Journal of Energy Storage 101 (2024) 113844

Contents lists available at ScienceDirect

Journal of Energy Storage

journal homepage: www.elsevier.com/locate/est

Review Article

A state-of-the-art review on numerical investigations of liquid-cooled battery thermal management systems for lithium-ion batteries of electric vehicles

Ashutosh Sharma [a], Mehdi Khatamifar [a], Wenxian Lin [a,*], Ranga Pitchumani [b]

[a] College of Science and Engineering, James Cook University, Townsville, QLD 4811, Australia
[b] Department of Mechanical Engineering, Virginia Tech, Blacksburg, VA 24061, USA

A R T I C L E I N F O

Keywords:
Liquid-cooled battery thermal management system
Electric vehicle
Numerical simulation
Review

A B S T R A C T

In recent decades, the electric vehicle (EV) industry has expanded at a quicker rate due to its numerous environmental and economic advantages. The battery thermal management system (BTMS) is an essential part of an EV that keeps the lithium-ion batteries (LIB) in the desired temperature range. Amongst the different types of BTMS, the liquid-cooled BTMS (LC-BTMS) has superior cooling performance and is, therefore, used in many commercial vehicles. Considerable ongoing research is underway to improve the performance of LC-BTMS, with most of the focus on numerical simulations. In view of this, the present article conducts a comparative assessment of the numerical simulation methodologies adopted for the analysis of LC-BTMS and systematically reviews the recent investigations of the design, operational, and performance aspects of LC-BTMS designs. The recently studied designs of LC-BTMS for both cylindrical and prismatic batteries are considered and further classified on the basis of main design attributes. Based on the existing literature, challenges with the current LC-BTMS technologies are analyzed, and areas of further development are identified. The review will serve as the basis for guiding future numerical simulations and the advancement of LC-BTMS technologies.

1. Introduction

In the modern world, energy needs are drastically rising. Currently, fossil fuels are the primary sources of the world's energy needs, contributing to about 80 % of all energy produced. The use of fossil fuels has drawbacks due to their limited supply and unfriendly burning [1]. Transportation is one of the major industries that utilize fossil fuels and is thus responsible for a great deal of pollution [2]. The second-biggest contributor to global greenhouse gas (GHG) emissions in 2022, with an estimated 14 % share, was the transport sector [3]. Therefore, researchers and entrepreneurs worldwide are becoming more interested in clean, alternative transportation technologies.

Electric vehicles (EVs) powered by chemical batteries have become a very viable substitute for traditional internal combustion engine automobiles [4]. In an EV, the battery, electric motor, and chassis are the essential parts, with the battery as the most important one, as it is the primary component that determines the charging/discharging rate and, in turn, the vehicle's range [5]. Amongst the several chemical battery types, lithium-ion batteries (LIBs) find extensive use in EVs owing to their extended cycle life, low self-discharge rate, and high specific energy and power [6]. LIB offers many benefits, but one drawback is that its operating temperature range is limited. According to Lu et al. [7], the ideal operating temperature range for LIBs is between 15 °C and 40 °C. Furthermore, the temperature differential between the cells in the battery pack causes an imbalance in the discharging phenomena, which eventually results in a loss in the capacity of the batteries. The primary goals of an EV are an extended range and quick charging, which necessitate maintaining the battery temperature. The rise in temperature of a LIB during rapid charging and discharging is a primary concern that results in further adverse consequences, including a reduction in battery capacity, thermal runaway, and potential explosion [8–12]. Therefore, the design of an effective and efficient battery thermal management system (BTMS) is much needed.

Both external and internal changes may control the temperature within a LIB. The electrode thickness, cathode/anode materials, and cathode/anode particle size are amongst the internal modifications [13]. The structural alterations to the batteries are limited by the manufacturing limitations and related expenses [14]. The external BTMS techniques include controlling battery temperature via the

* Corresponding author.
E-mail address: wenxian.lin@jcu.edu.au (W. Lin).

https://doi.org/10.1016/j.est.2024.113844
Received 22 May 2024; Received in revised form 24 August 2024; Accepted 15 September 2024
Available online 28 September 2024

Nomenclature

A_s	surface area of active particle material
C	capacitance
C_L	concentration of Lithium-ions in electrolyte
C_p	heat capacity
C_S	concentration of Lithium-ions
D_L^{eff}	effective diffusion coefficient
DoD	degree of discharge
D_S	diffusion coefficient for Lithium-ions in solid phase
f_+	electrolyte activity coefficient
F	Faraday's constant
i_s	current density in solid phase
I	current
I_l	current density in liquid phase
Q_{gen}	battery heat generation rate
$Q_{irr.}$	irreversible heat generation
$Q_{ohm.}$	ohmic heat generation
$Q_{pol.}$	heat generation due to polarization
$Q_{rev.}$	reversible heat generation rate
Q_{RX}	heat generation due to electro-chemical reaction
Re	Reynolds Number
$R_{int.}$	internal resistance of the battery
R_O	Ohmic Resistance
SoC	State of Charge
t	time
t_+^o	transfer number of lithium ion
T	temperature
T_{max}	maximum temperature of the battery module
ΔT	temperature difference of batteries in a module
U	voltage
U_{OC}	open circuit voltage
$V_{bat.}$	volume of the battery

Greek symbols

δ^{eff}	effective conductivity of solid phase
ε_L	volume fraction of electrolyte
$\eta_{pol.}$	over potential
ρ	density
ρ_i	local current density
τ	time constant
φ_s	solid phase potential

Abbreviations

AC-BTMS	Air Cooled Battery Thermal Management System
BTMS	Battery Thermal Management System
CFD	Computational Fluid Dynamics
CP	Cooling Plate
ECM	Equivalent Circuit Model
EG	Ethylene Glycol
EV	Electric Vehicle
HWFET	Highway Fuel Economy Test
HTF	Heat Transfer Fluid
LC-BTMS	Liquid Cooled Battery Thermal Management System
LIB	Lithium-ion Battery
MCDM	Multi Criteria Decision Making technique
MHPA	Micro Heat Pipe Array
MWCNT	Multiwall Carbon Nano-tube
P2D	Psuedo-2-Dimensional Thermo-electric model
PCM	Phase Change Material

battery's exterior case. The battery temperature can be successfully kept within the specified temperature range with the use of an external BTMS [15].

External BTMSs can be categorized as active and passive systems, as shown in Fig. 1 [16]. In an active BTMS, the heat from the battery pack is removed by a flowing fluid (air, water, or any other miscellaneous). In a passive BTMS, the battery's heat management is handled without the need for any energy-intensive systems (using phase change materials (PCM) or heat pipes). A hybrid BTMS combines passive and active techniques to achieve a higher level of performance than either approach alone. BTMSs may be used, depending on the situation, to raise or decrease the battery pack's temperature. This work focuses on cooling BTMSs since the greater temperature of LIB is linked to significant issues.

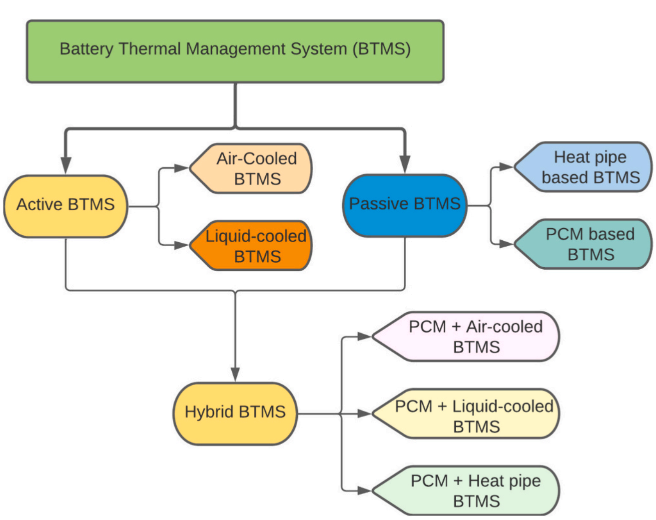

Fig. 1. Classification of different types of BTMSs [16].

There are many BTMS types available to maintain the battery temperature within an appropriate range. For cooling, an active BTMS uses an active system that moves the cooled fluid (heat transfer fluid - HFT) through it. Despite its high complexity and operating costs, the active BTMS provides quick cooling [17]. On the other hand, the low operating cost of a passive BTMS stems from its lack of need for fluid movement. However, passive systems are limited in their cooling or storage capabilities [18]. In comparison to active or passive BTMSs, hybrid BTMSs have marginally better cooling performance. Nonetheless, they have limited practical use due to their intricate construction and associated costs [19]. For example, using a leak-proof container for the battery modules is essential to the PCM implementation but incurs additional manufacturing and maintenance costs that preclude its practicality. Moreover, some PCMs are highly inflammable and, thereby, are less suited to be used in BTMSs [20]. Considering all these aspects, most EV manufacturers use active BTMSs. Amongst the air-cooled (AC) and liquid-cooled (LC) active BTMSs, the LC-BTMS is more effective due to better heat transfer and fluid dynamic properties of liquid compared to air [21]. Since the battery pack must be kept within the intended temperature range during intense charging and discharging, an effective and efficient LC-BTMS must be designed and developed.

In view of this, the primary objective of the present article is to review and comparatively investigate the various recently studied designs of LC-BTMSs based on design, operational, and performance parameters. Published reviews on the different designs of LC-BTMS [22–27], as summarized in Table 1, have considered the cylindrical and prismatic battery designs. These reviews further highlight the use of numerical modeling for the investigation of the performance of the LC-BTMS designs. However, the numerical modeling details in these reviews on

Table 1
Summary of recent reviews on LC-BTMSs.

Ref.	Year	Review specification	Considerations		Parameters	Key findings	Remarks
			BTMS type	Battery design			
[22]	2023	Various designs of LC-BTMSs and their optimization	• LC-BTMS • LC-based hybrid-BTMS	• Cylindrical • Prismatic	• Design • Operational	For LC-BTMS, LC-based hybrid-BTMS with PCM cooling, external coolant channel, and AC system design enhancement approaches work well.	LC-BTMSs for cylindrical and prismatic LIBs are not presented separately.
[23]	2021	Different designs of LC-BTMSs with a focus on the HTF type	• Direct and indirect contact type LC-BTMSs	• Cylindrical • Prismatic (few studies)	• Design • Operational • HTF type	Compared to other HTFs, water cooling was more effective and efficient. Nonetheless, a heat transfer barrier is the main drawback of the water-cooling system.	Different studies are categorized based on the HTF type, not on the kinds of LIBs and LC-BTMS designs.
[24]	2023	Review and comparison of LC-BTMSs	• Direct and indirect contact type LC-BTMSs	• Prismatic	• Design • Operational • HTF type • Comparison of designs	Different LC-BTMS designs were recreated and compared to numerical results. Every variant possesses unique merits, and no scheme exhibits absolute superiority in all aspects of the assessment.	It is necessary to include working conditions, application scenarios, and additional variables in the final design.
[25]	2023	Recent advancements in LC-BTMSs	• LC-BTMS • LC-based hybrid-BTMS	• Cylindrical • Prismatic	• Design • Operational • HTF type	Coolant plate designs provide better performance for prismatic batteries, whereas coolant channel designs are advantageous for cylindrical batteries.	Most of the studies included are numerical investigations.
[26]	2023	Recent progress on LC-BTMSs	• LC-BTMS • LC-based hybrid-BTMS	• Cylindrical • Prismatic	• Design • Operational • HTF type	Water is the most commonly used HTF in the studies and has been commercialized as well. Since liquid metal has superior thermophysical properties than water, it is essential to investigate its application in LC-BTMS.	The design has not been studied based on the battery configuration. Moreover, the details of numerical studies were not presented.
[27]	2019	Issues in LIBs due to high temperature and LC-BTMS as a solution	• LC-BTMS • LC-based hybrid-BTMS	• Cylindrical • Prismatic	• Design • Operational	Many researchers have studied PCM-based and direct contact-type LC-BTMSs. Still, these designs have practical limitations which suppress their applicability in the EV industry.	Most of the studies included are numerical investigations. However, there is no presentation of the numerical simulation specifics.

BTMSs are not extensively presented. Therefore, the second objective of this article is to provide the details of the numerical simulations. Moreover, in most of the reviews, the studies on both cylindrical and prismatic are presented separately. The design and operational parameters of the cylindrical and prismatic LIBs are different and affect the numerical simulation methodology. The third objective of this article is to compare the range of various design, operational, and performance parameters of the LC-BTMS designs studied with cylindrical and prismatic LIBs. This study will help researchers and entrepreneurs design effective LC-BTMS designs for both cylindrical and prismatic LIBs.

The rest of the present review is organized as follows: in Section 2, LC-BTMS designs are classified in several ways; in Section 3, different LC-BTMS designs for cylindrical LIBs are described, discussed and analyzed comparatively; in Section 4, similar description, discussion and comparative analysis are conducted for different LC-BTMS designs for prismatic LIBs; in Section 5, a comparison of LC-BTMS for cylindrical and prismatic LIBs is made; in Section 6, some major issues and challenges are identified and future work is recommended; and finally in Section 7, the conclusion is presented.

2. Classification of LC-BTMS designs

It is possible to categorize LC-BTMS designs in several ways, as seen in Fig. 2. One categorization is based on the battery design. Three distinct forms of LIBs are available for commercial use: pouch, prismatic, and cylindrical. Since pouch cells have low mechanical strength, they are susceptible to being damaged by physical forces, which prohibits them from being effectively used in EVs. The layout of the cooling

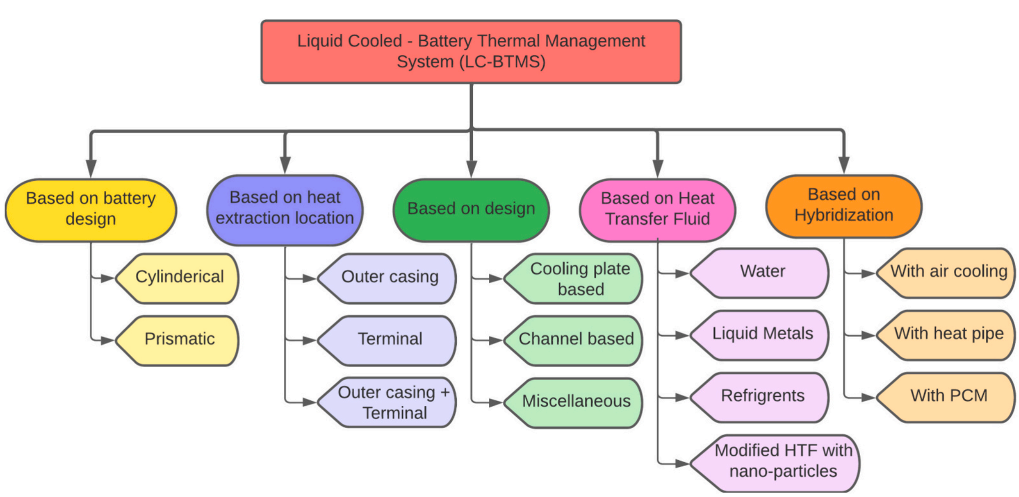

Fig. 2. Classification of different LC-BTMS designs.

channels is yet another method that may be used to categorize LC-BTMS devices. Regarding commercial applications, cooling plate (CP) based and channel-based LC-BTMS devices have been used and researched more often. It is also possible to classify LC-BTMS designs according to the location of the heat extraction, which might result from the outer casing, taps, or a mix of these elements or according to the kind of heat transfer fluids that are used.

Additionally, LC-BTMS designs have been investigated in conjunction with other BTMS designs in order to provide further insight, thus LC-BTMS designs may also be categorized according to the sort of hybridization that is used. The categorization of LC-BTMS designs based on the configuration of LIBs is the most prominent amongst the several classifications that are available. As a result, the following sections will discuss several LC-BTMS designs that are based on the configuration of LIBs, including prismatic LIBs and cylindrical LIBs. Fig. 3 diagrammatically illustrates the organizational framework of the present review paper.

3. LC-BTMS designs for cylindrical LIBs

The cylindrical LIB is a ubiquitous design used in many applications. In EVs, many manufacturers are using cylindrical LIB designs for battery modules because of their high heat dissipation rate and higher performance consistency [28–30]. Therefore, numerous LC-BTMS designs for cylindrical LIBs have been studied. In most of these designs, either CP-based or channel-based LC-BTMS designs have been studied. The following sub-sections discuss these studies in detail.

3.1. CP-based LC-BTMS designs

A cold plate (CP) is basically a flat rectangular plate with embedded liquid channels. The passage of the HTF through the CP keeps it cool and maintains the temperature of the battery module. CPs can be further classified based on the size and shape of the liquid channel.

Many types of CP-based LC-BTMS designs have been studied. Huang et al. [31] carried out a numerical investigation of an LC-BTMS design for cylindrical 18,650 Li-ion cells. In the battery pack, 48 cells were arranged, and cold plates were arranged on both terminals of the cells, as shown in Fig. 4(a). The effect of the Reynolds number of flow (*Re*) was studied to reveal that the temperature of the battery pack decreased when *Re* increased up to a certain point and became steady afterward. The optimum value of *Re* was found to be 475. They also reported a cooling hysteresis with the flow rate, i.e., the battery temperature did decrease immediately with an increase in the flow rate. Moreover, as shown in Fig. 5, the battery surface temperature decreased rapidly with an initial rise in the flow rate. Then, it became almost constant afterward for all C values considered, where C is a measure of the discharge rate at which a battery is discharged relative to its maximum capacity, with 1C rate meaning that the discharge current will discharge the entire battery in 1 h. For a battery with a capacity of 100 Amp-hrs, a 1C rate equates to a discharge current of 100 Amps, and a 5C rate for this battery would be 500 Amps. Yang et al. [32] carried out a numerical investigation to evaluate the cooling performance of a hybrid PCM + LC-BTMS. The hexagonal battery module, having cylindrical batteries, PCM, and CPs arranged, as shown in Fig. 4(b), was used for the study. Their results showed that the designed system was very capable of keeping the maximum battery temperature (T_{max}) and the temperature difference (ΔT) below 309.15 K and 3.8 K, respectively. The pressure drop in the

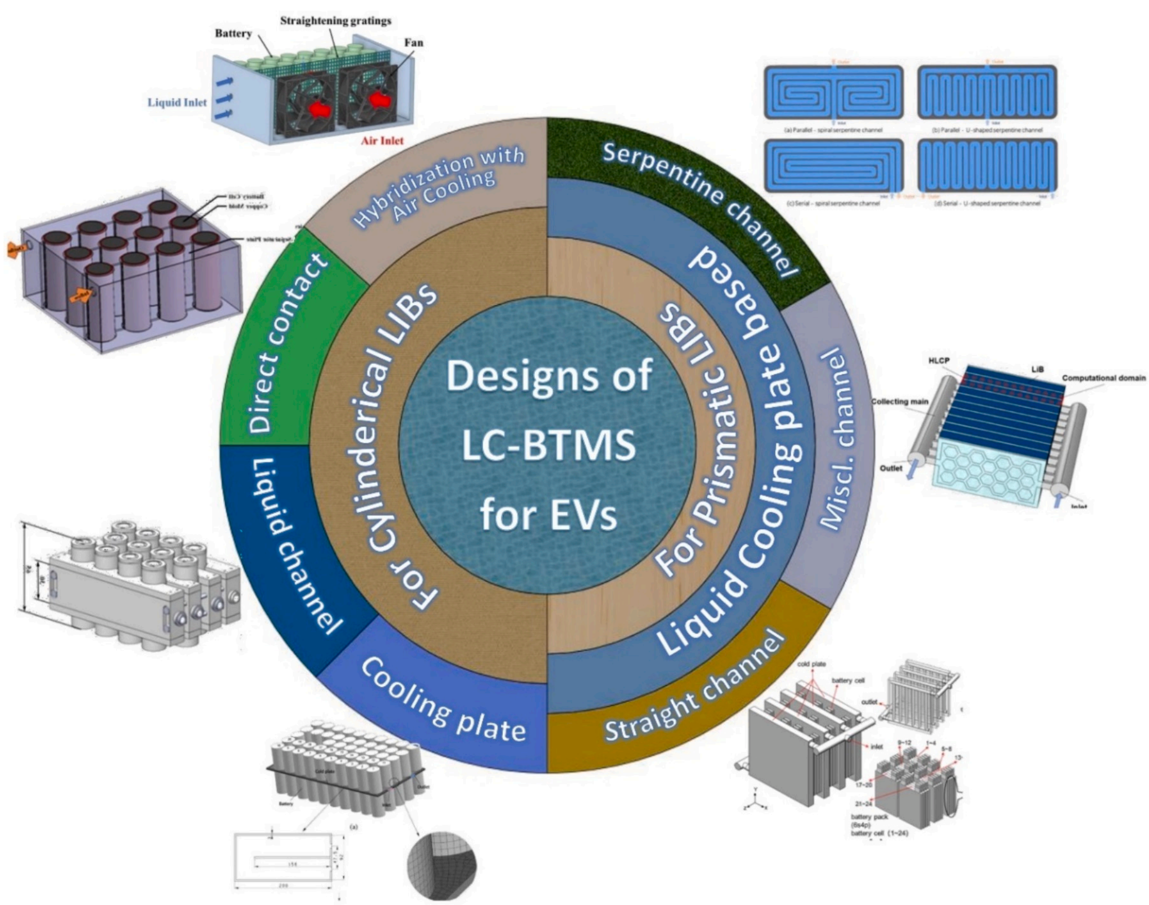

Fig. 3. Structure of the present review article.

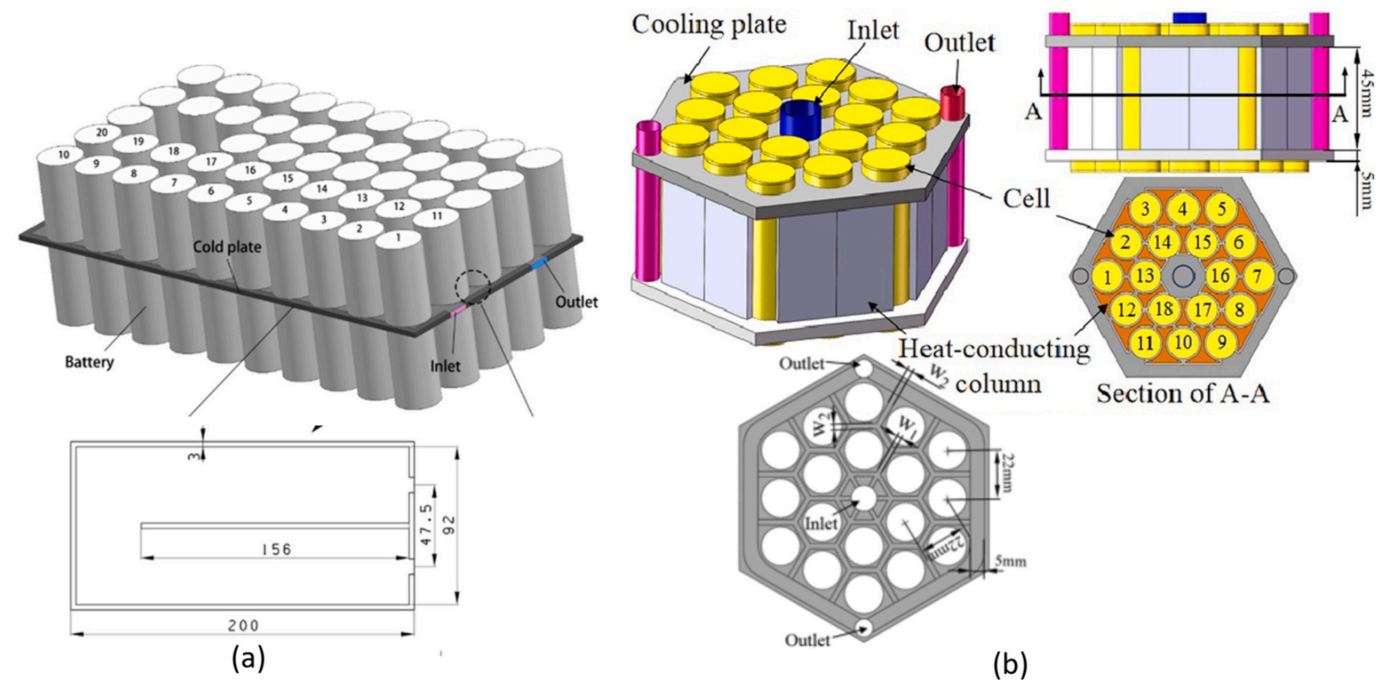

Fig. 4. CP-based LC-BTMS designs were studied by (a) Huang et al. [31] and (b) Yang et al. [32].

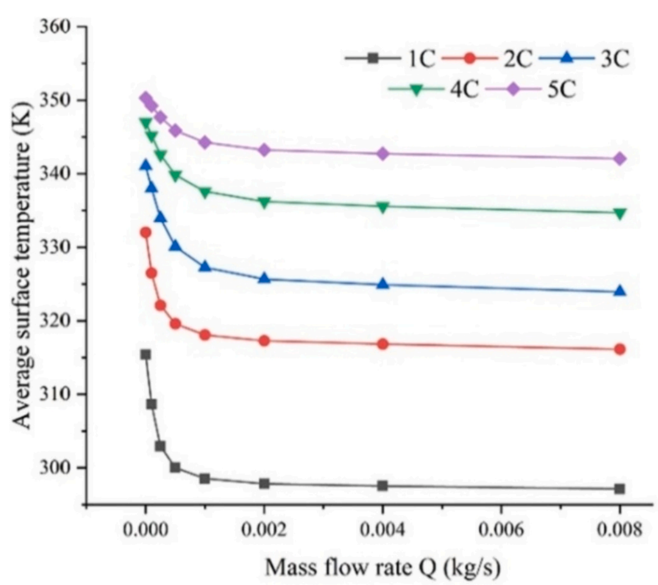

Fig. 5. Variation of the average surface temperature with the mass flow rate for different C values (Obtained with permission from Huang et al. [31]).

designed honeycomb channels was also found to be below 11.95 Pa. The performance of the CP with a honeycomb channel was found to be comparatively better than the CP with a straight channel. This trend may be attributed to the more turbulent fluid mixing and eventually improved heat transfer rate in the honeycomb channels as compared to the straight channel.

Zeng et al. [33] investigated the thermal performance of an LC-BTMS having reciprocating flow. The LC-BTMS was made up of a micro heat pipe array (MHPA), CPs, tubes, and a solenoid valve. Instead of using a single fluid flow direction (as in other studies), the solenoid valve was used to alter the flow direction after a specific time. Two critical parameters of the reciprocating flow, i.e., velocity and reciprocating frequency, were thoroughly investigated. It was found that the reciprocal flow reduces both the temperature differential and energy usage by 55.3 % and 15.6 %, respectively.

Amongst different CP-based LC-BTMS designs, some had the flow of the HTF from the CP and the channels designed on the outer casing of the LIB. Many such designs have been studied that are able to extract heat from both the taps and outer casing of the cylindrical LIB. Zhao et al. [34] carried out a numerical investigation to evaluate the thermal performance of a mini-channel-based LC-BTMS. The design included a thin metallic jacket around each cell of the battery pack with eight mini channels, as shown in Fig. 6. The effect of the flow direction in the channels was studied in terms of T_{max} and ΔT. The results revealed that the LC-BTMS design was able to keep T_{max} below 40 °C.

In another study, Dong et al. [35] conducted a numerical analysis to evaluate the cooling performance of an LC-BTMS. A cylindrical jacked around the cylindrical cells with a helix-shaped cooling channel was used for the LC-BTMS. The optimization for the helix pitch, tube diameter, and HTF flow rate was carried out using the multiple criteria decision-making (MCDM) technique. The designed system kept the module's T_{max} and ΔT below 32.36 °C and 6.98 °C, respectively. Similarly, Lai et al. [36] numerically investigated the thermal performance of a lightweight LC-BTMS at a discharge rate of 5C. The designed system included two CPs on both sides of the cylindrical LIB and thermal conductive structures (TCS). The effects of the TCS's mass flow rate, inner diameter, contact surface height, and contact surface angle were examined. It is found that when the liquid flow rate is $>1 \times 10^{-4}$ kg/s, T_{max} can be kept within 313 K for the battery pack.

3.2. Channel-based LC-BTMS designs

Another typical design of LC-BTMSs that has been widely studied is the channel-based LC-BTMS, wherein the HTF passes through different channels, which are generally placed on the outer casing of the LIB. Wang et al. [37] carried out both experimental and numerical investigations for the thermal performance evaluation of a novel modular LC-BTMS. The modular design included a rectangular channel with staggered indents on both long sides for cylindrical cell placement, as shown in Fig. 7. The parallel and series flow arrangements were investigated for the LC-BTMS design at a 3C discharge rate. The performance

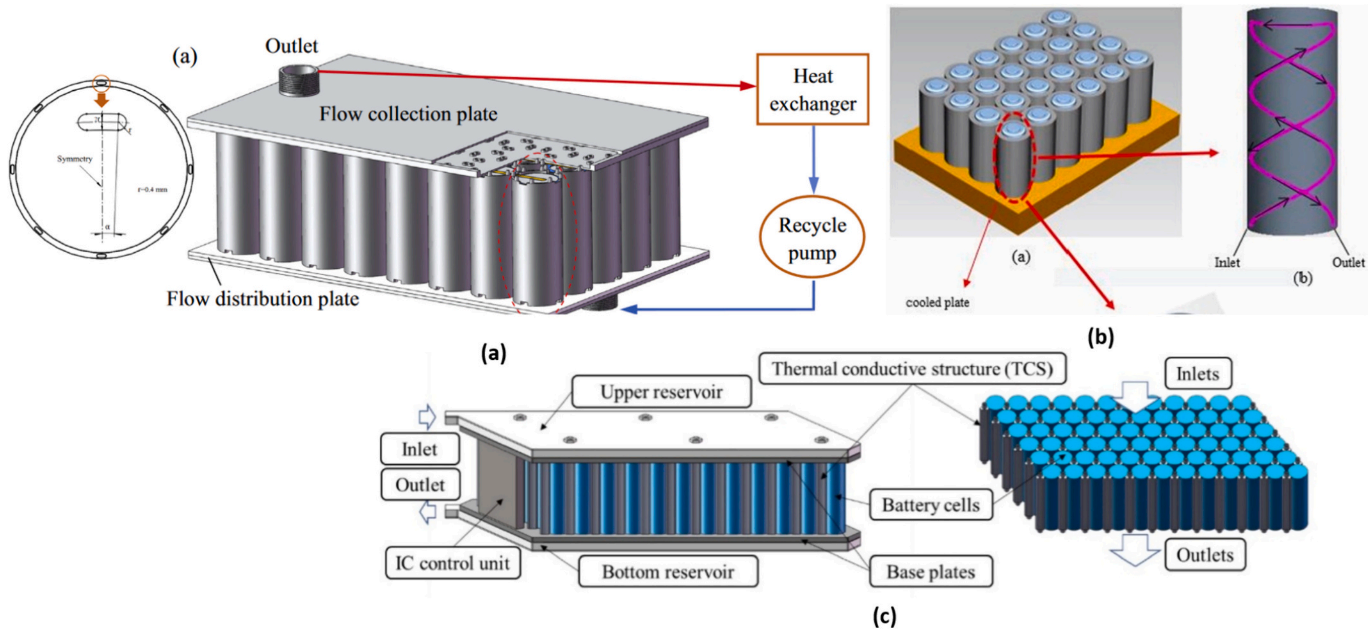

Fig. 6. LC-BTMS designs studied by (a) Zhao et al. [34], (b) Dong et al. [35], and (c) Lai et al. [36].

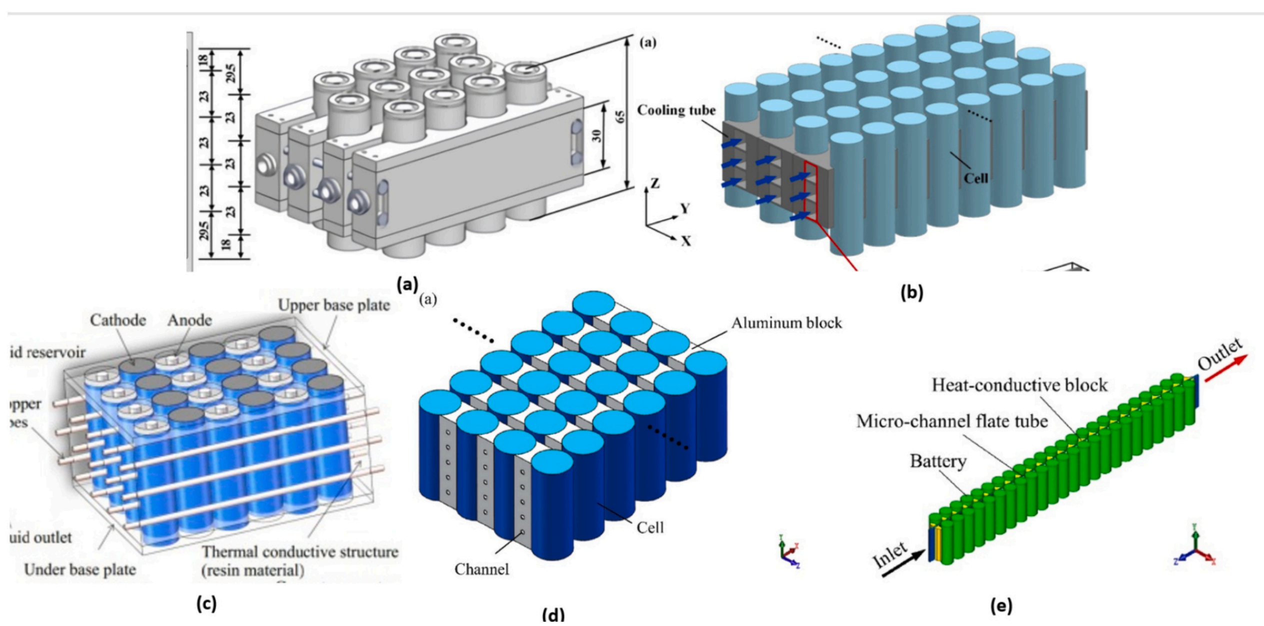

Fig. 7. Channel-based designs of LC-BTMSs for cylindrical LIBs studied by (a) Wang et al. [37], (b) Gao et al. [38], (c) Liu et al. [39], (d) Rao et al. [40], and (e) Tang et al. [41].

of the LC-BTMS design, which had a parallel flow channel, was found to be superior to that of the series arrangement. The designed system was able to keep T_{max} and ΔT at 37.67 °C and 5.76 °C, respectively.

Gao et al. [38] numerically and experimentally investigated a novel gradient channel design (GCD) based LC-BTMS. The design of the LC-BTMS is also presented in Fig. 7. The performance of the designed system was compared with the uniform large channel design (ULCD) and uniform small channel design (USCD). Compared with the ULCD and USCD, ΔT of the battery module with the optimal GCD is significantly reduced in the whole flow range, especially at low inlet flow rates, which is effective in reducing external power consumption. Liu et al. [39] studied the performance of an LC-BTMS for cylindrical battery cells with liquid metal (gallium indium alloy, $Ga^{80}In^{20}$) as the HTF. The system's performance was compared to that of a system with water as the HTF. It was observed that the system with liquid metal as the HTF performed significantly more effectively as compared to that with water as the HTF, as shown in Fig. 8. Moreover, a variable flow velocity strategy (VFVS) was designed based on the discharging rate and ambient conditions and the performance was compared to the traditional constant flow velocity strategy (CFVS). Results show that the designed VFVS can maintain the same T_{max} in the battery module as CFVS with 47 % less pump power consumption.

Rao et al. [40] carried out a numerical investigation to evaluate the cooling performance of an LC-BTMS for cylindrical LIB cells. The LC-BTMS was made up of concave aluminum blocks placed between the cylindrical cells for a larger heat transfer area, and five cylindrical

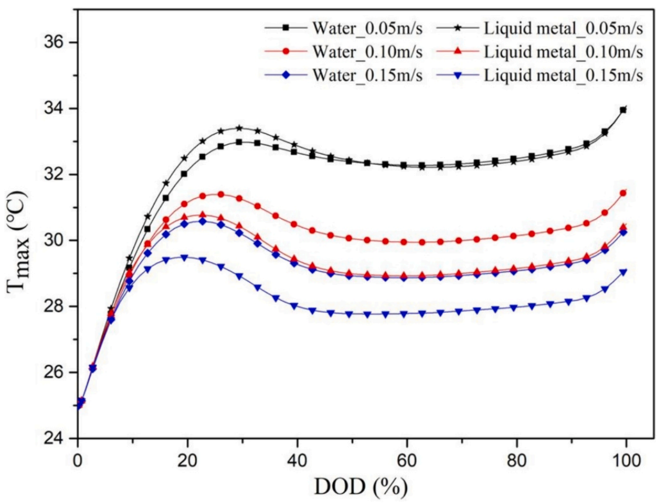

Fig. 8. Variation of T_{max} with depth of discharge (DOD) for water and liquid metal as the HTF at different flow velocities (Obtained with permission from Liu et al. [39]).

channels were passed through them for the HTF passage. They reported that the designed system was able to significantly reduce T_{max} and ΔT in the battery cell to be below 40 °C and 5 °C, respectively, when the HTF flow rate was 0.5 m/s. Tang et al. [41] numerically studied the thermal performance of an LC-BTMS having heat-conducting blocks with gradient contact surface angles. A novel approach for varying the contact surface angle in the LC-BTMS was adopted. The straight LC-BTMS was divided into four equal parts, and different contact angles were selected for different sections. Results demonstrated that when the contact angle near the inlet and outlet was the smallest and largest respectively, the minimum ΔT between the cells was observed to be 8.05 °C. In another study, an almost similar design was evaluated similarly [42]. Instead of flat microchannel, five microtubes were used and almost the same designs of the heat conductive blocks were studied. The designed system kept T_{max} and ΔT below 34.6 °C and 2.9 °C, respectively, at the discharging rate of 2C. Fan et al. [43] reported a different type of strategy for improving the charging time of the EV in conjunction with an LC-BTMS. A genetic algorithm was developed based on the cell temperature for charging current and voltage. During charging, the LC-BTMS actively cooled the battery. Results showed that the designed charging method cuts 11.9 % off the time it took to charge compared to the constant current-constant voltage method. Mitra et al. [44] experimentally investigated the cooling performance of different nano-fluids in LC-BTMSs. Two serpentine rectangular tubes were used for the LC-BTMSs. Multiwalled carbon nanotubes (MWCNT) were added in different fractions (0.15 %, 0.3 %, and 0.45 %) within the water + Ethylene Glycol (EG) mixture. Three different arrangements of fluid flow, namely single channel flow, double channel-parallel flow, and double channel-counter flow, were investigated at different battery discharging rates. It was observed that at the 2.1C discharge rate, T_{max} reached 47.2 °C, which can be effectively reduced by 30.5 % with the help of nano-fluid of 0.45 % MWCNT in the flow arrangement of the double channel – counter flow.

Another primary channel design for LC-BTMSs is a flexible channel. There are many studies on LC-BTMSs with flexible channels, generally in a serpentine shape in the LC-BTMS. Xie et al. [45] numerically investigated the thermal performance of an LC-BTMS, which is an improvement of the patent design of the Tesla-S model BTMS, as shown in Fig. 9 (a). A baffle was introduced on the sides of the serpentine tube for better fluid mixing. The Psuedo-2-Dimensions (P2D) model was used for the battery heat generation. The result revealed that the modification in the LC-BTMS design significantly improved the heat transfer rate. Yin et al. [46] studied the thermal performance of an LC-BTMS in a vibrating

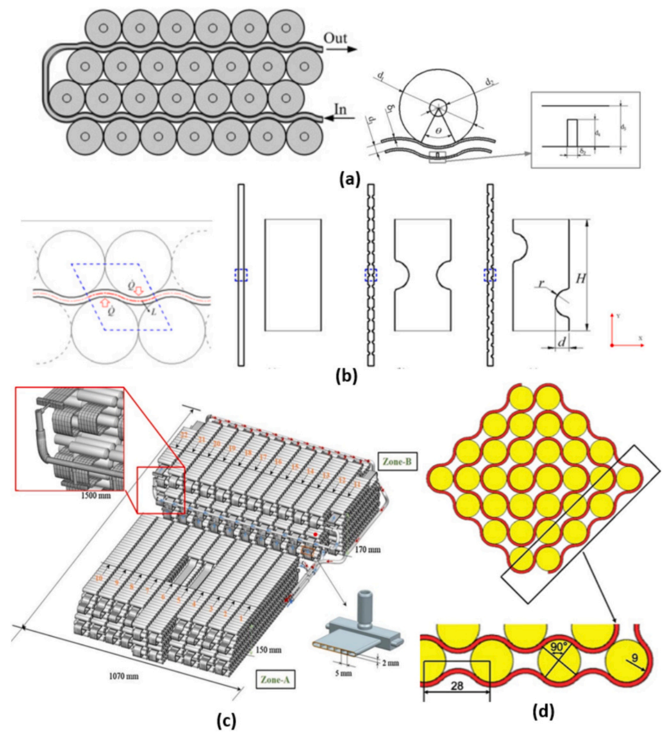

Fig. 9. Flexible rectangular channel-based designs of LC-BTMSs for cylindrical LIB studied by (a) Xie et al. [45], (b) Yin et al. [46], (c) Cao et al. [47], and (d) Qi et al. [48].

environment. They studied three different designs of LC-BTMSs, i.e., plain rectangular channel, rectangular channel with protrusions on side walls opposite to each other, and rectangular channel with protrusions on side walls in a staggered scheme, as shown in Fig. 9(b). Their results showed that the LC-BTMS design with the plain rectangular channel did not have any effect of the vehicle vibration. In contrast, the heat transfer rate was found to be improved with vibration for the second and third designs because of vortex formation near the protrusion design. They found that the average Nusselt Number on the wall for the third design was twice that of the first design. Cao et al. [47] investigated the thermal performance of an LC-BTMS for a full-size cylindrical battery pack, as shown in Fig. 9(c). The design of the LC-BTMS included a wavy rectangular pipe with mini channels for the HTF passage. The study included the consideration of a battery pack at the full scale, consisting of 22 modules, which held a total of 5664 LIBs of the 18,650 type. The results revealed that the designed system was able to keep the battery temperature below 40 °C and 11 °C under the discharging rates of 0.5C and 1C, respectively. The study on the effect of the HTF flow rate found that the performance improved with increasing the HTF flow rate.

Qi et al. [48] numerically investigated the thermal performance of a flexible Swiss-roll type LC-BTMS, as shown in Fig. 9(d). The performance of the designed LC-BTMS was analyzed, and optimization of channel width and height was carried out by forming orthogonal test combinations. T_{max} and ΔT for the optimized design were found to be 300.4 K and 3.3 K, respectively. They also compared the performance of the designed system with the serpentine flow channel type LC-BTMS and found that T_{max} and ΔT for the developed system were 1.2 K and 0.2 K lower than the conventional system, respectively. Ke et al. [49] experimentally evaluated the performance of the serpentine-type LC-BTMS having micro-channels for the retardation of thermal runaway propagation. The effect of the HTF flow rate on the thermal runaway propagation was studied. They reported that the thermal runaway propagation in the battery pack is inversely proportional to the HTF flow rate. For the 96 l/h flow rate, the thermal runaway propagation rate was found to be minimal.

Apart from the conventional rectangular flexible channels, some other shapes of the channels have also been studied. Bohacek et al. [50] study numerically the cooling performance of the LC-BTMS design made up of polymeric hollow fibers. The selected design of the LC-BTMS used alternating hot and cold tubes on the circumference of the cylindrical cells, as shown in Fig. 10(a). The performance of the designed system was studied at a 1C discharging rate, and it was found that the designed system maintained T_{max} and ΔT in the ranges of 49 °C–35 °C and 14.6 °C–4.6 °C, respectively. Zhou et al. [51] conducted a numerical investigation to analyze the performance of the LC-BTMS design, which included the spiral screw-thread-type jackets for the cylindrical batteries made up of half-helical tubes as shown in Fig. 10(b). The effect of the liquid flow rate, pitch, diameter, and number of starts was investigated. It was shown that T_{max} decreased from 66.7 °C to 30.8 °C and ΔT decreased from 31.8 °C to 5.4 °C when the intake mass flow rate increased from 1×10^{-5} kg/s to 3×10^{-4} kg/s.

Another subtype of the channel-based LC-BTMS is the block-based design. In this design, a block with an embedded HTF channel is used. Many researchers studied different block-based LC-BTMS designs. Yates et al. [52] conducted a numerical study and compared the thermal performance of two different block-based LC-BTMS designs, which are the channel-cooled heat sink (CCHS) design and mini-channel-cooled cylinder (MCC) design, as shown in Fig. 11(a). Results of the study revealed that the thermal performance of both systems improved with the increase in the flow rate. The optimized designs of MCC and CCHS were able to keep T_{max} and ΔT below 213 K and 5 K, respectively. The MCC design offers superior cooling capabilities compared to the CCHS design. However, these advantages are accompanied by challenges related to greater design complexity, hence imposing limitations on its economic viability. Coleman et al. [53] carried out a numerical investigation to evaluate the thermal performance of an LC-BTMS consisting of a cold block, HTF tube, and cylindrical LIB, as shown in Fig. 11(b). The effect of cell spacing and block material was investigated. Two different block materials, aluminum (*Al*) and composite wax/metal material (CW), were studied. They reported that both the bock material and cell spacing play a significant role in cooling performance, especially in the case of a particular cell failure. The cell spacing of 10 mm and block material of CW 5 % provided the best results comparatively.

Liu et al. [54] conducted a numerical investigation to investigate the thermal performance of two layouts of LC-BTMSs comparatively. The LC-BTMS design consisted of an aluminum frame, HTF pipes, and cylindrical LIB. In one layout, the HTF tubes were arranged horizontally, whereas vertical HTF tubes were used in the second design, as shown in Fig. 11(c). Alongside the comparative investigation, the effect of the step variation in flow rate and tube diameter was also investigated. The results revealed that the configuration with the vertical HTF tubes performed significantly better than the other design. It was also found that the cooling performance improved with the step variation of the HTF flow rate and tube diameter. For the optimized design, T_{max} and ΔT were limited at 30 °C and 2.88 °C at a 3C discharge rate, respectively. Sheng et al. [55] carried out a numerical investigation to evaluate the thermal performance of a cellular cooling jacket (CCJ) type LC-BTMS, as shown in Fig. 11(d). The effects of the HTF flow rate, tube diameter, and flow direction were studied. Results advocated that interlaced flow directions could achieve better temperature uniformity. Cooling performance was also found to be improved with an increase in the HTF flow rate and tube diameter. The cooling effect of water and 50%GAS (glycol aqueous solution) as the HTF was also comparatively investigated, and better performance was observed in the case with 50%GAS as the HTF.

3.3. Direct contact type LC-BTMS designs

Tete et al. [56] carried out a numerical investigation to evaluate the thermal performance of a direct contact type LC-BTMS. The schematic of the designed system is shown in Fig. 12(a). 25 cylindrical cells were considered in the battery module, and water was used as the HTF. The performance of the system was compared with that of the same system, which had no water flow velocity. Results showed that the temperature in the natural convection case increased up to 60 °C, whereas T_{max} and ΔT for the designed system were found to be 28 °C and 0.12 °C, respectively, at a 5C discharge rate. Tousi et al. [57] conducted a numerical investigation to evaluate the thermal performance of an LC-BTMS consisting of a leak-proof container with separators and copper molds for cell placement, as shown in Fig. 12(b). The serpentine liquid channel path was designed in the system with the help of separators. Water with AgO nanoparticles in volume fractions of 1 %, 2 %, and 3 % were used as the HTF. The results of the study revealed that the thermal performance of the designed system with the nano-fluid was significantly improved. It was able to maintain T_{max} and ΔT below 305.59 K and 1.07 K, respectively. Kumar et al. [58] comparatively investigated the effect of different fluids on the cooling capacity of a BTMS, with air and naphthenic oil considered for the simulation. Results showed that compared to air, the use of oil demonstrated a considerable drop in the average temperature of a battery module cell of 6.6 °C during a 1C discharge rate and 9.8 °C with a 2C discharge rate.

Zhou et al. [59] comparatively investigated the thermal performance of an immersion-BTMS and direct contact LC-BTMS for the batteries. Pouch cells were considered for the study, and a lumped battery model was used to simulate the batteries. They reported that the direct contact LC-BTMS performed better than the immersion-BTMS even when the flow rate was minimal, i.e., at 1 mm/s. Kant and Pitchumani [60] reported the comparative assessment of two designs of LC-BTMS, as shown in Fig. 12(c). One design included a channel (Case I) and another without a channel (direct contact) (Case II). The results of the study showed that the cooling performance of Case II was significantly better than that of Case I due to comparatively less thermal resistance.

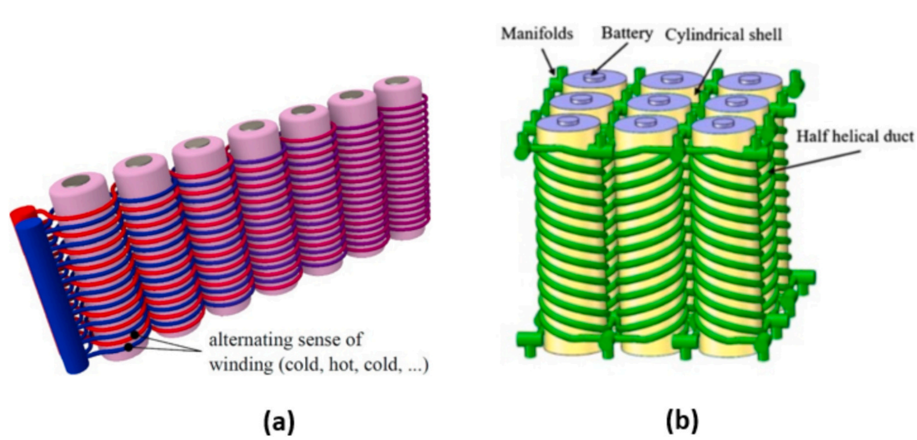

Fig. 10. Flexible circular channel-based LC-BTMS designs for cylindrical LIB studied by (a) Bohacek et al. [50] and (b) Zhou et al. [51].

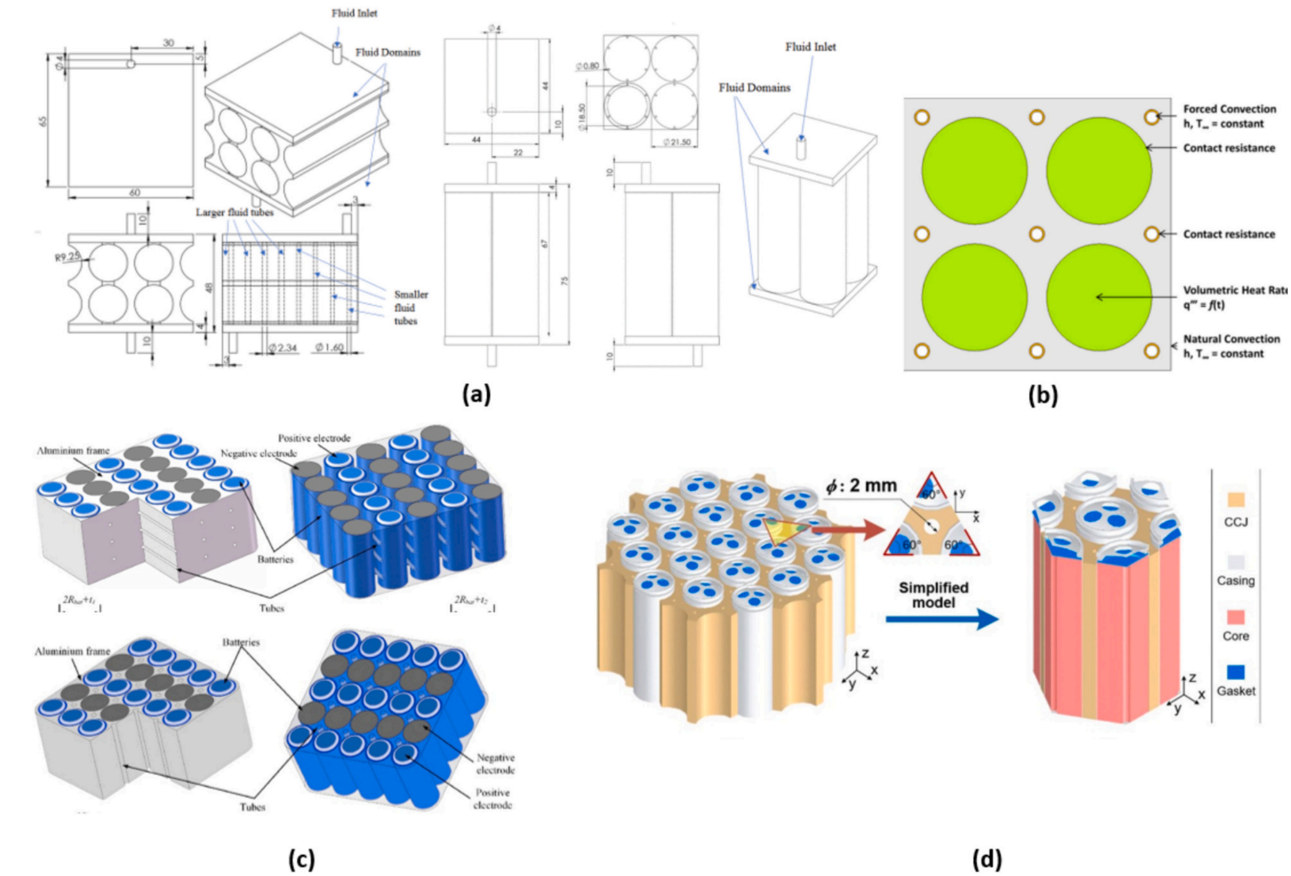

Fig. 11. Block-based LC-BTMS designs studied by (a) Yates et al. [52], (b) Coleman et al. [53], (c) Liu et al. [54], and (d) Sheng et al. [55].

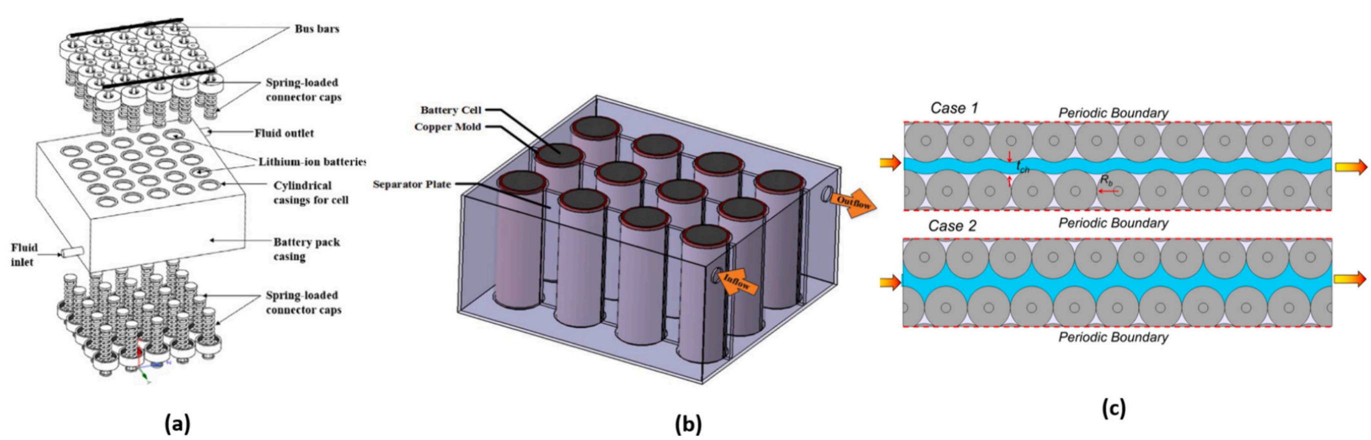

Fig. 12. Direct contact type LC-BTMS designs studied by (a) Tete et al. [56], (b) Tousi et al. [57], and (c) Kant and Pitchumani [60].

3.4. Hybridization with air cooling

Air cooling (AC) of LIB in EVs has been widely studied in the literature. The combination of this technology with liquid cooling improves the overall performance of the system. Many researchers studied the hybridization of air and liquid cooling. Xin et al. [61] conducted a numerical investigation to evaluate the thermal performance of a combined AC + LC-BTMS, as shown in Fig. 13(a). For liquid cooling, the cooling blocks were used, and the effect of the cooling block number was investigated. Results showed that T_{max} and ΔT were 34.41 °C and 1.53 °C, respectively, while using only liquid cooling. T_{max} and ΔT were both reduced by 3.75 °C and 0.96 °C, respectively, when AC was added. Zhao et al. [62] conducted a numerical investigation to evaluate the thermal performance of a hybrid AC + LC-BTMS, as shown in Fig. 13(b). For liquid cooling, the cylindrical LIB cells were placed in a corrugated type channel, and the air was allowed to pass on the outer surface of the channel. Results of the study showed that the cooling performance improved with an increase in the width of the cooling channel. Moreover, T_{max} and ΔT decrease with an increase in the HTF flow rate; however, the cooling efficiency decreases. The designed system was able to maintain the temperature criteria for the LIB at a 4C discharge rate. Angani et al. [63] conducted both numerical and experimental investigations to evaluate the thermal performance of a hybrid AC + LC-BTMS, as shown in Fig. 13(c). The performance of the designed system was compared with the same BTMS but with liquid cooling only. Results revealed that the developed hybrid system had 28 % better cooling

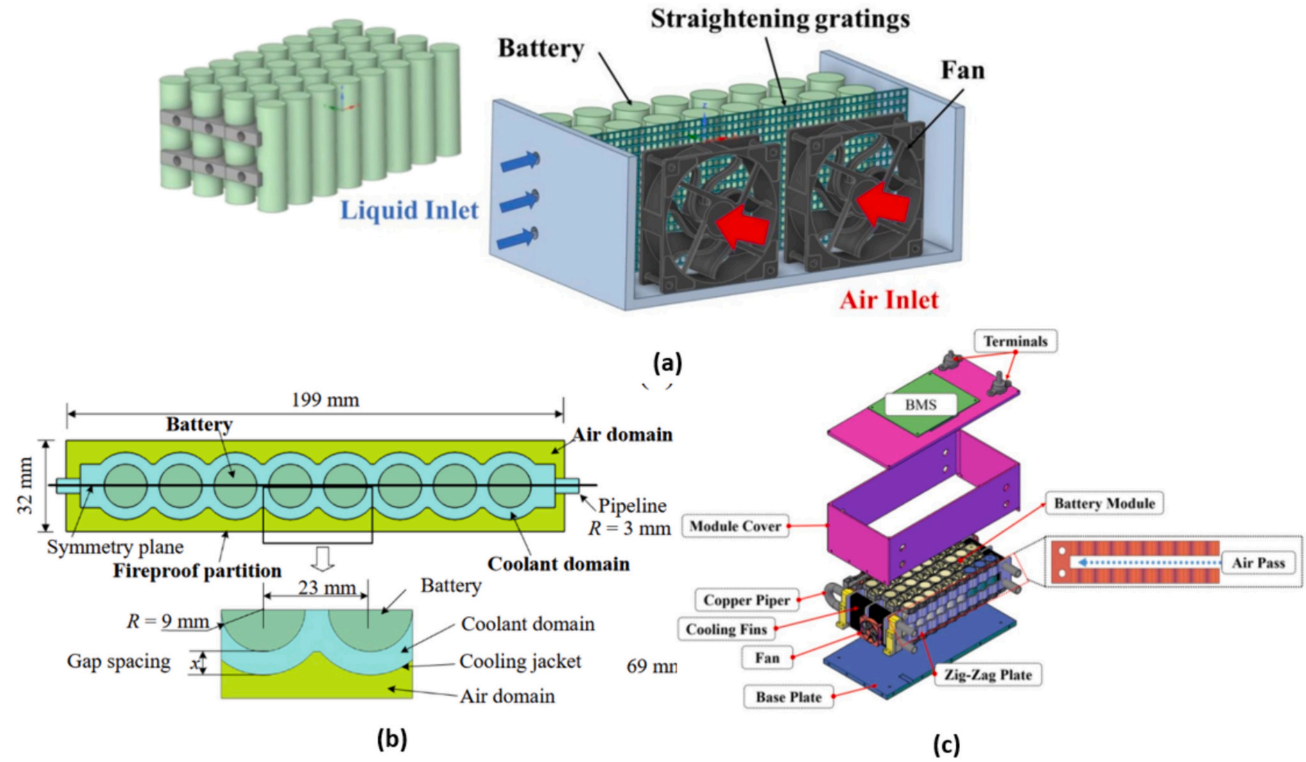

Fig. 13. Hybridization of LC-BTMSs with air cooling studied by (a) Xin et al. [61], (b) Zhao et al. [62], and (c) Angani et al. [63].

performance than the standalone system, with T_{max} and ΔT in the designed system to be 35 °C and 1.4 °C, respectively.

Apart from the hybridization of both AC-BTMS and LC-BTMS, some researchers studied the comparative performance of both systems. Vita et al. [64] comparatively investigated the thermal performance of AC-BTMS and LC-BTMS for prismatic battery cells. For the AC-BTMS, the direct placement of batteries in the air channel was studied. For the LC-BTMS, the cold plates were stacked in between the consecutive prismatic cells. Results showed that the LC-BTMS is far superior to the AC-BTMS for maintaining the batteries in the desired temperature range. However, the LC-BTMS was found to be more complex and heavier than the AC-BTMS. A general comparison of LC-BTMS and AC-BTMS is given in Table 2. Some other studies studied the same comparison and found similar results [65–67].

A summary of different studies on LC-BTMSs for cylindrical LIBs is presented in Table 3.

3.5. Discussion on LC-BTMSs for cylindrical LIBs

Literature review shows that many studies have focused on LC-BTMSs for cylindrical LIBs. The number of these studies has increased substantially in the past few years. The broad objective of most of these studies was to design and optimize an LC-BTMS design for the selected type of cylindrical LIB. Notably, most of the studies have utilized the 18,650 type of LIB because of its easy availability and lower price. Many studies reported the performances of their designs and compared them with the conventional commercially available designs.

The optimization in most of the studies has been reported for both the design and the operational parameters. The design parameters are dependent on the particular studied LC-BTMS design. For CP-based designs, the typical design attributes are the position, number, and dimensions of the CP, as well as the hybridization with other battery jacket channels. Similarly, for the channel-based designs, the typical design attributes are the number, dimensions, position, and contact area of the channel with the battery.

The most studied operational attributes for all the designs are the flow rate, flow direction, inlet HTF temperature, and ambient temperature. Ambient temperature is influenced by the surrounding environment and is determined by the researchers based on the ambient temperature of a specific geographical area. The inlet HTF temperature has also been selected in the range of −10 °C to 30 °C for most of the studies. The performance of the designs had been found to improve with a lower HTF inlet temperature. Many studies have observed the significant effect of the HTF flow rate and flow direction on the LC-BTMS performance. Some studies show that the performance of an LC-BTMS design (in terms of T_{max}) improved with an increase in the HTF flow rate initially and then became almost steady afterward. However, there are also some studies which reported that ΔT did improve significantly with an increase in the flow rate. The HTF flow direction, on the other hand, has a significant effect on T_{max} and ΔT. Many investigations studied the uni-directional, counter-directional, and reciprocating types of flow patterns. The reciprocating flow arrangements were found effective in terms of both T_{max} and ΔT. Fig. 14 presents the comparison of unidirectional and reciprocating flow arrangements. It shows that ΔT and T_{max} for the reciprocating flow scheme are significantly better than the unidirectional scheme at a low flow rate.

Table 2
Comparison of an LC-BTMS and an AC-BTMS (Vita et al. [64]).

LC-BTMS	AC-BTMS
Pro	
Heat transport capacity	Simple design
Temperature uniformity	Lower cost
Better temperature control	No leakage concern
Compact design	
Con	
Weight	Low heat transfer capacity
High cost	Less temperature control
Complex design	More temperature variation in the module
Chances of leakage	Blower noise

Table 3

A summary of previous studies on LC-BTMS designs for cylindrical LIBs (Note: In all studies summarized here, except in [43], a laminar flow model was used).

Ref.	Main objectives	Design and operation parameters						Simulation			Results		
		Battery details	Battery module and BTMS design details	HTF	Discharging rate (C)	Ambient temperature (K)	Flow rate (kg/s, m/s, l/s)	Battery heat generation model	Simulation software	Flow model	ΔT (K)	T_{max} (K)	Others
CP-based LC-BTMS designs													
[31]	To study transient temperature variation in battery modules with BTMS during discharging	18,650 LIB	Cold plate with two compartments at the bottom of cells	Water	1–5	288	0–0.008 kg/s	Bernardi Model	ANSYS Fluent	Laminar flow model	0.35	345	–
[32]	Thermal performance analysis of the designed BTMS	18,650 LIB, 2.6 Ah, 2.8–4.2 V	Honeycomb-shaped module with dual CP and PCM	Water	2–4	298.15–308.15	0.0005–0.002 kg/s	Equivalent Circuit Model (ECM)	ANSYS Fluent	Laminar flow model	5.5	312.7	An increased HTF flow rate suppresses PCM melting.
[33]	Effect of reciprocating flow on performance	18,650 LIB, 2.6 Ah, 2.8–4.2 V	Design with heat pipe, CPs, and mechanism for reciprocating flow	Water	3	298	0.002–0.5 m/s	Bernardi Model	COMSOL	Laminar flow model	2	312	Reciprocating flow was found effective from both uni-directional and cross-directional.
[34]	Thermal performance analysis of the designed BTMS	42,110 $LiFePO_4$battery, 10 Ah capacity	Dual CP with a mini channel-based liquid jacket around each battery	Water	5	298.15	5×10^{-6} –1×10^{-3} kg/s	Bernardi Model	ANSYS Fluent	Laminar flow model	10.8	311.9	Different flow directions in mini-channel-based jacked improved performance.
[35]	Thermal performance analysis of the designed BTMS	18,650 LIB	Single CP at the bottom with a mini channel-based liquid jacket around each battery	Water	5	298.15	5×10^{-5} –2×10^{-3} kg/s	Bernardi Model	–	Laminar flow model	9	311.5	Pressure drops by 5 kPa.
[36]	Thermal performance analysis of the designed BTMS	18,650 LIB	Dual CPs with thermal conductive structure	Water	5	300	1×10^{-5} –2×10^{-3} kg/s	Bernardi Model	ANSYS Fluent	Laminar flow model	4.8	313	Pressure drop increases from 11 Pa to 7.2 kPa with an increase in flow rate.
Channel-based LC-BTMS designs													
[37]	Thermal performance analysis of the designed BTMS	18,650 LIB	Rectangular channel with staggered indents on both sides for cell placement	Water	3	303	3.3×10^{-5} –1.8×10^{-3} l/s	Bernardi Model	ANSYS Fluent	Laminar flow model	4.17	308.74	Parallel flow with alternate directions was found to be most effective.
[38]	Investigation and comparison of designed BTMS with conventional system	18,650 LIB	Gradient channel-based design	Water	0.5–2	298	0.003–0.015 l/s	Bernardi Model	ANSYS Fluent	Laminar flow model	2.5	312	ΔT with the designed system was found to be significantly lower than the conventional system at the same flow rate.
[39]	Use of liquid metal in the designed BTMS	18,650 LIB	An array of cells in conductive resin material with straight micro pipes for HTF	Ga^{80} In^{20}	3–5	298–308	0.05–0.2 m/s	Lumped 3D thermal model	COMSOL	Laminar flow model	3.7	312.4	The system was able to reduce energy consumption by 47 % as compared to water as the HTF.

(continued on next page)

Table 3 (*continued*)

Ref.	Main objectives	Design and operation parameters						Simulation			Results		
		Battery details	Battery module and BTMS design details	HTF	Discharging rate (C)	Ambient temperature (K)	Flow rate (kg/s, m/s, l/s)	Battery heat generation model	Simulation software	Flow model	ΔT (K)	T_{max} (K)	Others
[45]	To study a modified LC-BTMS design for commercial vehicle	18,650 LIB, 2.2 Ah LIBs	A baffle was added to the rectangular flexible HTF channel of the Tesla Model S	Water	5	298.15	0.2 m/s	Pseudo two-dimensional (P2D) thermal model	COMSOL	Laminar flow model	4.83	303.86	Pressure drop increases from 233 Pa to 295 kPa with the implementation of a baffle.
[47]	Thermal performance of a full-scale battery pack	18,650 LIB, 3.65 V, 2.75 Ah	Rectangular flexible channel with six mini-channels	H_2O (47 %) – 2 (CH_2OH) (53 %)	0.5–2	298	0.3–0.6 l/s	Bernardi Model	ANSYS	Laminar flow model	11	312	
[48]	Thermal performance of a flexible Swiss-roll type LC-BTMS	18,650 LIB, 3.65 V, 2.5 Ah	Rectangular channel-based LC-BTMS in the shape of a Swiss roll	Water	3	298	6×10^{-4} –4.5×10^{-3} kg/s	Bernardi Model	–	–	3.3	300.4	The performance of the designed system was superior to the conventional serpentine channel.
[52]	Comparison of the thermal performance of two separate designs	18,650 LIB, 3.6 V	Block-based designs	Water	5	298	1×10^{-5} –5×10^{-4} kg/s	Bernardi Model	ANSYS Fluent	Laminar flow model	3.05	310.26	The performance of one design was superior but uneconomical.
[53]	Optimization of the compactness of the battery module	Length; 200 mm, Dia; 55 mm, 30 Ah	A rectangular nano-enhanced metal block with an array of holes for cells and HTF tubes	50/50 propylene glycol water	11	313	0.05 l/s	Bernardi Model	ANSYS Fluent	Laminar flow model	–	360.5 (Cell core temp.)	The peak cell core temperature was found to decrease with increased cell-to-cell spacing.
Direct contact type LC-BTMS designs													
[56]	Thermal performance analysis of the designed BTMS	Samsung INR18650–30Q Lithium-Ion cell	Rectangular duct with battery casings and connections	Water	0.5–5	298	0.01 m/s	Constant heat generation	ANSYS Fluent	Laminar flow model	2.89	300.95	Flow direction plays a significant role in the cooling of particular cells in battery packs.
[57]	Thermal performance analysis of the designed BTMS	18,650 LIB	Rectangular channel with multi-pass for HTF	Water + AgO nano-HTF	0.5–4	296–298	0.2–0.28 m/s	Bernardi Model	ANSYS Fluent	Laminar flow model	1.04	308.03	Nano-enhanced HTF improves thermal performance but increases pressure drop.
Hybridization with AC-BTMS													
[61]	Thermal performance analysis of the designed BTMS	18,650 LIB, 2 Ah, 4.2 V	Metallic blocks with HTF channels and cross-air flow	Water + Air	3	298	0.0005–0.0035 kg/s	Bernardi Model	ANSYS Fluent	Laminar flow model	1.53	307.41	Air cooling lowers T_{max} by 3.75 °C and ΔT by 0.96 °C, respectively.
[62]	Thermal performance analysis of the designed BTMS	18,650 LIB, 1.25 Ah	Corrugated type channel for liquid HTF and air on the outer surface	Water + Air	4	298	0.001–0.005 kg/s (water); 0–1.5 m/s (air)	Bernardi Model	COMSOL	Laminar flow model	4.15	303.6	It was suggested to keep air velocity below 0.4 m/s to achieve efficiency
[63]	Thermal performance analysis of the designed BTMS	21,700 LIB, 5 A, 3.7 V	Zig-zag plate-based cooling structures and HTF channel	Water + Air	1.25	286	2.5 m/s (Water); 1.5 m/s (air)	Constant heat generation	–	Laminar flow model	1.4	308	The hybrid system cooled 28 % better than the standalone system.

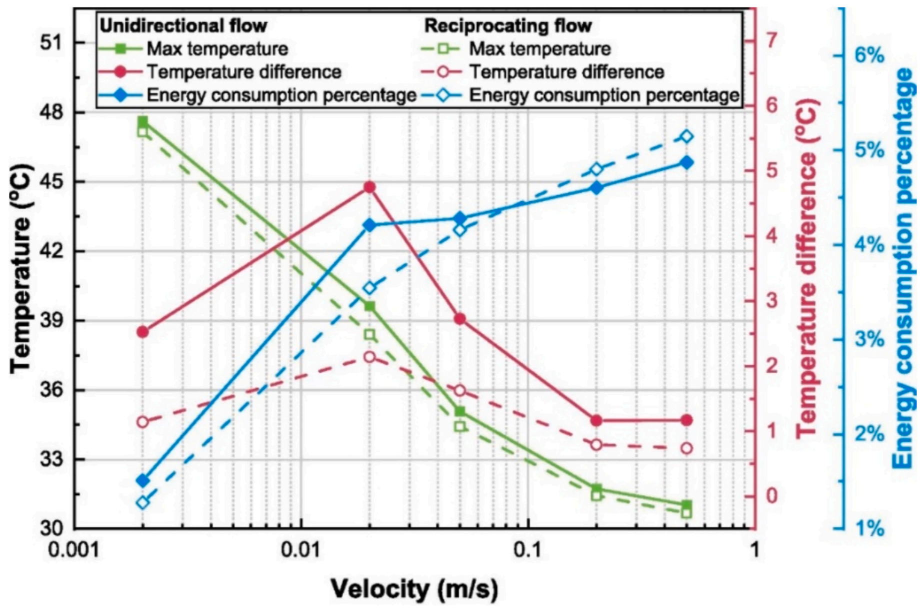

Fig. 14. Comparison of cooling performance of LC-BTMS with different flow schemes (obtained with permission from Zeng et al. [33]).

Fig. 15 represents the types of HTF used by different studies considered in the present review. The chart advocates that pure water has been widely used as the HTF in most of the studies. This is due to the good thermo-physical properties of water and less pumping power requirements. Notably, the studies that used the HTF temperature below 0 °C had used a mixture of water and EG. This is because of the lower freezing point of the mix. Moreover, the use of nanoparticles in water has also been reported by some studies. It has been found that the performance was improved substantially with the use of conductive nanoparticles on the cost of large pumping power requirements. Some studies also reported the use of liquid metal as HTFs and reported high performance of the systems. However, the other economic, health, and environmental aspects of liquid metals as HTFs in EVs have not been reported.

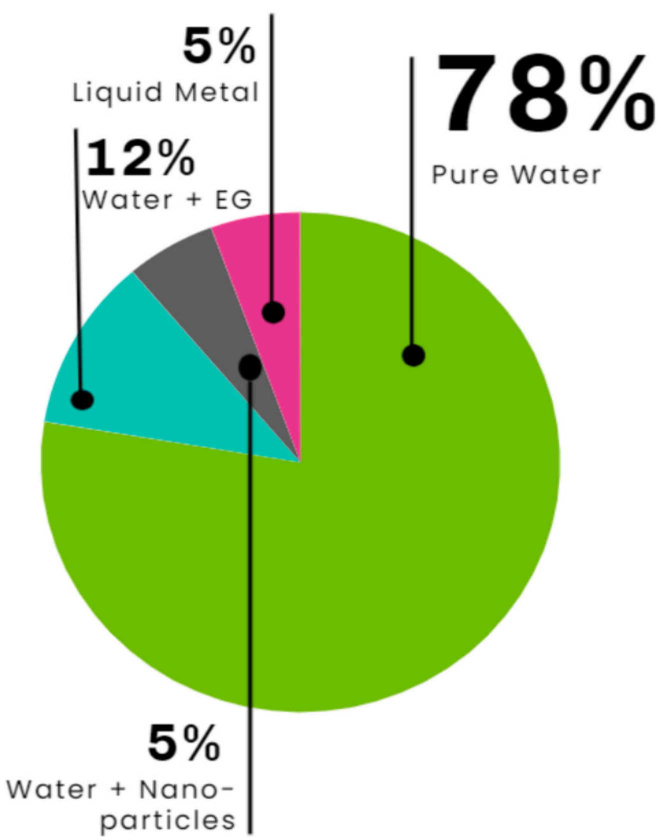

Fig. 15. Pie chart showing the HTF types reported in the selected LC-BTMS investigations for cylindrical LIBs.

3.5.1. Comparative analysis of LC-BTMSs for cylindrical LIBs

A comparative analysis is carried out here to evaluate the performance of different designs of LC-BTMSs for cylindrical LIBs based on the design and operational parameters. Some of the studies from each design of LC-BTMS for cylindrical LIBs were identified and compared with the available quantitative data. The effects of different operational and design parameters on the performance of LC-BTMS is discussed in detail below.

3.5.1.1. Effect of design parameters. The design of an LC-BTMS plays a significant role in its performance. Researchers have tried different designs of LC-BTMSs for cylindrical LIBs. Commonly, these designs are categorized as cooling plate-based designs, channel-based designs, direct contact type designs, and other hybrid designs. Fig. 16 shows the comparative analysis of these different designs of LC-BTMSs for cylindrical LIBs. Although many design parameters can be identified for these designs of LC-BTMSs, two prominent design parameters have been selected for this comparison, namely, the capacity of the battery module and the relative heat transfer area.

The capacity of the battery module (in Ah) is directly proportional to the heat generation rate. If the capacity of the battery module is large, i.e., more numbers of LIBs in the module, the heat generation rate will be high. The capacity of the battery module was identified for each study by multiplying the capacity of each LIB by the number of LIBs in the considered design.

Fig. 16 shows that the average module capacity for most of the considered cases is between the range of 30–150 Ah, and the mean value is around 60 Ah. The performance of the different designs has been comparatively evaluated by considering attributes like T_{max}, ΔT, and pressure drop. For any suitable design, all the considered performance parameters should be as low as possible. The figure clearly depicts that most of the performance parameters are directly proportional to the capacity of the battery module. Ideally, the number of joints should be as

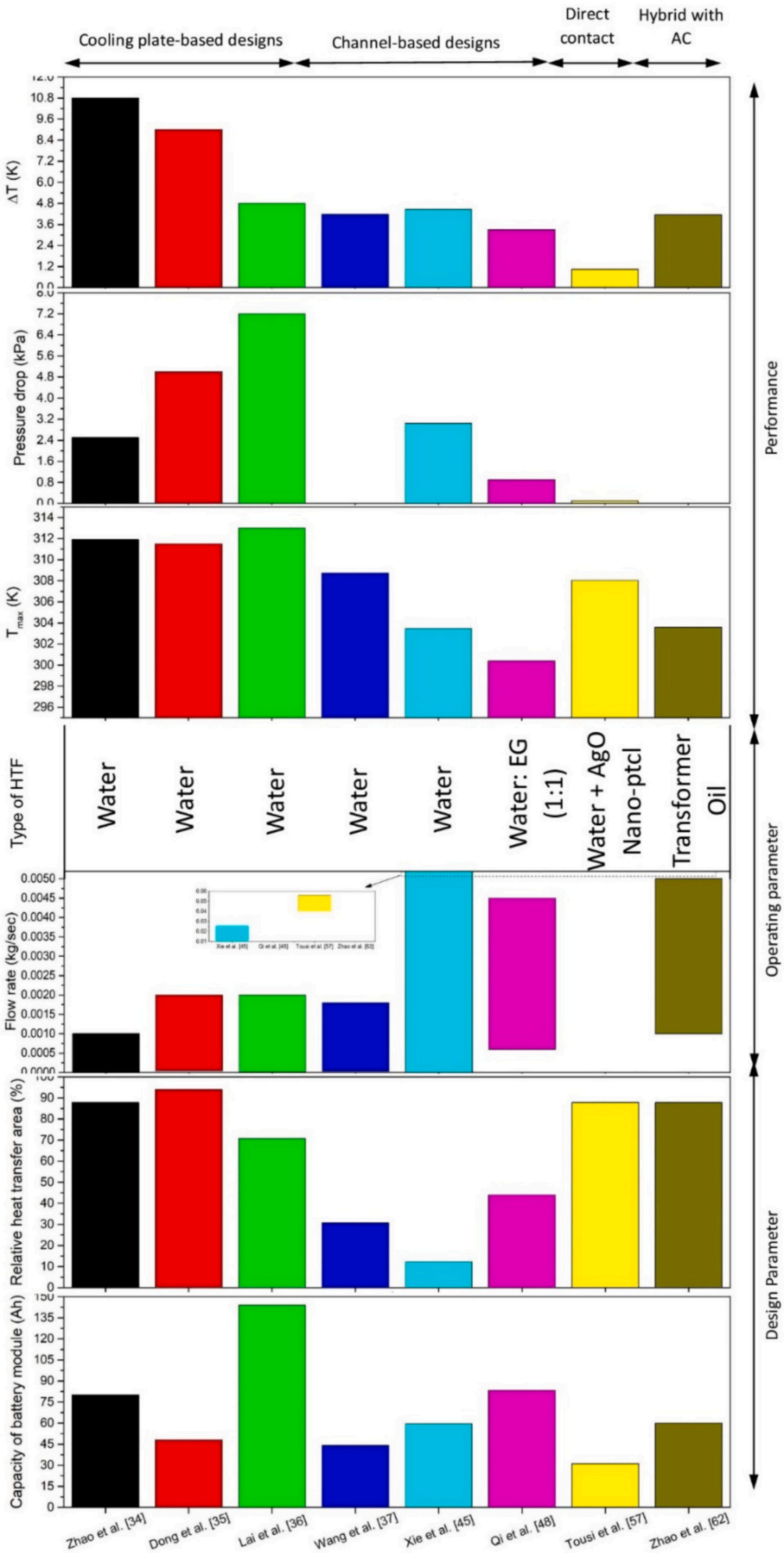

Fig. 16. Comparative analysis of different LC-BTMS designs for cylindrical LIBs.

small as possible in a battery pack of EVs, which can be achieved by increasing the module size. Therefore, the optimization of battery module size is necessary.

Another considered design parameter is the relative heat transfer area (in %). This parameter has been evaluated by the ratio of the heat transfer area for a single LIB to the total surface area of the considered LIB. This parameter can help us identify how effective a particular LC-BTMS design is. Most of the CP-based LC-BTMS designs have cylindrical jackets for the individual LIBs; therefore, the relative heat transfer area for these designs is high. Similarly, the direct contact type and hybrid designs also have high relative heat transfer areas. On the other hand, the channel-based designs have comparatively less relative heat transfer areas. Ideally, the performance of the designs with less relative heat transfer area should be low as compared to the designs with high relative heat transfer area. However, Fig. 16 shows that no such sharp variations were observed. Even the design having a relative heat transfer area of about 15 % and a module capacity of 59.4 Ah has better performance than the designs with similar module capacities and higher relative heat transfer areas. This trend may be attributed to the supremacy of other operational parameters, which have been discussed in the following sub-section. Remarkably, the higher value of the relative heat transfer area is also linked with the complexity of the design of the LC-BTMS. Complex designs generally have higher manufacturing costs. Therefore, the cost optimization of the LC-BTMS design can be achieved by optimizing the relative heat transfer area for a particular design.

3.5.1.2. Effect of operational parameters. The operational parameters also significantly affect the performance of an LC-BTMS design. In this comparative analysis, three such operational parameters are considered: discharge rate, HTF type, and HTF flow rate. To justify the comparison, only studies which have almost similar discharge rates have been selected.

The discharge rate range has been chosen in the range of 4 to 5C. The direction of the HTF flow is another parameter that significantly affects the performance of the system. However, no studies have been considered from the alternating HTF flow direction in this comparison because of significant dissimilarities.

The types of HTF for the selected studies can be seen in Fig. 16. For most of the studies, water has been used as the HTF. Few studies have used other alternatives like water and EG mixture (1:1), nano-enhanced HTF, and transformer oil. HTFs with better thermo-physical properties are most suitable for LC-BTMSs. The comparative analysis also shows that comparatively better performance was observed for the studies with unconventional HTFs than the conventional HTFs in terms of ΔT and T_{max}. The lowest values of ΔT and T_{max} were observed in the studies with unconventional HTFs. From an economic viewpoint, the cost of unconventional HTFs is more than that of conventional HTFs. Therefore, optimization of the HTF selection should be carried out by considering both performance and economic prospects.

HTF flow rate is another parameter that directly affects the system's performance and operational cost. Generally, the HTF flow rate is directly proportional to the system's performance and operating costs. Therefore, the optimization of the HTF flow rate is a crucial parameter in many studies. Fig. 16 shows that the HTF flow rates for the CP-based BTMS designs are in the range of 1×10^{-5} to 2×10^{-3} kg/s. Therefore, T_{max} and ΔT for these designs are comparatively higher. Moreover, the friction factor, which defines the pressure drop, is inversely proportional to the flow rate. Therefore, the pressure drops for CP-based BTMS designs have also been found to be comparatively significant. For the channel-based and hybrid designs, the flow range is 5×10^{-4} to 2×10^{-2} kg/s. Therefore, the performance of these designs is significantly better than that of the other designs. The direct contact type BTMS designs have studied the highest range of the HTF flow rate, i.e., 0.04 to 0.056 kg/s. A higher flow rate requires high and constant pumping power, which increases the operating cost of the system. Therefore, optimization of the flow rate is crucial for the effective design of an LC-BTMS.

3.5.2. Details of numerical simulation

From the literature on LC-BTMS for cylindrical LIBs, it is noted that the majority of the research work has studied the performance and optimization of LC-BTMS designs through numerical simulation. The numerical method involves the simulation of the battery as a heat source and flowing HTF for heat transfer and fluid mechanics. Several commercial CFD software are available to model LC-BTMSs. It was observed that ANSYS Fluent and COMSOL were the software packages that were most often employed in the investigations. These two CFD applications are fully outfitted to simulate any LC-BTMS design with meticulous detail. Battery heat generation models are used to simulate the LIBs in any CFD package. To date, many battery heat generation models have been developed by considering various parameters. However, most of the reported studies on LC-BTMS have utilized only a few battery heat generation models, namely, the Bernardi model [68,69], equivalent circuit model (ECM) [70,71], pseudo-2-dimensional (P2M) model [72,73], etc. A detailed description of these battery heat generation models is presented subsequently.

3.5.2.1. Bernardi battery heat generation model. The Bernardi equation model is one of the most uncomplicated and most utilized battery heat generation models in the literature. Basically, the Bernardi equation for estimating the battery heat generation rate is based on the energy balance. It means that the total heat generation within the battery during discharging is the summation of reversible and irreversible heat generation. The heat generation within the battery due to a change in entropy is regarded as the reversible component, while the Joule heating is the irreversible component. The Bernardi equation is as follows [74],

$$Q_{gen} = Q_{irr.} + Q_{rev.} = \frac{I}{V_{bat.}}(U_{OC} - U) + \frac{I}{V_{bat.}}T\frac{dU_{OC}}{dT}$$

or

$$Q_{gen} = \frac{I}{V_{bat.}}\left(IR_{int.} + T\frac{dU_{OC}}{dT}\right) \tag{1}$$

where Q_{gen} is the heat generation rate of the battery, $Q_{rev.}$ and $Q_{irr.}$ are the reversible and irreversible heat generation, I is the discharge current of the battery, $V_{bat.}$ is the volume of the battery, U is the battery terminal voltage, U_{OC} is the battery open circuit voltage, dU_{OC}/dT is the thermal entropy coefficient of the battery, T is the temperature, and $R_{int.}$ is the internal resistance of the battery, respectively. For the battery simulation using the Bernardi Model, $R_{int.}$ dU_{OC}/dT are evaluated experimentally at different C-rates and state of charge (*SoC*) using a hybrid pulse power characterization (HPPC) test. The *SoC* is a function of the nominal capacity of the battery and the discharging/charging time, which is calculated by the following equation,

$$SoC = SoC_{t=0} - \frac{1}{Cap.}\int I(t).dt \tag{2}$$

where $SoC_{t=0}$ represents the initial value of *SoC*, *Cap.* represents the nominal capacity of the battery, and t is time, respectively. As a general practice, correlations are developed for both $R_{int.}$ and dU_{OC}/dT in terms of *SoC*. After that, a user-defined function (UDF) is written for the battery heat generation rate using the equation and complies with the simulation software. The correlations for $R_{int.}$ in many studies have developed as a function of SoC and temperature. The developed correlations for $R_{int.}$ and dU_{OC}/dT from some studies are given in Table 4.

3.5.2.2. Equivalent circuit model (ECM). In the equivalent circuit model, the battery is mimicked as an electric circuit. The heat generation in this pseudo-electric circuit due to a change in potential is regarded as the

Table 4
Correlations developed for the $R_{int.}$ and dU_{OC}/dT in various studies.

Ref.	Correlations
Lai et al. [36]	$R_{int.} = \begin{cases} 992.SoC^6 - 3406.SoC^5 + 4667.SoC^4 - 3263.SoC^3 + 1225.SoC^2 - 233.SoC + 48, T = 60^\circ C \\ 1559.SoC^6 - 5374.SoC^5 + 7367.SoC^4 - 5121.SoC^3 + 1898.SoC^2 - 355.SoC + 58, T = 50^\circ C \\ 1559.SoC^6 - 5365.SoC^5 + 7378.SoC^4 - 5181.SoC^3 + 1962.SoC^2 - 382.SoC + 66, T = 40^\circ C \\ 2989.SoC^6 - 10480.SoC^5 + 14700.SoC^4 - 10514.SoC^3 + 4036.SoC^2 - 793.SoC + 107, T = 30^\circ C \\ 4301.SoC^6 - 15496.SoC^5 + 22391.SoC^4 - 16531.SoC^3 + 6559.SoC^2 - 1334.SoC + 166, T = 20^\circ C \end{cases}$
	$\frac{dU_{OC}}{dT} = 0.355 + 2.154.SoC - 2.869.SoC^2 + 1.028.SoC^3$
Wang et al. [37]	$R_{int.} = 0.0852 + 0.00623\ sin\ \frac{\pi.(SoC - 0.23727)}{0.18}$
	$\frac{dU_{OC}}{dT} = 3.18467 - 62.787.SoC + 425.05.SoC^2 - 1330.74.SoC^3 - 2134.38.SoC^4 - 1701.34.SoC^5 - 533.88.SoC^6$
Huang et al. [31]	$R_{int.} = \frac{141.19 - 20.66.SoC - 4.167.T + 0.09886.T^2 - 7.211 \times 10^{-4}.T^3}{1 - 1.1684.SoC + 3.7948.SoC^2 - 4.181.SoC^3 + 0.00993.T + 2.65 \times 10^{-4}.T^2}$
	$\frac{dU_{OC}}{dT} = 2.74 - 9.75.SoC - 8.27.SoC^2 + 75.15.SoC^3 - 102.6.SoC^4 + 42.969.SoC^5$
Zhou et al. [51]	$U_{OC} = 4.17 - 0.0151.DoD + 0.00121.DoD^2 - 6.96 \times 10^{-5}.DoD^3 + 1.85 \times 10^{-6}.DoD^4 - 2.58 \times 10^{-8}.DoD^5 + 1.82 \times 10^{-10}.DoD^6 - 5.15 \times 10^{-13}.DoD^7$
	$U = 3.78 - 0.0302.DoD + 0.00206.DoD^2 - 8.77 \times 10^{-5}.DoD^3 + 1.96 \times 10^{-6}.DoD^4 - 2.38 \times 10^{-8}.DoD^5 + 1.48 \times 10^{-10}.DoD^6 - 3.73 \times 10^{-13}.DoD^7$
	$\frac{\partial U_{OC}}{\partial T} = 0.651 - 6.61.DoD + 59.4.DoD^2 - 198.DoD^3 + 286.DoD^4 - 156.DoD^5 - 17.3.DoD^6 + 32.1.DoD^7$
	where, $DoD = 1 - SoC$ $(100\% = Empty; 0\% = Full)$

heat generation rate of the battery. The schematic for the pseudo-electric circuit is given in Fig. 17. The irreversible heat generation in the battery is given as,

$$Q_{irr.} = I^2R_o + I(V_{RC1} + V_{RC2} \cdots + V_{RCn}) \tag{3}$$

in which R_0 is the Internal ohmic resistance, and V_{RCi} are dynamic overpotentials which are calculated as follows,

$$V_{RCi} = \int_0^t \left(\frac{I}{C_i} - \frac{V_{R_iC_i}}{R_iC_i}\right)dt, i = 1, 2, 3 \ldots n \tag{4}$$

where Ri is the pair resistance and C_i is the RC pair capacitance, respectively.

The estimation of the parameters like R_0, R_1, R_2, etc., is done using the HPPC test. Some studies have considered this model as the battery heat generation model in numerical simulations. The estimated values of parameters for a second-order ECM by Yang et al. [32] are shown in Fig. 18. Similarly, the identified values for a third-order ECM are given in Table 5. These parameters were utilized to evaluate the heat generation rate in the LIBs. For more detailed information about the computation and implementation of the ECM model, readers are referred to the supplementary data provided by Baveja et al. [75].

3.5.2.3. P2D model. The P2D model is considered the most complex and accurate model for simulated heat generation rate in LIBs. This model finds the energy, mass, and charge balance together. Firstly, the structure of a LIB is defined. Generally, it consists of five layers, as shown in Fig. 19. Positive and negative current collectors are considered as the solid materials whereas the separator, positive and negative electrodes are considered porous solid matrices and immersed in an electrolyte. Afterwards, the energy, mass, and charge balance are applied to the LIB. A brief detail about the model is given below.

Conservation of Mass:

$$\text{Solid Phase}: \frac{\partial C_S}{\partial t} = \frac{D_S}{r^2}\frac{\partial}{\partial r}\left(r^2\frac{\partial C_S}{\partial r}\right) \tag{5}$$

$$\text{Liquid Phase}: \varepsilon_L\frac{\partial C_L}{\partial t} = D_L^{eff}\frac{\partial^2 C_L}{\partial x^2} + \frac{(1 - t_+^0)}{F}j \tag{6}$$

Conservation of Charge:

$$\text{Solid Phase}: \delta^{eff}\frac{\partial^2 \varphi_S}{\partial x^2} = i_S \tag{7}$$

$$\text{Liquid Phase}: \nabla\varphi_L = -\frac{i_L}{\varphi_L^{eff}} + \frac{2RT}{F}(1 - t_+^0)\left(1 + \frac{d\ lnf_+}{d\ lnc_L}\right)\nabla ln\ c_L \tag{8}$$

Conservation of Energy:

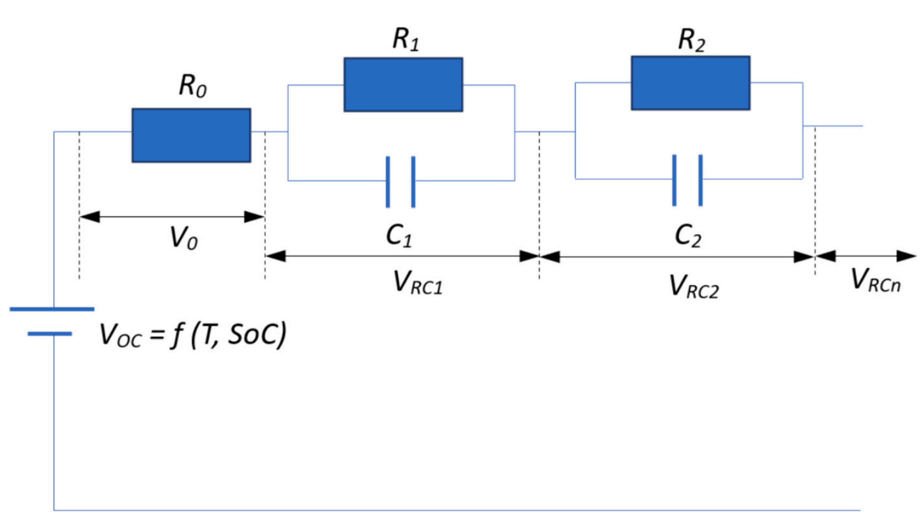

Fig. 17. Multi-order ECM for the LIBs.

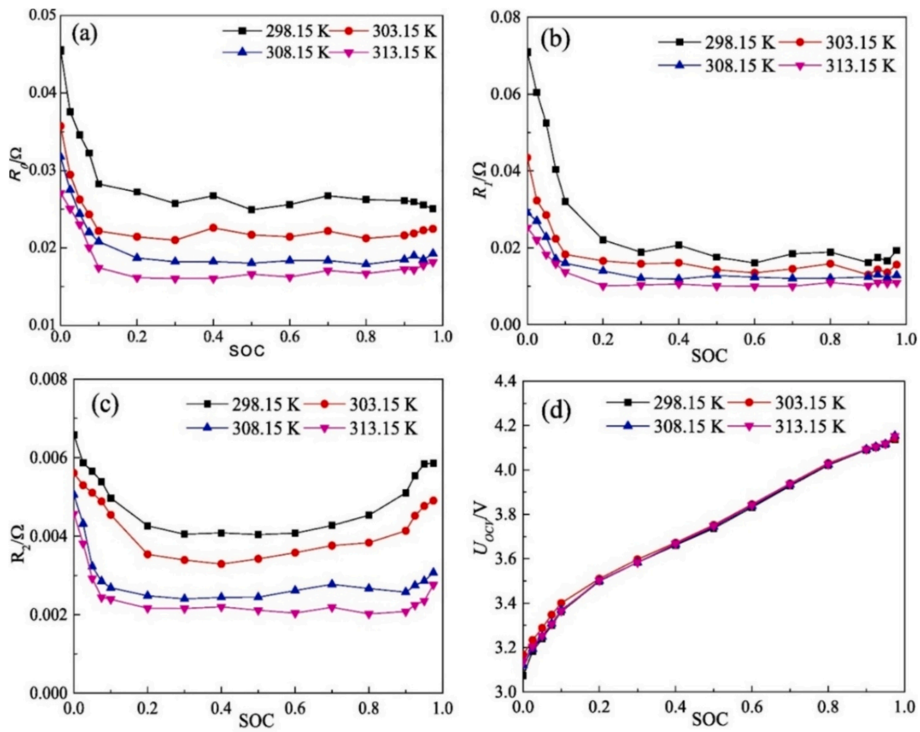

Fig. 18. Estimated values of parameters for second-order ECM (Obtained with permission from Yang et al. [32]).

Table 5
Estimated values of parameters by Baveja et al. [75] at 25.5 °C for third-order ECM.

SoC	U_{OC}	R_0	R_1	R_2	R_3	τ_1	τ_2	τ_3
0	3.296	0.003	0.002	0.0015	0.001	10	150	1500
0.1	3.5999	0.5279	0.0028	0.0015	0.001	14.182	153.59	1486.408
0.2	3.20006	0.07691	0.00221	0.00373	0.00112	16.1987	198.687	1040.745
0.3	3.25405	0.09051	0.0021	0.00198	0.00153	8.9301	184.685	1202.766
0.4	3.27307	0.089	0.0026	0.00263	0.00195	9.60397	189.286	1201.888
0.5	3.2836	0.08609	0.00206	0.00252	0.00229	13.2178	147.267	1200
0.6	3.28748	0.07968	0.00217	0.00412	0.00172	9.85578	141.657	544.126
0.7	3.29234	0.076	0.00213	0.00188	0.0001	9.09792	199.806	1441.04
0.8	3.27108	0.0304	0.00233	0.00208	0.00125	8.23996	172.849	1550.81
0.9	3.296	0.00299	0.00221	0.0015	0.001001	9.343754	150	1455.727
1	3.296	0.003	0.002	0.0015	0.001	10	150	1500

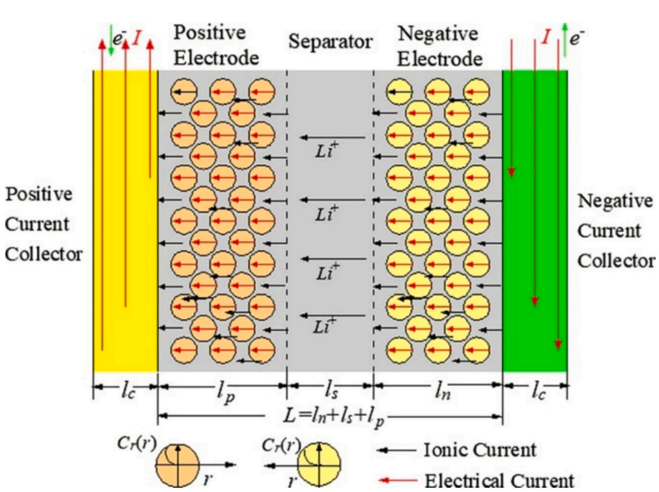

Fig. 19. Structure of LIB for the P2D model (Obtained with permission from Xie et al. [45]).

$$\frac{\partial}{\partial t}(\rho C_p T) - k\nabla^2 T = Q_{RX} + Q_{pol.} + Q_{ohm.} \tag{9}$$

$$Q_{pol.} = A_s \rho_i \eta_{pol.} \tag{10}$$

$$Q_{RX} = A_s \rho_i \frac{\partial U_{OC}}{\partial T} \tag{11}$$

$$Q_{ohm.} = -\left(i_L \left(\frac{\partial \varphi_L}{\partial x} \right) + i_S \left(\frac{\partial \varphi_S}{\partial x} \right) \right) \tag{12}$$

These equations are solved in the computational domain to obtain the heat generation rate of the LIBs. More details about the parameters of LIB related to the P2D model (including the definitions of the various symbols in the above equations) can be found in Xie et al. [45].

3.5.3. Battery heat generation model selection for numerical simulation

One of the most important decisions to make during the numerical simulation of a LC-BTMS is selecting a specific battery heat generation model. Almost all of the chosen studies have used experimental or published data to verify their battery heat generation model. As a result, it is difficult to recommend a model for a particular situation. Herrera et al. [76] comparatively investigated the different battery heat generation models for both constant discharge rates and highway fuel economy test (HWFET)-driving cycle. It is noteworthy that this research used the terms “Lumped Model” and “3D-CFD” to refer to the Bernardi and P2D models, respectively. The comparison's findings are shown in Fig. 20, which demonstrates that all models can roughly represent the rate at which heat generated in batteries is in line with experimental findings. The NTGK model yielded the highest divergence at a discharge rate of 1.5C. On the other hand, every model executed the HWFET driving cycle with the same precision. As a result, depending on the computing facility's simulation capacity, any model may be used for the battery heat production rate simulations.

4. LC-BTMS designs for prismatic LIBs

Similar to that for cylindrical LIBs, various designs of LC-BTMSs for prismatic LIBs have also been extensively studied, as summarized in Table 6. In most of the LC-BTMS designs for prismatic LIB, cold plates (CPs) have been used. This is because of the cartesian geometry of the LIB, the leak-proof nature of the CPs, and the safe operation of the CPs. The further classification of the LC-BTMS designs for prismatic LIBs is based on the design of the HTF channel in the CPs.

4.1. LC-BTMS designs with straight HTF channels in the CP

The most conventional LC-BTMS design for a prismatic LIB is one with a straight HTF channel in the CP. The flow through these channels in three different flow directions, i.e., parallel, series, and reciprocating, have been studied. Many studies have reported the utilization of the CP with straight HTF channels for EV battery packs. Zhang et al. [77] numerically investigated the thermal performance of an LC-BTMS for a battery pack with 24 prismatic battery cells of dimensions of 140 mm × 70 mm × 7 mm, as shown in Fig. 21(a). The NTGK MSMD battery model was used to quantify the heat generation within the battery. The cold plates had vertical parallel liquid channels inserted between the batteries. The effects of the fluid flow rate and temperature were investigated. They reported that at a 5C discharge rate, the designed system was able to maintain T_{max} and ΔT at 40 °C and 5 °C, respectively.

Wang et al. [78] conducted a numerical investigation to evaluate the cooling performance of a mini-channel-based LC-BTMS. The schematic of the studied design is shown in Fig. 21(b). The effects of the CP width, mini-channel interval, and mass flow rate were investigated. The optimum values for these parameters were found to be 90 mm, 4 mm, and 80 g/s, respectively. T_{max} and ΔT for the optimum set of the parameters were found to be 301.57 K and 3.10 K, respectively. Duan et al. [79] studied a CP-based LC-BTMS with parallel liquid channels in the CP, as shown in Fig. 21(c). The system was optimized for channel height and HTF flow rate. Results revealed that the effect of thermal contact resistance between the CP and battery is significant and needs to be considered. Additionally, the impact of the HTF flow rate was found to be more substantial than that of the channel height, and the energy consumption could be reduced by up to 80 % with the optimum strategy compared to the constant HTF flow rate.

Guo et al. [80] carried out a numerical investigation to evaluate the thermal performance of a mini-channels direct-contact type LC-BTMS, as shown in Fig. 21(d). Different configurations of the system were comparatively studied, and the optimization of the most effective configuration was carried out using a multi-criteria decision-making technique, Non-dominated Sorting Genetic Algorithm II (NSGA-II). The results showed that the optimized design kept the battery's T_{max} and ΔT below 36 °C and 0.65 °C, respectively, at a 3C discharging rate. Xia et al. [81] investigated the performance of a CP-based LC-BTMS with an improved channel design, as shown in Fig. 21(e). The designed system's performance was tested for an entire battery pack of an EV and compared with the commercially available LC-BTMS. Results of the study revealed that the battery pack with the designed LC-BTMS had T_{max} and ΔT of 1 °C and 2 °C, respectively, lower than that of the commercially available LC-BTMS. Shang et al. [82] numerically investigated the effect of different designs and operational parameters of CP-based LC-BTMS with embedded liquid channels placed at the bottom of the prismatic battery cells. Effects of the HTF inlet temperature, HTF flow rate, and CP width were investigated. It was found that the battery's T_{max} is directly proportional to the HTF inlet temperature but inversely proportional to the CP width. When the input temperature is 18 °C, the CP width is 70 mm, and the mass flow rate is 0.21 kg/s, the optimum cooling performance is achieved. Yang et al. [83] conducted a numerical study to evaluate the thermal performance of a taper-type manifold-based LC-BTMS. The performance of the system was compared with the conventional rectangular-type manifold-based LC-BTMS, and it was found that the developed system was able to maintain T_{max} and ΔT of the battery in the effective range with 86.3 % less power consumption than the conventional design.

Jiaqiang et al. [84] carried out a numerical investigation to evaluate the thermal performance of an LC-BTMS consisting of prismatic batteries, HTF channel, and CP. The effects of the HTF flow rate, cooling channel height, width, and number were investigated. An orthogonal matrix with 16 alternatives was designed, and the impact of different parameters was evaluated. They reported that the most significant parameters were the HTF flow rate and number of cooling channels, whereas the cooling channel height and width had a trivial effect on the thermal performance of the LC-BTMS. Mei et al. [85] conducted a numerical investigation to evaluate the cooling performance of an LC-BTMS with the CP along with flat heat pipes inserted between the consecutive cells. The effect of the designed system was analyzed using different discharging rates and HTF flow rates. The results showed that the developed system was able to maintain T_{max} and ΔT of the battery module within the suitable range. Lan et al. [86] conducted a numerical investigation to evaluate the thermal performance of a mini-channel-based LC-BTMS in which aluminum tubes having 4 and 8 channels were wrapped around the prismatic batteries for thermal management. Four different configurations of tubes, one tube with four channels

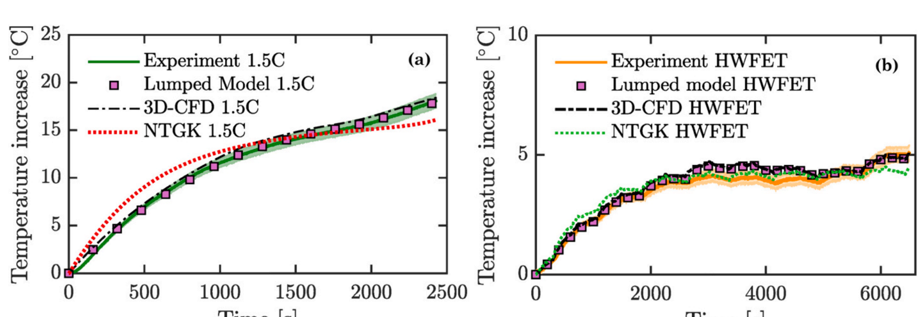

Fig. 20. Comparison of different battery heat generation models with experimental results under (a) 1.5C discharge rate and (b) HWFET drive cycle discharge rate [76].

Table 6
A summary of past studies on LC-BTMS designs for prismatic LIBs.

Ref.	Main objective	Design and Operation Parameters						Simulation			Results		
		Battery details	Battery module and BTMS design details	HTF	Discharging rate (C)	Ambient temperature (K)	Flow rate (kg/s, m/s, l/s)	Battery heat generation model	Simulation software	Flow model	ΔT (K)	T_{max} (K)	Others
CP with straight HTF channels													
[77]	Thermal performance analysis of the designed system	140 × 70 × 7 mm, 3.2 V, 5 Ah	Array of prismatic cells with CPs inserted in between	Water	5	283–303	0.1–2 m/s	NTGK	ANSYS Fluent	k-ε turbulence model	5	308	Under external shorting conditions, T_{max} rises to 50 °C.
[78]	Use of a novel battery model for the designed LC-BTMS	115 × 100 × 10 mm, 3.6 V, 10 Ah	LIBs are arranged in rows and placed over CP.	Water	1–5	298.15	0.022–0.08 kg/s	1D electrochemical and 3D simplified models	–	Standard k-ε turbulence model	3.1	301.57	T_{max} and ΔT can further be reduced by 4.9 % and 9.2 %, respectively, with the use of aluminum fins in between the LIBs.
[79]	Performance investigation of the designed LC-BTMS	207 × 157 × 7 mm LIBs	Array of prismatic cells with CPs inserted in between	Water	1–4	298	0.0005–0.01 kg/s	Bernardi Model	ANSYS Fluent	Laminar flow model	5	313	A control strategy was developed based on flow rate variation to maintain the module temperature in the desired range.
[81]	Designed the system's thermal performance analysis	CATL PHEV-2, Fujian, China	Commercial prismatic battery module (CATL HJL, Fujian, China)	–	–	305	0.1 l/s	Bernardi Model	–	k-ε Turbulence Model	2.5	312.7	The improvement in the flow channel design improved the thermal performance of the system.
[82]	Optimization of the designed LC-BTMS	230 × 175 × 73 mm, 3.7 V, 49 Ah	LIBs are arranged in rows and placed over CP.	A mixture of water and EG	–	303	0.17–0.29 kg/s	Bernardi Model	–	–	4.5	312.65	HTF inlet temperature varied between 15 and 24 °C, and the optimum value was found at 18 °C.
[86]	Designed LC-BTMS's optimization	173 × 168 × 39 mm, 3.7 V, 55 Ah	The LIBs with a jacket of CP	Water	1–2	300	0.0033–0.0167 l/s	Constant heat generation	COMSOL	Laminar flow model	1.26	301.27	The mini-channel cooling jacket was found to be significantly effective
[87]	Thermal analysis of silica-based CPs for LC-BTMS	152 × 120 × 22 mm, 20 Ah	Silica-based CPs attached on both sides of prismatic LIB	Water	5	303	0.1–0.4 m/s	Constant heat generation	COMSOL	Laminar flow model	–	315	The flow direction had an insignificant role with a single battery system.

(*continued on next page*)

Table 6 (*continued*)

Ref.	Main objective	Design and Operation Parameters						Simulation			Results		
		Battery details	Battery module and BTMS design details	HTF	Discharging rate (C)	Ambient temperature (K)	Flow rate (kg/s, m/s, l/s)	Battery heat generation model	Simulation software	Flow model	ΔT (K)	T_{max} (K)	Others
[91]	Effect of different flow paths on the performance of the system	148 × 97 × 27 mm, 3.6 V, 38 Ah	LIBs are arranged in rows and placed over CP.	Water	1–2	298	0.21–0.29 kg/s	Constant heat generation	–	k-ε turbulence model	9.65	308.68	The inlet and exit should be in the center of the first and second collecting mains for maximum heat dissipation.
[92]	Effect of reciprocating flow pattern on the thermal performance	148 × 91 × 40 mm, 3.75 V, 70 Ah	LIBs arranged in rows and placed over CP and reciprocating flow mechanism	1:1 EG: water	–	293–315	0.0083–0.083 l/s	Equivalent circuit model	–	–	0.3	316	The reciprocating system's HTF flow rate is 11.5 % of the unidirectional flow BTMS under the same thermal performance.
[93]	Thermal performance analysis of the system with supercritical CO_2 as HTF	300 × 225 × 24.5 mm, 3.7 V, 100 Ah	CP was placed over the top of the LIB	Supercritical CO_2	1–5	304.79–314.76	0.00014 kg/s	Bernardi Model	ANSYS Fluent	Turbulence model	–	308	The T_{max} rise in the module can be reduced by 36.26 % with the use of supercritical CO_2 as compared to water as HTF.
[95]	Performance analysis of the system with the nano-enhanced HTF	100 × 180 × 14 mm, 3.7 V, 45 Ah	Array of prismatic cells with CPs inserted in between	(Water, EG, Engine oil) + 2 % - 5 % Al_2O_3 nanoparticles	1–3	298.15	4.46 × 10^{-3} l/s	Bernardi Model	ANSYS Fluent	Laminar flow model	9.48	25.02 (Temperature rise)	The addition of nanoparticles significantly reduces T_{max} but has an insignificant effect on the ΔT
CP with serpentine HTF channels													
[99]	Optimization of the designed LC-BTMS	Rechargeable LIB TLP80A5E6-50 Ah	Array of prismatic cells with CPs inserted in between	Water	0.8	296	0.3 m/s	Constant heat generation	Ansys Fluent	Laminar flow model	13.1	308.6	The pressure drop in the designed system decreased by 13.28 % after the optimization of design parameters.
[100]	Designed LC-BTMS's optimization	194 × 91 × 8.5 mm, 17.5 Ah	LIBs arranged in rows, placed over CP, and fins attached in-between LIBs	Water	0.5–2	298	0.4 m/s	Bernardi Model	Ansys Fluent	Laminar flow model	6.9	304.9	The alternate flow direction of HTF in consecutive liquid plates can significantly improve the performance.

(*continued on next page*)

Table 6 (*continued*)

Ref.	Main objective	Design and Operation Parameters						Simulation			Results		
		Battery details	Battery module and BTMS design details	HTF	Discharging rate (C)	Ambient temperature (K)	Flow rate (kg/s, m/s, l/s)	Battery heat generation model	Simulation software	Flow model	ΔT (K)	T_{max} (K)	Others
[101]	Use of MOGA approach for optimization of LC-BTMS design	Soft pack LIB, 3.6–4.2 V, 8 Ah	CP with a U-shaped channel inserted between two LIBs	Water	1	298.15	–	Bernardi Model	Ansys Fluent	Laminar flow model	2.8	304.35	Optimized design reduces T_{max} and ΔT by 1.85 °C and 0.35 °C.
[103]	Use of the MOGA approach for the optimization flow rate of designed LC-BTMS	LIB, 3.6–4.2 V, 5 Ah	CP with a U-shaped channel inserted between two LIBs	Water	1	300	45×10^{-5} kg/s	Bernardi Model	–	Laminar flow model	0.23	300.34	Instead of a constant flow rate, an optimized flow rate combination produced the same cooling effect with 43.56 % reduced power usage.
Other miscellaneous designs													
[104]	Optimization of the LC-BTMS design	200 × 105 × 7 mm, 3.7 V, 21 Ah	CPs with spiral channels inserted between LIBs	Water	2	298	1.2×10^{-3} kg/s	Bernardi Model	Ansys Fluent	Laminar flow model	3.95	307.65	The pressure drop in the optimized design was found to be 8.82 Pa.
[105]	Optimization of the LC-BTMS design	148 × 91 × 27 mm, 3.65 V, 40 Ah	An array of LIB arranged over the CP with a tree shaped like HTF channel	Water	0.5–3	300	0.005–0.025 kg/s	Bernardi Model	Ansys Fluent	Laminar flow model	0.99	310.64	The pressure drop in the optimized design was found to be 181.75 Pa.
[106]	Optimization of the LC-BTMS design	100.5 × 145.3 × 21.3 mm, 3.2 V, 27 Ah	CPs with fishbone-inspired channels inserted between LIBs	1:1 EG: water	6	298	0.01–0.05 kg/s	Bernardi Model	Ansys Fluent	Laminar flow model	8.6	308.4	The pressure drop in the optimized design was found to be 3106.9 Pa.
[107]	Performance analysis of the designed LC-BTMS	118.5 × 63 × 13 mm, 3.2 V, 8 Ah	CPs with honey-comb channel inserted between LIBs	Water	5	298.15	0.01–0.5 m/s	Constant Heat generation	COMSOL	Laminar flow model	4.1	302.5	Design in which coolant flows in opposing directions in two neighboring HLCPs improves LIB temperature uniformity.
[109]	Optimization of the LC-BTMS design	20,100,140-type LIBs	Lightweight design consisting of HTF tubes on the outer edges of LIB and thin fin in-between two LIBs attached with HTF tube	1:1 EG: water	0.7–2	298.15 for HTF and 313 for battery	0.1–1 m/s	Constant heat generation	Ansys Fluent	Standard k-ε model	5	313	The LC-BTMS developed improves battery module temperature uniformity and minimizes BTMS weight ratio

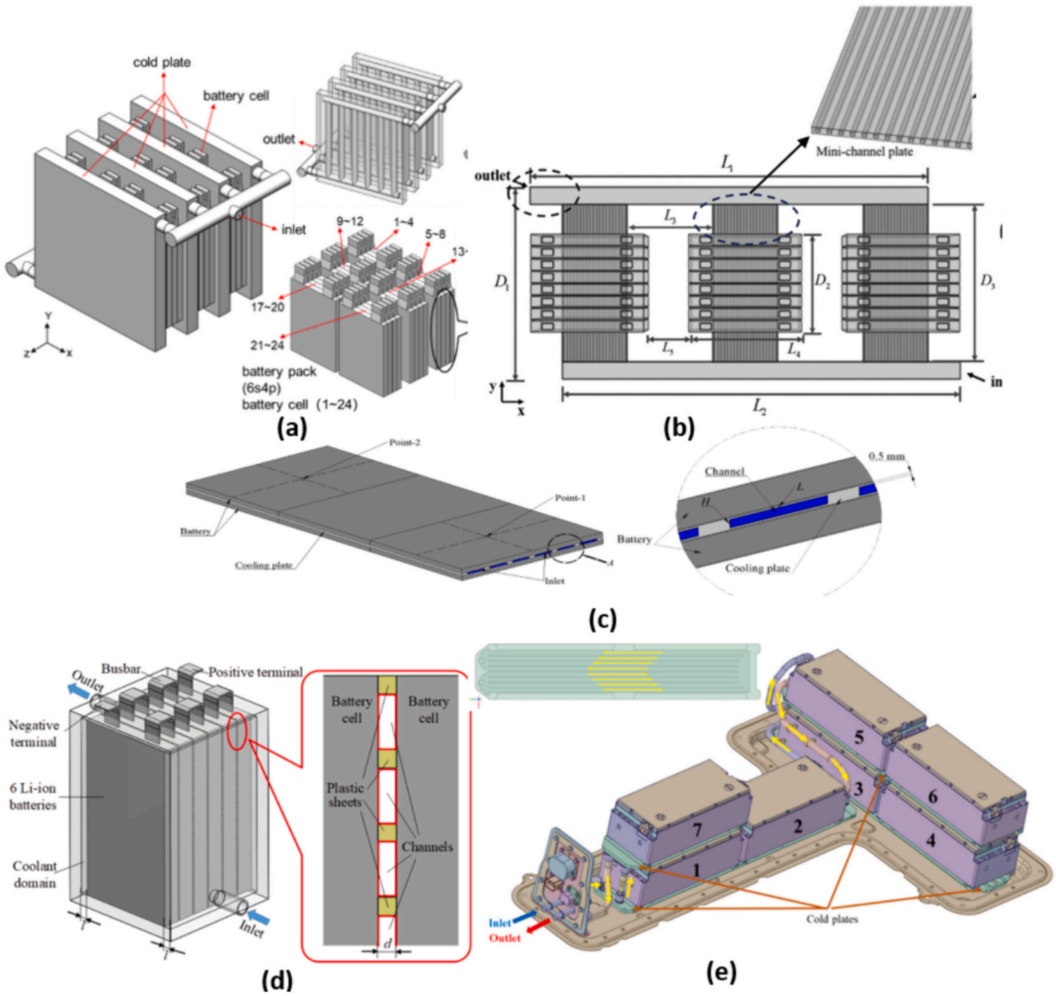

Fig. 21. LC-BTMS designs with straight HTF channels in the CP studied by (a) Zhang et al. [77], (b) Wang et al. [78], (c) Duan et al. [79], (d) Guo et al. [80], and (e) Xia et al. [81].

(Design-I), one tube with eight channels (Design-II), two tubes with four channels (Design-III) and four tubes with four channels (Design-IV) were investigated. Design-IV was found to be the best. The results revealed that for a 2C discharge rate, the flow rate of 1 m/s (pumping power of 5.27e-3 W) is required to maintain the maximum battery temperature below 28.27 °C.

The effect of flow direction is a crucial parameter that dictates T_{max} and ΔT within the LIB module. Many studies reported the impact of different flow arrangements within the LC-BTMS for prismatic LIBs. Wang et al. [87] carried out a numerical investigation for the design optimization of a silica plate/liquid coupled CP (SLCP), as shown in Fig. 22(a). The optimization for the number of tubes, flow rate, and flow direction was carried out at different battery discharge rates. The optimum number of tubes was found to be five. The flow rates at 3C and 5C were found to be 0.1 m/s and 0.25 m/s, respectively. In another study [88], the designed LC-BTMS was tested for the battery module of five cells with series connections, and noticeably different results were observed. Chung and Kim [89] numerically evaluated the thermal performance of a pack-level LC-BTMS, which includes the CP, rectangular fins, and prismatic batteries, as shown in Fig. 22(b). Three different configurations of the LC-BTMS, including vertical batteries + one CP, vertical batteries + two CPs, and horizontal batteries + two CPs, were investigated. Results showed that the configuration with the horizontal batteries performed significantly better than the other designs. Wang et al. [90] conducted a control analysis for the flow direction of liquid in the LC-BTMS. Three cases, namely, unidirectional, constant cycle reciprocating, and actively controlled reciprocating flow directions, were comparatively studied. They reported that the LC-BTMS with the reciprocating flow direction was significantly better than that with the unidirectional flow.

Yang et al. [91] studied the effect of the inlet and outlet positions and the number of coolant inlets and outlets on the cooling performance of an LC-BTMS. Four CPs with batteries placed on the top were connected parallelly, and four different locations of the main inlet and outlet were studied, as shown in Fig. 22(c). Results revealed that when the inlet and outlets were placed at the center of the four CPs, the performance was comparatively better. In extension to this, the effect of the number of inlets and outlets was also studied, and it was found that the performance improved with an increase in the number of the main inlets and outlets. The system with three inlets and outlets was able to keep cell T_{max} and ΔT below 27.98 °C and 2.69 °C, respectively, at the discharge rate of 1C. Chang et al. [92] carried out a numerical investigation of an LC-BTMS with reciprocating flow directions, as shown in Fig. 22(d). A CP placed at the base of the LIB was used in the LC-BTMS. It was found that when the reciprocating flow direction was used, T_{max} and ΔT were observed to be 1.67 °C and 3.77 °C lower than that with the unidirectional flow under the same flow rate, discharge conditions, and environment temperature.

In addition to the HTF flow direction, the HTF type also affects the performance of an LC-BTMS design with a straight HTF channel in the CP. Many researchers have studied the effect of different HTFs on the cooling performance of such systems for prismatic LIBs. Yang et al. [93]

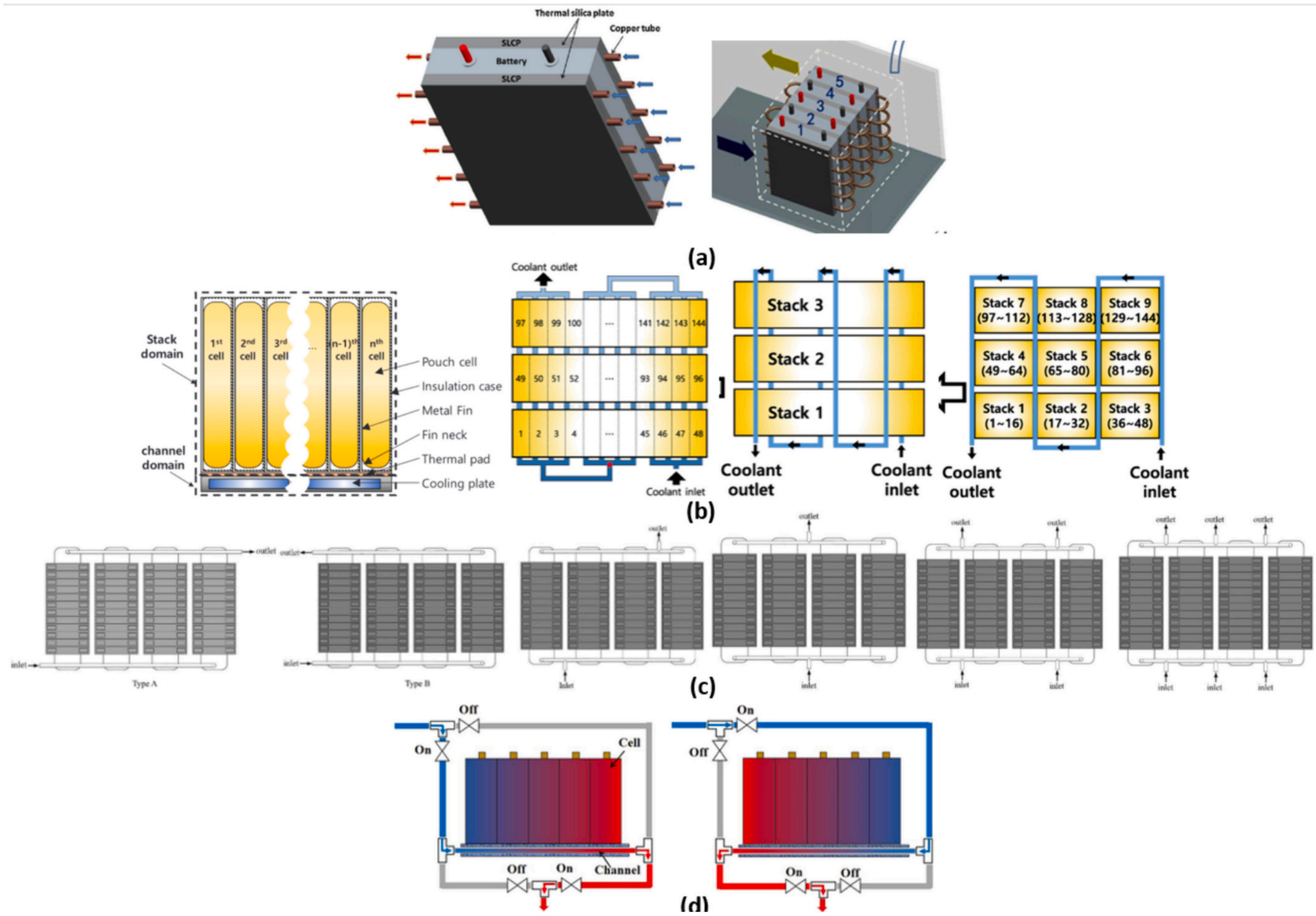

Fig. 22. Effect of flow directions on the LC-BTMS designs with straight HTF channel in the CPs studied by (a) Wang et al. [87], (b) Chung and Kim [89], (c) Yang et al. [91], and (d) Chang et al. [92].

numerically investigated the performance of supercritical CO_2 as the HTF in an LC-BTMS design with parallel cooling tubes in the CP. The performance of the supercritical CO_2 was compared with the LC-BTMS with water as the HTF. It was reported that supercritical CO_2 combines the effect of both the HTF and PCM in the system. T_{max} rises in the battery pack with water and supercritical CO_2 as the HTF was observed to be 9.1 °C and 5.8 °C, respectively. Yang et al. [94] carried out a numerical investigation to evaluate the thermal performance of an LC-BTMS design with liquid metals as the HFT. Gallium Indium alloy ($Ga^{80}In^{20}$) was used as the liquid metal, and the performance of the system was compared with that of water as the HTF. Results show that the thermal performance of the system improved significantly with the use of liquid metals (Fig. 23). Moreover, the pumping power at the same flow rate was also observed to be less for the liquid metal than for the HFT.

Liu et al. [95] carried out a numerical investigation to study the effect of a nano-enhanced LC-BTMS, as shown in Fig. 24(a). Three base fluids, i.e., water, ethylene glycol (EG), and engine oil (EO), were considered and tested with Al_2O_3 nanoparticles. For the LC-BTMS, the CP with parallel mini channels was used. Results revealed that the addition of nanoparticles significantly improved the effectiveness of the LC-BTMS. On the other end, the pumping power also increased substantially because of the addition of nanoparticles. An et al. [96] carried out an experimental investigation for flow boiling in a mini channel type LC-BTMS, as shown in Fig. 24(b). The CP with parallel channels was used for the LC-BTMS. Dielectric hydrofluoroether liquid, having a boiling temperature of 34 °C, was used as the HTF. Results revealed that the designed system was able to keep the module temperature below 40 °C at the discharge rate of 5C. The effect of different flow rates was also analyzed, and it was found that the cooling rate improved with the increase in the HTF flow rate.

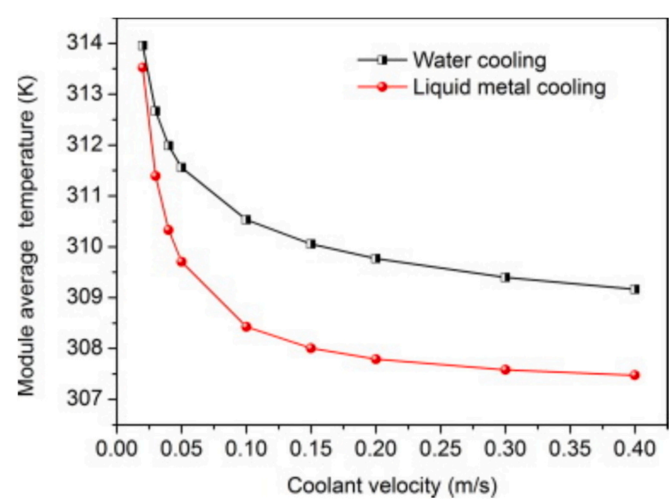

Fig. 23. Variation of the average module temperature with the HTF velocity for different HTFs. (Obtained with permission from Yang et al. [94]).

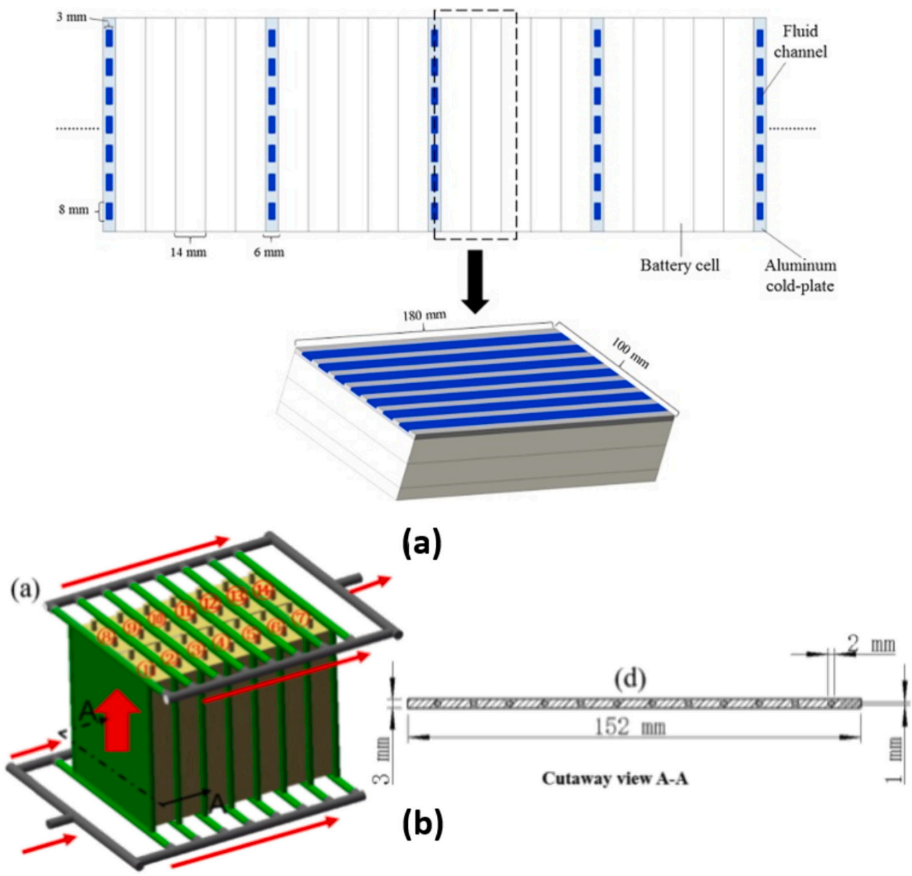

Fig. 24. Effect of different HTFs on the LC-BTMS designs with straight HTF channel in the CPs studied by (a) Liu et al. [95] and (b) An et al. [96].

4.2. LC-BTMS designs with serpentine HTF channel in the CP

Another widely studied design of the HTF channel in the CP-based LC-BTMSs for prismatic LIBs is a serpentine HTF channel. Many researchers have reported studies of serpentine channels of different shapes, sizes, and configurations in LC-BTMS designs with serpentine HTF channels in the CP for prismatic LIBs. Sheng et al. [97] conducted a numerical study to evaluate the cooling performance of an LC-BTMS design with a serpentine HTF channel in the CP, as shown in Fig. 25 (a). Seven different configurations of the HTF flow in the serpentine channel were studied. Results revealed that compared to the CP channels with a single inlet and outlet, those with two inlets and outlets had a greater capacity for thermal management. It was shown that placing the channel's intake and exit on the opposite sides rather than the same side had advantages. They also reported that increasing the fluid flow rate effectively lowered the cell's T_{max} without significantly altering the temperature differential across cells. Guo and Li [98] studied the effect of different channel configurations in an LC-BTMS design with a serpentine HTF channel in the CP, which consisted of a CP, L-shaped aluminum fins, and prismatic LIB, as shown in Fig. 25(b). Four different configurations of the liquid channel, i.e., parallel-spiral, parallel-U-shape, series-spiral, and series-U-shape serpentine channels, were studied. Results showed that T_{max} and ΔT were comparatively lower for the parallel configurations than for the series configurations, especially the parallel-spiral serpentine channel. Optimization of the channel design was also reported for the parallel-spiral serpentine channel. Wang et al. [99] investigated the cooling performance of an LC-BTMS design with a serpentine HTF channel in the CP for prismatic LIB cells. Three different configurations of flow connections to different CPs were studied, as shown in Fig. 25(c). The configuration with inlet and outlet staggered was found to produce the best results in terms of cooling performance. The designed system kept the T_{max} of the battery pack below 311.25 K. Zhao et al. [100] conducted a numerical investigation to evaluate the thermal performance of a liquid CP (LCP) based LC-BTMS. Two configurations of the BTMS, one with a single LCP and another with double LCP on the top and bottom, were studied. The serpentine channel was used for the HTF passage in the LCP. Optimization of the structural parameters of the serpentine channel was also reported. It was found that the BTMS with double LCP performed better than that with the single LCP. T_{max} and ΔT for the single LCP and double PCP designs were found to be 31.9 °C, 27.7 °C and 5.2 °C, 1.9 °C, respectively. In addition, it was reported that the designed system was able to keep T_{max} below 32.1 °C when the ambient temperature was increased from 25 °C to 40 °C.

Amongst different serpentine channel designs, the U-shaped channel design is quite popular and has been investigated by several studies. Chen et al. [101] numerically investigated and optimized the design of CP for an LC-BTMS, as shown in Fig. 26(a), with a multi-objective genetic algorithm used for the optimization of the CP aiming at a high heat dissipation rate and low-pressure drop. Results revealed that without much complexity in manufacturing, the optimized design could reduce T_{max} and ΔT deviations in the module by 1.85 °C and 0.35 °C, respectively. Chen et al. [102] carried out an experimental investigation for scheduling effect on the performance of an LC-BTMS design with a U-shaped HTF channel in the CP. The discharging process was divided into three equal parts, and different HTF flow rates were used for various periods. It was shown that the cooling performance was superior when a higher flow rate was used initially and a lower flow rate was used toward the end of the discharge cycle. Karthik et al. [103] conducted a numerical investigation to optimize the flow rate of the HTF in an LC-BTMS design with a U-shaped HTF channel in the CP, as shown in Fig. 26(b). Three HTF flow rates were used for cooling during the discharging

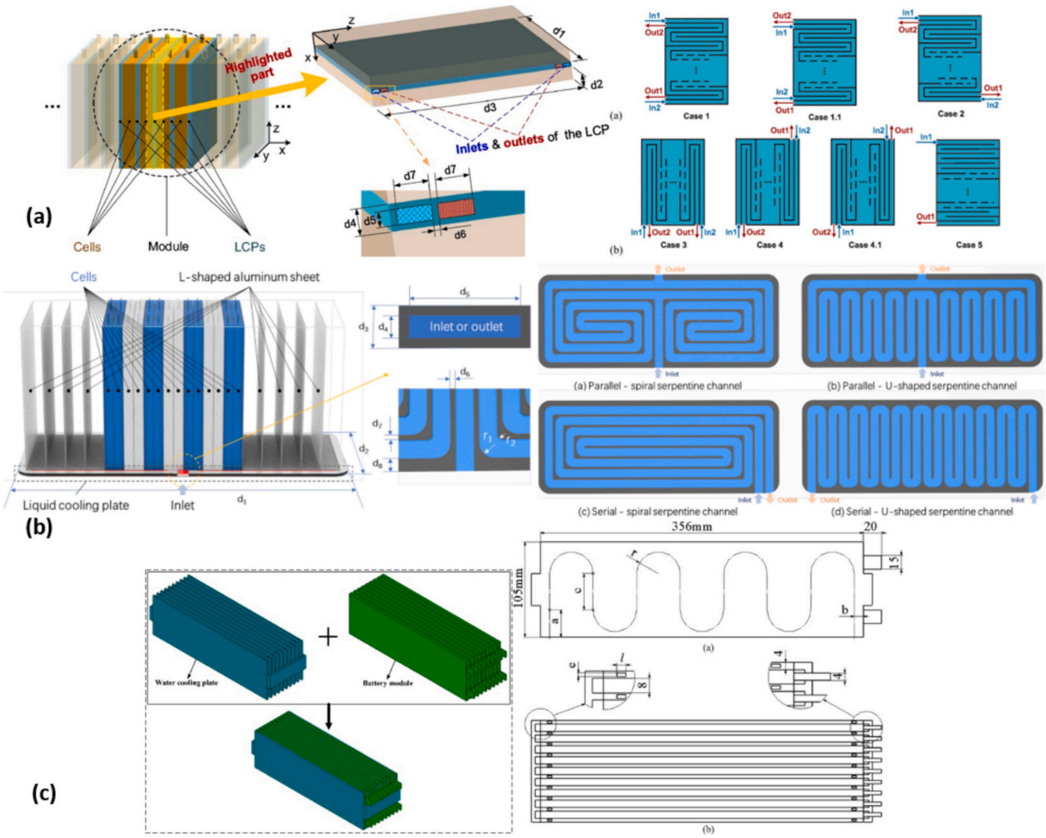

Fig. 25. LC-BTMS designs with serpentine HTF channels in the CPs studied by (a) Sheng et al. [97], (b) Guo et al. [98], and (c) Wang et al. [99].

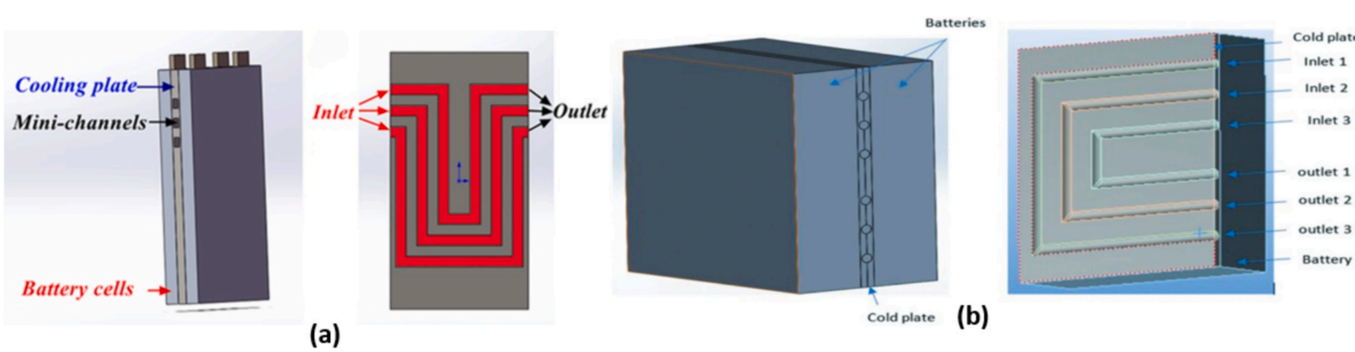

Fig. 26. LC-BTMS designs with U-shaped HTF channels in the CPs studied by (a) Chen et al. [101] and (b) Karthik et al. [103].

process. Thirteen combinations were designed based on the orthogonal array, and optimization was carried out using the response surface method (RSM). Results revealed that when the optimized combination of the flow rate was used instead of a constant flow rate, the same cooling effect was achieved with 43.56 % less power consumption.

4.3. LC-BTMS designs with miscellaneous HTF channels in the CP

Apart from the conventional straight and serpentine HTF channels in CP-based LC-BTMS designs for prismatic LIBs, many other configurations of the channels have also been studied. Li et al. [104] conducted a numerical investigation to evaluate the thermal performance of a CP-based LC-BTMS having spiral channels, as shown in Fig. 27. Their results showed that the designed LC-BTMS was able to keep T_{max}, ΔT, and pressure drop below 34.65 °C, 3.95 °C and 8.82 Pa, respectively. Fan et al. [105] conducted a numerical investigation of a CP-based LC-BTMS having tree-shaped channels, and the performance of the system was compared with the conventional system having serpentine liquid channels, as shown in Fig. 27(b). The optimization of the geometrical parameters of the design was also carried out. Results of the study showed that T_{max}, ΔT, and pressure drop for the optimized design were 1.79 %, 69.25 %, and 79.13 % lower than that in the conventional LC-BTMS, respectively. Fan et al. [106] investigated how to improve the liquid channel design in a CP-based LC-BTMS. Four fishbone-based designs with different configurations were studied, as shown in Fig. 27(c). The result revealed that the single inlet and double outlet symmetric bionic fishbone channel (D2) design provided the best results. Furthermore, the optimization of the D2 design was also reported. T_{max}, ΔT, and pressure loss for the optimized design were found to be 35.4 °C, 8.6 °C, and 3106.9 Pa, respectively. Zhao et al. [107] conducted a numerical investigation to evaluate the thermal performance of a CP-based LC-BTMS having a honeycomb-shaped channel, as shown in Fig. 27(d). The effect of the HTF flow rate was investigated. The results showed that the cooling performance improved with the increase in the HTF flow rate up

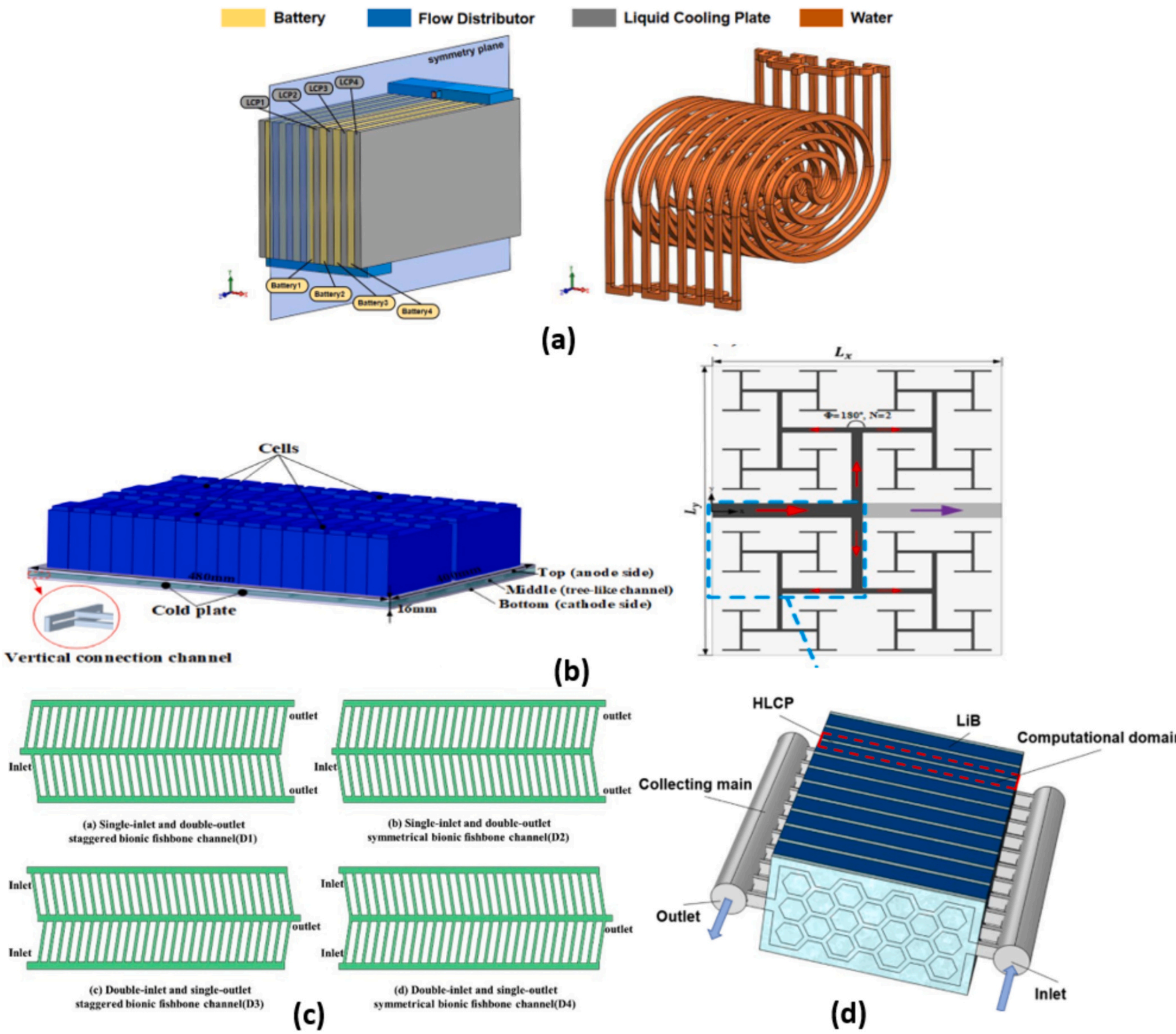

Fig. 27. CP with miscellaneous-shaped HTF channel-based designs studied by (a) Li et al. [104], (b) Fan et al. [105], (c) Fan et al. [106], and (d) Zhao et al. [107].

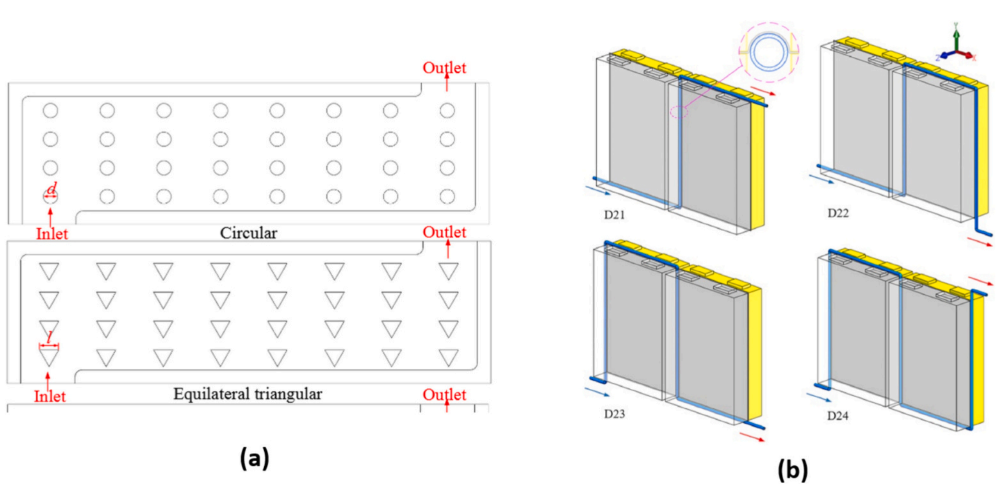

Fig. 28. CP with other miscellaneous-shaped HTF channel-based designs studied by (a) Xiong et al. [108] and (b) Tang et al. [109].

to a certain point and became almost constant afterward. T_{max} and ΔT for the 0.1 m/s flow rate were found to be 302.5 K and 4.1 K, respectively.

In addition to the mentioned channels, some other miscellaneous channels have also been studied. Xiong et al. [108] conducted a numerical investigation to evaluate the performance of the CP-based LC-BTMS designs that had pin-fins in the CPs, as shown in Fig. 28(a). The effects of pin-fin shapes, numbers, and distribution were studied. It was found that the square-shaped pin fins performed significantly better than the other designs in terms of reducing T_{max} and pressure drop. T_{max} was also found to decrease with the increase in the fin numbers; however, the pressure drop increased. Tang et al. [109] designed and investigated a lightweight LC-BTMS for a prismatic LIB. The LC-BTMS consisted of a thin metallic plate as a fin and a microtube on the periphery of the fin for the HTF passage. Different arrangements of the tube placement around the fin were studied for four cells, as shown in Fig. 28(b). Amongst the selected configurations, D22 and D24 were able to keep T_{max} and ΔT at safe levels below 40 °C and 5 °C, respectively. Xu et al. [110] numerically investigated the effect of a nano-enhanced EG on the cooling performance of the LC-BTMS. Two different LC-BTMS for cylindrical cells and prismatic cells were investigated for three different nanofluids, i.e., CuO-EG, Al_2O_3-EG, and TiO_2-EG. It was reported that the performance of CuO-EG and Al_2O_3-EG was found to be the maximum with the LC-BTMS designed for cylindrical cells and prismatic cells, respectively. Table 6 presents a summary of the existing studies on LC-BTMS designs for prismatic LIBs.

4.4. Discussion of studies on LC-BTMS for prismatic LIBs

The literature review on LC-BTMS for prismatic LIBs shows that extensive research has been carried out on the topic. Many researchers have investigated and optimized their LC-BTMS designs. Some have compared the performance of their designs with the conventional designs used in commercial vehicles. Notably, all of the LC-BTMS designs for prismatic batteries are based on CP. Designs have been done using single or double CP in a LIB module. Similarly, the positioning of the CP is also studied either on top, on bottom, in-between, or both on top and bottom. Most of the designs claimed to maintain the LIB's T_{max} and ΔT in the working ranges.

In the present review, the LC-BTMS designs for prismatic LIBs have been classified based on the design of the HTF channel in the CP. Most of the studies have utilized the CP with straight HTF channels. This is because of easy manufacturing, less pressure drop, and lower cost of these types of CPs. Another type of CP that has been studied is serpentine channels. Many researchers studied the different configurations of the serpentine channels and did optimization. Apart from straight and serpentine channel-based CPs, some other CPs with miscellaneous HTF channels have also been studied. The previous studies showed significant improvement in the heat transfer rate, with CPs having serpentine and miscellaneous channel designs. The common problem with the CPs with complex HTF channels is their manufacturing cost and pressure drop. With the help of advanced manufacturing techniques, these designs are possible and eventually can be produced at less cost. Still, the pressure drop needs to be minimized in HTF channels for the commercialization of these LC-BTMS designs.

Unlike the LC-BTMS for cylindrical LIBs, prismatic LIBs have been studied in terms of dimensions and attributes, such as the prismatic LIBs having storage capacity in the range of 5–100 Ah. Therefore, the heat generation rate is different for these designs, and eventually, the flow parameters are very diverse. Similar to LC-BTMS for cylindrical LIBs, the foremost choice of many researchers is water as the HTF. The second most utilized type of HTF is the mixture of water and EG (generally in a ratio of 1:1). Many others studied the nano-enhanced HTFs and found superior performance on the compensation of high-pressure drops. Interestingly, Liu et al. [95] studied the comparative performance of different HTFs (engine oil (EO), EG, and water). The results for T_{max} and ΔT are presented in Fig. 29, which shows that water demonstrated the most effective performance amongst the selected HTFs. The figure also shows that the performance improved with the use of nanoparticles (2 % Al_2O_3). Moreover, one study also used the supercritical CO_2 as the HTF and found that the system performance improved with the utilization of the CO_2 [93]. Liquid metals have also been studied as HTF and found to improve cooling significantly [94].

The discharge rate for most of the studied cases was in the range of 1–5C. Notably, the prismatic batteries have higher storage capacity; therefore, many researchers have studied their applicability in medium to heavy vehicles as well. Heavy vehicles require high discharge rates; hence, further testing of these LC-BTMS can be done at higher discharge rates. Similarly, the ambient temperature in most of the studies was in the range of 283–303 K. Tropical regions have higher ambient temperatures, which can affect the overall performance of a system. Therefore, the performance of these systems needs to be analyzed at higher ambient temperatures.

4.4.1. Comparative analysis of LC-BTMSs for prismatic LIBs

A comparative study was conducted to assess the performance of several designs based on their design and operational factors. Using the available quantitative data, a subset of the experiments from each LC-BTMS design for prismatic LIBs were selected and contrasted. The subsequent sections have explored the impact of various operating and design factors on the performance of LC-BTMS.

4.4.1.1. Effect of design parameters. The design parameters that significantly affect the performance of the LC-BTMS are the nominal capacity of the battery module and the relative heat transfer surface area. The results of the comparative analysis for LC-BTMS designs for prismatic

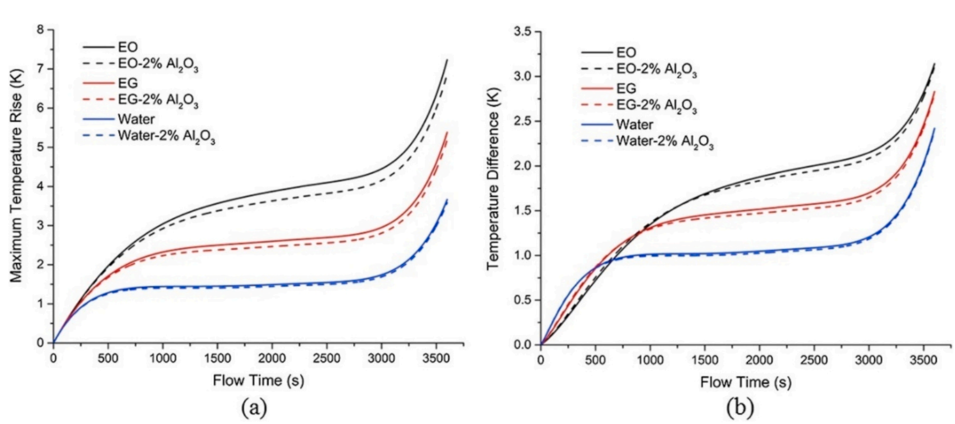

Fig. 29. Variation of (a) T_{max} and (b) ΔT with time for different HTFs. (Obtained with permission from Liu et al. [95]).

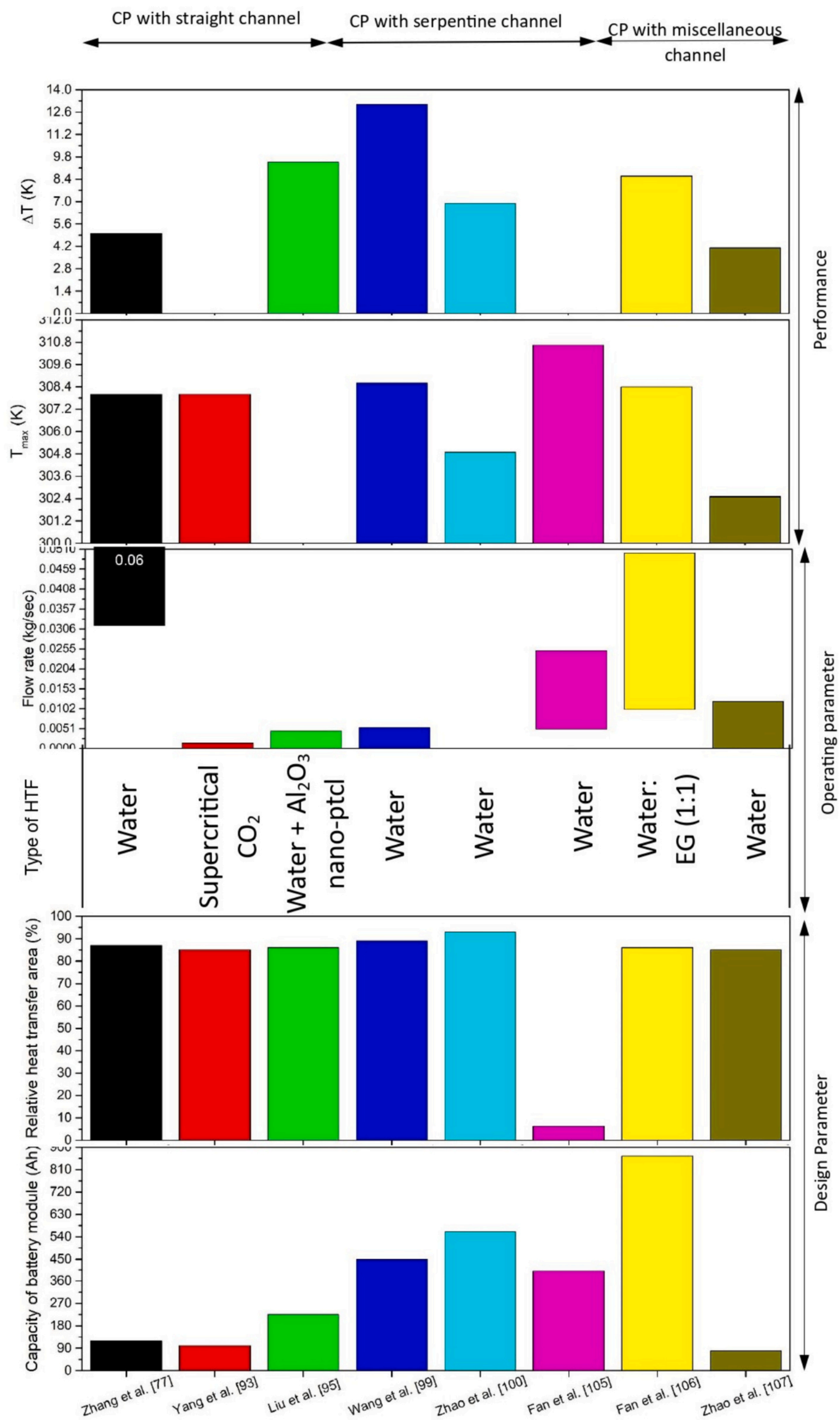

Fig. 30. Comparative analysis for the LC-BTMS for prismatic LIBs.

LIBs are presented in Fig. 30. The figure shows that the nominal capacity of the selected designs lies between 100 and 900 Ah. Higher values of nominal module capacity lead to higher heat generation rates in the module. The other significant design parameter of the LC-BTMS is the relative heat transfer area. The value for the relative heat transfer area has been evaluated as described in Section 3.5.1.1. For most of the studied designs, the relative heat transfer surface area is above 80 %. The cartesian configuration of prismatic LIB and CP provides a relatively higher heat transfer area. For one study, the relative heat transfer area is about 6 %. As a result, the comparatively highest T_{max} was observed for this design. The design with the highest value of nominal module capacity has >80 % relative heat transfer surface area. Hence, the performance of this design is found to be better than that of the design with the least relative heat transfer area, indicating that the relative heat transfer surface area while designing LC-BTMS should be kept as high as possible.

4.4.1.2. Effect of operational parameters. The operational parameters of the LC-BTMS can significantly affect its performance. For this comparison, the type of HTF and HTF flow rate have been selected as operational parameters. The discharging rate range for selected studies is 3 – 6C. For most of the studies, water has been chosen as HTF. However, some unconventional HTFs like supercritical CO_2, nano-enhanced HTF, and water-EG mixture have also been studied. The thermal performance of most of these designs was found to be comparatively better. Similarly, relatively better thermal performance was observed for a higher HTF flow rate. The optimization of the HTF flow rate is necessary to reduce the overall operational cost of the LC-BTMS. Notably, the HTF flow rates for the studies having supercritical CO_2 and nano-enhanced HTF are comparatively low. However, due to the lack of pressure drop data, it is not easy to compare the overall performance of these studies.

The performance of these different designs of LC-BTMS for prismatic LIBs is a function of both design and operational parameters. Designs with low nominal capacity, higher relative heat transfer area, better HTF, and higher HTF flow rates have shown significantly better performance. Notably, researchers and entrepreneurs are interested in comparatively evaluating the effect of different parameters on performance so that the desired performance can be met by adjusting the most crucial parameters only. Therefore, a detailed comparative analysis of these design and operational parameters needs to be done using multi-criteria decision-making techniques (MCDM) in the future.

4.4.2. Battery heat generation models

The numerical simulations have been widely utilized to study the performance of different LC-BTMS designs for the prismatic LIBs. Similar to the cylindrical LIBs, the battery heat generation models are used to estimate the heat generation rate of the prismatic LIB. The cylindrical LIBs come in standard sizes like 18,650, 4680, etc. Therefore, the heat generation model developed for a LIB from the same manufacturer can be used for an identical LIB. However, the prismatic LIBs do not have any fixed standards, and sizes vary from manufacturer to manufacturer. Therefore, most of the reported studies have validated their developed heat generation model with the experimental data. The most used models are the Bernardi heat generation model and the transient heat generation model. The details of some studied models are presented below.

4.4.2.1. Transient heat generation model. This model is considered the simplest heat generation model. The heat generation rate during discharging or charging of a battery is studied for different charging/discharging rates. Equations are eventually developed for the heat generation rate as a function of time or SoC. Some of the developed correlations in some studies are shown in Table 7.

4.4.2.2. Bernardi Model. The Bernardi equation-based model has also been widely studied for the analysis of LC-BTMS for prismatic LIBs. The different equations developed by various studies are shown in Table 8.

4.4.3. Details of numerical simulation

The numerical simulation of the LC-BTMS for prismatic LIBs has been researched in a way that is similar to the LC-BTMS for cylindrical LIBs. This is because the two types of LIBs operate similarly. In order to adequately cool prismatic LIBs, higher flow rates have been required than those utilized for cooling cylindrical LIBs. This is because the nominal capacity of the prismatic LIBs is significantly greater than the cylindrical LIBs. Because of this, turbulence models have been used to represent the fluid dynamics present in the system. The conventional k-ε model is the turbulence model that is typically used in the majority of the investigations. In addition, a significant number of studies have investigated the influence of flow directions. Research has been conducted on a wide variety of flow patterns, including series, parallel, and reciprocating flow. It has been determined that the recirculating flow has produced the most substantial improvements in outcomes. It is important to note that the reciprocating flow scheme calls for additional active components, and a comprehensive study has to be carried out in order to evaluate the system's overall performance. The majority of the research has been conducted using the ANSYS FLUENT platform, with COMSOL coming in second most often.

5. Comparison of LC-BTMS for cylindrical and prismatic LIBs

Literature review shows that numerous studies have been reported on LC-BTMS systems involving cylindrical and prismatic LIBs. In this section, the different design, operational, and performance parameters of the designs for both LIB configurations are evaluated comparatively. A comparison of the studied module capacity range shows that the module capacity for prismatic LIBs is significantly larger than that of cylindrical LIBs, as shown in Fig. 31. In EVs, modules with higher nominal capacity are preferred because of the reduction in total modules required for the entire battery pack. The figure shows that the relative heat transfer surface area for most of the designs studied, either with cylindrical LIB or prismatic LIB, is almost the same. The relative heat transfer area also represents the complexity of the LC-BTMS design. Therefore, optimization of the relative heat transfer area should be carried out for a designed LC-BTMS. The comparison of HTF flow rate suggests that a higher range of flow rates has been studied with the prismatic LIBs than with the cylindrical LIBs. This could be due to the higher nominal capacity and heat generation rate of the prismatic LIB module. Because of the higher flow rates with the prismatic LIBs, turbulence gets involved in the physics of flow dynamics in fluid channels. Therefore, turbulence models have been utilized in most numerical studies for prismatic LIBs, whereas laminar models have been used in the numerical investigation of cylindrical LIBs. The heat transfer rate can be improved with the increase in turbulence and flow mixing in the fluid channel. Therefore, the effect of turbulence promotors in the LC-BTMS designs for prismatic LIBs can be studied in the future.

The comparison of performance parameters for cylindrical and prismatic LIBs shows that T_{max} and ΔT can be kept below the extreme limits using the devised designs. The range of ΔT for the prismatic LIBs is slightly higher than that of the cylindrical LIBs. This phenomenon could be due to the large physical size of prismatic cells and modules. Notably, the T_{max} range for the prismatic LIBs was found to be lesser than that of the cylindrical LIBs. The comparison shows that the design and

Table 7
Correlations for the various heat generation models.

Ref.	Correlation
Zhao et al. [100]	$Q_{gen.} = \begin{cases} 1535SoC^5 - 11936SoC^4 + 12154SoC^3 + 366.79SoC^2 - 3118.3SoC + 3250, 0.5C \\ 188118SoC^5 - 47133SoC^4 + 407725SoC^3 - 133945SoC^2 + 8857.2SoC + 12074, 1C \\ 250833SoC^5 - 644645SoC^4 + 495505SoC^3 + 60110SoC^2 - 56976SoC + 55948, 2C \end{cases}$
Yang et al. [83]	$Q_{gen.} = 3.2235 \times 10^{-12}t^6 - 8.2542 \times 10^{-9}t^5 + 7.7851 \times 10^{-6}t^4 - 3.2303 \times 10^{-3}t^3 + 0.6157t^2 - 59.9607t + 148414.7651$
Liu et al. [95]	$Q_{gen.} = \begin{cases} 4.91 \times 10^{-16}t^6 - 3.77 \times 10^{-12}t^5 + 1.06 \times 10^{-8}t^4 - 1.34 \times 10^{-5}t^3 + 0.0076t^2 - 2.22t + 17151.7, 1C \\ 1.25 \times 10^{-13}t^6 - 4.83 \times 10^{-10}t^5 + 6.83 \times 10^{-7}t^4 - 4.29 \times 10^{-4}t^3 + 0.12t^2 - 17.76t + 66623.33, 2C \\ 3.22 \times 10^{-12}t^6 - 8.25 \times 10^{-9}t^5 + 7.78 \times 10^{-6}t^4 - 3.23 \times 10^{-3}t^3 + 0.61t^2 - 59.96t + 148414.76, 3C \end{cases}$

Table 8
Correlations for Bernardi model by various studies for prismatic LIBs.

Ref.	Correlations
Yang et al. [93] and Fathabadi [111]	$R_{int.} = \begin{cases} 2.258 \times 10^{-6}.SoC^{-0.3952}, T = 20^{\circ}C \\ 1.857 \times 10^{-6}.SoC^{-0.2787}, T = 30^{\circ}C \\ 1.659 \times 10^{-6}.SoC^{-0.1692}, T = 40^{\circ}C \end{cases}$ $\Delta S = \begin{cases} 99.88SoC - 76.67, 0 < SoC < 0.77 \\ -30, 0.77 < SoC < 0.87 \\ -20, 0.87 < SoC < 1 \end{cases}$
Li et al. [104]	$R_{int.} = \begin{cases} 0.0039.SoC^5 - 0.0049.SoC^4 + 0.0054SoC^3 - 0.0039SoC^2 + 0.0008.SoC + 0.0023, T = 5^{\circ}C \\ -0.0034.SoC^4 + 0.0099.SoC^3 - 0.0077.SoC^2 + 0.0017.SoC + 0.0016, T = 15^{\circ}C \\ 0.06.SoC^6 - 0.1751.SoC^5 + 0.1880.SoC^4 - 0.0828.SoC^3 + 0.0097.SoC^2 + 0.0011.SoC + 0.0032, T = 25^{\circ}C \\ 0.4679.SoC^6 - 1.2613.SoC^5 + 1.2574.SoC^4 - 0.5506.SoC^3 + 0.0923.SoC^2 - 0.0019.SoC + 0.0043, T = 35^{\circ}C \\ -0.0054.SoC^4 + 0.0178.SoC^3 - 0.017.SoC^2 + 0.0047.SoC + 0.0039, T = 45^{\circ}C \end{cases}$
Fan et al. [106]	$R_{int.} =$ $\begin{cases} 642.65 - 5.2T - 259.42SoC + 0.013T^2 + 1.406T \times SoC + 61.74SoC^2 - 1.21 \times 10^{-5}T^3 - 0.0019T^2 \times SoC - 0.136T \times SoC^2 - 10.69SoC^3, C - rate = 5 \\ 620.22 - 5.14T - 215.63SoC + 0.014T^2 + 1.125T \times SoC + 60.01SoC^2 - 1.30 \times 10^{-5}T^3 - 0.0015T^2 \times SoC - 0.132T \times SoC^2 - 10.19SoC^3, C - rate = 6 \end{cases}$ $\frac{dU_{OC}}{dT} = -0.13847 + 2.55.SoC - 19.92.SoC^2 + 92.72.SoC^3 - 191.71.SoC^4 + 175.08.SoC^5 - 58.47.SoC^6$
Guo et al. [80]	$R_{int.} = (8.655 - 4.43.SoC + 3.022.SoC^2).exp\left(\frac{13.605}{T + 19.49}\right)$ $\frac{dU_{OC}}{dT} = -0.34 + 2.72.SoC - 5.43.SoC^2 + 3.85.SoC^3 - 0.61.SoC^4$

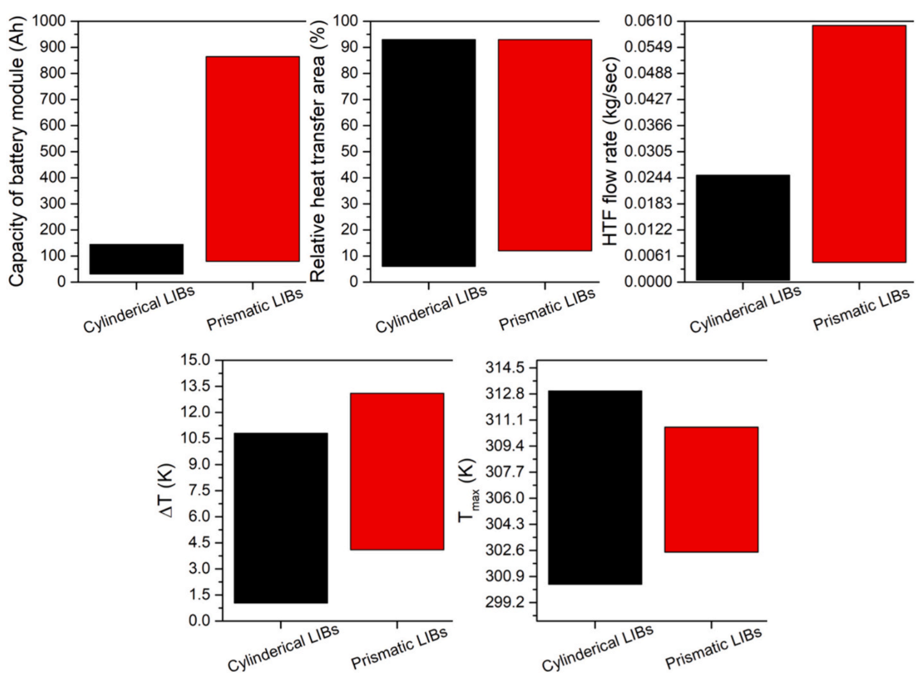

Fig. 31. Comparison of design, operational, and performance parameter range for LC-BTMS designed for cylindrical and prismatic LIBs.

operational parameters for designs of both cylindrical and prismatic LIBs are significantly different. Future studies can be carried out on both systems to optimize the design and operational parameters.

6. Major issues and challenges and recommended future work

The present literature review shows that the performance of an LC-BTMS could be improved with the design and operational optimization. However, this review also suggests that some issues exist with the current LC-BTMS technologies, and further improvements need to be carried out to refine the reliability and safety of the systems under extreme working conditions. These works could be done on the LC-BTMS analysis in the future. More specifically,

1. The relative heat transfer area is directly proportional to the performance of the system. However, its higher values also lead to more system complexity and higher cost of the LC-BTMS. Therefore, optimization of the relative heat transfer surface area for designs of LC-BTMSs needed to be carried out.
2. The flow direction of HTF plays a crucial role in the performance of an LC-BTMS. The most effective flow scheme found in the literature is the reciprocating flow scheme. Notably, the reciprocating flow scheme necessitates additional active components, and a thorough study is essential for the comprehensive assessment of the system's overall performance.
3. The performance of an LC-BTMS was found to improve with some unconventional HTFs like liquid metals and supercritical CO_2. However, the other economic, health, and environmental aspects of these unconventional HTFs in EVs have not been reported and need further exploration.
4. The nano-enhanced HTFs were also found to be superior to the conventional HTFs. The biggest hurdle with the use of nano-

enhanced HTF is the increase in pumping power. Therefore, optimization of nano-enhanced HTFs can be carried out for different LC-BTMS designs.

5. For LC-BTMS for prismatic LIBs, many studies have seen a significant increase in the heat transfer rate while using CPs with serpentine and a variety of channel shapes. The pressure drop and manufacturing expense of the CPs with complicated HTF channels are prevalent issues. These designs are feasible and ultimately less expensive to build with the aid of sophisticated production processes. However, in order to commercialize these LC-BTMS devices, future work should be carried out to minimize pressure loss in HTF channels.
6. The LIB's discharge rate in most of the reported studies is in the range of 1 – 5C. This discharge rate is suitable for the light vehicle. However, for medium and heavy vehicles, the discharge rate is high. Further investigations should be done to improve the LC-BTMS for medium and heavy vehicles.
7. The ambient temperatures studied for most of the cases were in the range of 293–303 K. The ambient temperature is higher in tropical climates, which might have an impact on the system's overall performance. For this reason, it is necessary to analyze the performance of these systems at higher ambient temperatures. Moreover, higher energy will be required to maintain the HTF temperature in the desired range for high ambient temperatures. This will reduce the overall range of the vehicle. Further analysis can be carried out in the future to evaluate the overall performance of the EV in hot climatic regions.
8. The thermal runaway and heat propagation in an abusive scenario needed to be considered for the complete analysis of the LC-BTMS. The numerical modeling of such scenarios is currently being researched [112–115], but due to the complexity, it has not been utilized in the analysis of the LC-BTMS. Future numerical studies can be carried out by considering the extreme conditions.

7. Conclusion

The literature review of LC-BTMSs for different configurations of LIBs has been presented in this review work. Generally, cylindrical and prismatic LIBs are used in the EVs. Therefore, this article has been categorized based on the LC-BTMS designs for the cylindrical and prismatic configurations of the LIB. The broad conclusions from this review include the following,

1. The literature review shows that modifications in its design and operational parameters can significantly improve the thermal performance of an LC-BTMS.
2. For the cylindrical LIBs, both CP and channel-based designs have been extensively studied and have shown significant cooling performance. Moreover, the channel-based studies have reported more in numbers than CP-based designs for the cylindrical LIBs because of the larger heat transfer surface area in the former design.
3. For the prismatic LIBs, most of the LC-BTMS designs are made up of CPs. A large number of studies investigated the placement of the CP in a variety of positions, including on top, on bottom, in between, or both on top and bottom. Moreover, the different types of CPs with varying configurations of HTF channels have been studied. The most common types of HTF channels are straight and serpentine channels. In the majority of the investigations, the CP with straight HTF channels was used. This is because these types of CPs are simple to manufacture, have a lower pressure drop, and are inexpensive.
4. The performance of all designs was found to improve with an increase in the HTF rate. Several investigations indicated that the performance of an LC-BTMS design, in terms of T_{max}, is enhanced with an early rise in the HTF flow rate and stabilizes after that. However, several investigations have also shown that ΔT did not significantly improve with higher flow rates.
5. The HTF flow direction significantly affects the performance of the system. Several studies examined the unidirectional, counter-directional, and reciprocating flow patterns. The counterflow and reciprocating flow schemes were found to be significantly effective in reducing both ΔT and T_{max}.
6. The most studied types of HTFs in the LC-BTMS are water and a mixture of water and EG (Generally in the ratio of 1:1). Many researchers have also studied the effect of other HTFs like liquid metal and supercritical CO_2 for different designs. The nano-enhanced HTF has also shown significant performance improvement, but the increase in pumping power is their biggest issue, and it requires optimization.
7. A comparative analysis of the different designs of LC-BTMS for both cylindrical and prismatic LIBs has been carried out by considering design, operational, and performance parameters. Battery module capacity and relative heat transfer area were considered design parameters; HTF type, HTF flow rate, and discharging rate were operational parameters, ΔT and T_{max} were performance parameters. The results of comparative analysis for both cylindrical and prismatic LIBs show that the performance of the LC-BTMS design is significantly affected by the design and operational parameters. Higher and lower values of relative heat transfer area and module capacity lead to better design performance. Similarly, a higher HTF flow rate and better HTF type can also improve the LC-BTMS's performance. Moreover, the MCDM techniques can be employed to evaluate the effect of different parameters on the performance of a particular design of LC-BTMS comparatively.
8. A comparison of the range of different design, operational, and performance parameters on LC-BTMS for cylindrical and prismatic LIBs was carried out. The range of module capacity for the prismatic LIBs is significantly more extensive than the cylindrical LIBs. Similarly, the range of HTF flow rate for the prismatic LIBs is greater than that of the cylindrical LIBs.
9. Most of the investigations that have been reported on LC-BTMSs are numerical studies. Various battery heat generation models have been employed to simulate battery heat generation. The most commonly used battery models with cylindrical LIBs are the Bernardi model, ECM, and P2D. With prismatic LIBs, the most frequently studied heat generation battery models are the transient heat generation model and the Bernardi model.
10. For LC-BTMSs for cylindrical LIBs, the laminar flow model has been used in most of the studies, whereas the most common flow model for simulating the fluid flow for LC-BTMS designs for prismatic batteries is the standard k-ε turbulence model. The commonly used commercial CFD packages for these studies are ANSYS Fluent and COMSOL.

CRediT authorship contribution statement

Ashutosh Sharma: Writing – original draft, Methodology, Investigation, Formal analysis, Data curation, Conceptualization. **Mehdi Khatamifar:** Writing – review & editing, Supervision. **Wenxian Lin:** Writing – review & editing, Supervision, Methodology. **Ranga Pitchumani:** Writing – review & editing.

Declaration of competing interest

The authors declare that they have no known competing financial interests or personal relationships that could have appeared to influence the work reported in this paper.

Data availability

No data was used for the research described in the article.

References

[1] N. Armaroli, V. Balzani, The legacy of fossil fuels, Chem. Asian J. 6 (2011) 768–784, https://doi.org/10.1002/asia.201000797.

[2] US EPA, Carbon Pollution from Transportation. https://www.epa.gov/transportation-air-pollution-and-climate-change/carbon-pollution-transportation, 2015 (accessed November 3, 2023).

[3] Transportation emissions worldwide, Statista (n.d.). https://www.statista.com/topics/7476/transportation-emissions-worldwide/ (accessed May 10, 2024).

[4] X. Hao, Y. Yuan, H. Wang, M. Ouyang, Plug-in hybrid electric vehicle utility factor in China cities: influencing factors, empirical research, and energy and environmental application, eTransportation 10 (2021) 100138, https://doi.org/10.1016/j.etran.2021.100138.

[5] L. Zhang, C. Sun, G. Cai, L.H. Koh, Charging and discharging optimization strategy for electric vehicles considering elasticity demand response, eTransportation 18 (2023) 100262, https://doi.org/10.1016/j.etran.2023.100262.

[6] J. Luo, D. Zou, Y. Wang, S. Wang, L. Huang, Battery thermal management systems (BTMs) based on phase change material (PCM): a comprehensive review, Chem. Eng. J. 430 (2022) 132741, https://doi.org/10.1016/j.cej.2021.132741.

[7] Z. Lu, X.L. Yu, L.C. Wei, F. Cao, L.Y. Zhang, X.Z. Meng, L.W. Jin, A comprehensive experimental study on temperature-dependent performance of lithium-ion battery, Appl. Therm. Eng. 158 (2019) 113800, https://doi.org/10.1016/j.applthermaleng.2019.113800.

[8] G. Murali, G.S.N. Sravya, J. Jaya, V. Naga Vamsi, A review on hybrid thermal management of battery packs and it's cooling performance by enhanced PCM, renew, Sustain. Energy Rev. 150 (2021) 111513, https://doi.org/10.1016/j.rser.2021.111513.

[9] G. Wei, R. Huang, G. Zhang, B. Jiang, J. Zhu, Y. Guo, G. Han, X. Wei, H. Dai, A comprehensive insight into the thermal runaway issues in the view of lithium-ion battery intrinsic safety performance and venting gas explosion hazards, Appl. Energy 349 (2023) 121651, https://doi.org/10.1016/j.apenergy.2023.121651.

[10] Y. Yang, R. Wang, Z. Shen, Q. Yu, R. Xiong, W. Shen, Towards a safer lithium-ion batteries: a critical review on cause, characteristics, warning and disposal strategy for thermal runaway, Adv. Appl. Energy 11 (2023) 100146, https://doi.org/10.1016/j.adapen.2023.10 0146.

[11] Y. Wang, X. Feng, W. Huang, X. He, L. Wang, M. Ouyang, Challenges and opportunities to mitigate the catastrophic thermal runaway of high-energy batteries, Adv. Energy Mater. 13 (2023) 2203841, https://doi.org/10.1002/aenm.202203841.

[12] S. Bhavsar, K. Kant, R. Pitchumani, Robust model-predictive thermal control of lithium-ion batteries under drive cycle uncertainty, J. Power Sources 557 (2023) 232496, https://doi.org/10.1016/j.jpowsour.2022.232496.

[13] A.K. Thakur, M.S. Ahmed, H. Kang, R. Prabakaran, Z. Said, S. Rahman, R. Sathyamurthy, J. Kim, J.-Y. Hwang, Critical review on internal and external battery thermal Management Systems for Fast Charging Applications, Adv. Energy Mater. 13 (2023) 2202944, https://doi.org/10.1002/aenm.202202944.

[14] J. Lin, X. Liu, S. Li, C. Zhang, S. Yang, A review on recent progress, challenges and perspective of battery thermal management system, Int. J. Heat Mass Transf. 167 (2021) 120834, https://doi.org/10.1016/j.ijheatmasstransfer.2020.120834.

[15] M.M. Hamed, A. El-Tayeb, I. Moukhtar, A.Z. El Dein, E.H. Abdelhameed, A review on recent key technologies of lithium-ion battery thermal management: external cooling systems, Res. Eng. Des. 16 (2022) 100703, https://doi.org/10.1016/j.rineng.2022.100703.

[16] J.R. Patel, M.K. Rathod, Recent developments in the passive and hybrid thermal management techniques of lithium-ion batteries, J. Power Sources 480 (2020) 228820, https://doi.org/10.1016/j.jpowsour.2020.228820.

[17] P. Qin, J. Sun, X. Yang, Q. Wang, Battery thermal management system based on the forced-air convection: a review, eTransportation 7 (2021) 100097, https://doi.org/10.1016/j.etran.2020.100097.

[18] A.R.M. Siddique, S. Mahmud, B.V. Heyst, A comprehensive review on a passive (phase change materials) and an active (thermoelectric cooler) battery thermal management system and their limitations, J. Power Sources 401 (2018) 224–237, https://doi.org/10.1016/j.jpowsour.2018.08.094.

[19] Y. Zhao, B. Zou, T. Zhang, Z. Jiang, J. Ding, Y. Ding, A comprehensive review of composite phase change material based thermal management system for lithium-ion batteries, Renew. Sust. Energ. Rev. 167 (2022) 112667, https://doi.org/10.1016/j.rser.2022.112667.

[20] J. Weng, Q. Huang, X. Li, G. Zhang, D. Ouyang, M. Chen, A.C.Y. Yuen, A. Li, E.W. M. Lee, W. Yang, J. Wang, X. Yang, Safety issue on PCM-based battery thermal manage- ment: material thermal stability and system hazard mitigation, Energy Storage Mater. 53 (2022) 580–612, https://doi.org/10.1016/j.ensm.2022.09.007.

[21] C. Roe, X. Feng, G. White, R. Li, H. Wang, X. Rui, C. Li, F. Zhang, V. Null, M. Parkes, Y. Patel, Y. Wang, H. Wang, M. Ouyang, G. Offer, B. Wu, Immersion cooling for lithium-ion batteries – a review, J. Power Sources 525 (2022) 231094, https://doi.org/10.1016/j.jpowsour.2022.231094.

[22] G. Zhao, X. Wang, M. Negnevitsky, C. Li, An up-to-date review on the design improvement and optimization of the liquid-cooling battery thermal management system for electric vehicles, Appl. Therm. Eng. 219 (2023) 119626, https://doi.org/10.1016/j.applthermaleng.2022.119626.

[23] O. Kalaf, D. Solyali, M. Asmael, Q. Zeeshan, B. Safaei, A. Askir, Experimental and simulation study of liquid coolant battery thermal management system for electric vehicles: a review, Int. J. Energy Res. 45 (2021) 6495–6517, https://doi.org/10.1002/er.6268.

[24] J. Xu, Z. Guo, Z. Xu, X. Zhou, X. Mei, A systematic review and comparison of liquid-based cooling system for lithium-ion batteries, eTransportation 17 (2023) 100242, https://doi.org/10.1016/j.etran.2023.100242.

[25] R. Zhou, Y. Chen, J. Zhang, P. Guo, Research progress in liquid cooling technologies to enhance the thermal management of LIBs, Mater. Adv. 4 (2023) 4011–4040, https://doi.org/10.1039/D3MA00299C.

[26] J. Liu, H. Chen, S. Huang, Y. Jiao, M. Chen, Recent Progress and prospects in liquid cooling thermal management system for Lithium-ion batteries, Batteries 9 (2023) 400, https://doi.org/10.3390/batteries9080400.

[27] W. Wu, S. Wang, W. Wu, K. Chen, S. Hong, Y. Lai, A critical review of battery thermal performance and liquid based battery thermal management, Energy Convers. Manag. 182 (2019) 262–281, https://doi.org/10.1016/j.enconman.2018.12.051.

[28] J. Zhao, Z. Rao, Y. Huo, X. Liu, Y. Li, Thermal management of cylindrical power battery module for extending the life of new energy electric vehicles, Appl. Therm. Eng. 85 (2015) 33–43, https://doi.org/10.1016/j.applthermaleng.2015.04.012.

[29] P.H. Camargos, P.H.J. dos Santos, I.R. dos Santos, G.S. Ribeiro, R.E. Caetano, Perspectives on Li-ion battery categories for electric vehicle applications: a review of state of the art, Int. J. Energy Res. 46 (2022) 19258–19268, https://doi.org/10.1002/er.7993.

[30] Z. Azizi, R. Barzegarian, M. Behvandi, Design-expert aided thermohydraulic assessment of a nanofluid-cooled cylindrical microchannel heat sink: possible application for thermal management of electric vehicle batteries, Sustain Energy Technol Assess 50 (2022) 101876, https://doi.org/10.1016/j.seta.2021.101876.

[31] Y. Huang, S. Wang, Y. Lu, R. Huang, X. Yu, Study on a liquid cooled battery thermal management system pertaining to the transient regime, Appl. Therm. Eng. 180 (2020) 115793, https://doi.org/10.1016/j.applthermaleng.2020.115793.

[32] W. Yang, F. Zhou, Y. Liu, S. Xu, X. Chen, Thermal performance of honeycomb-like battery thermal management system with bionic liquid mini-channel and phase change materials for cylindrical lithium-ion battery, Appl. Therm. Eng. 188 (2021) 116649, https://doi.org/10.1016/j.applthermaleng.2021.116649.

[33] W. Zeng, C. Ma, S. Hu, S. Li, Y. Zhang, The performance investigation and optimiza- tion of reciprocating flow applied for liquid-cooling-based battery thermal manage- ment system, Energy Convers. Manag. 292 (2023) 117378, https://doi.org/10.1016/j.enconman.2023.117378.

[34] J. Zhao, Z. Rao, Y. Li, Thermal performance of mini-channel liquid cooled cylinder based battery thermal management for cylindrical lithium-ion power battery, Energy Convers. Manag. 103 (2015) 157–165, https://doi.org/10.1016/j.enconman.2015.06.056.

[35] F. Dong, Z. Cheng, J. Zhu, D. Song, J. Ni, Investigation and optimization on cooling performance of a novel double helix structure for cylindrical lithium-ion batteries, Appl. Therm. Eng. 189 (2021) 116758, https://doi.org/10.1016/j.applthermaleng.2021.116758.

[36] Y. Lai, W. Wu, K. Chen, S. Wang, C. Xin, A compact and lightweight liquid-cooled thermal management solution for cylindrical lithium-ion power battery pack, Int. J. Heat Mass Transf. 144 (2019) 118581, https://doi.org/10.1016/j.ijheatmasstransfer.2019.118581.

[37] H. Wang, T. Tao, J. Xu, X. Mei, X. Liu, P. Gou, Cooling capacity of a novel modular liquid-cooled battery thermal management system for cylindrical lithium ion batteries, Appl. Therm. Eng. 178 (2020) 115591, https://doi.org/10.1016/j.applthermaleng.2020.115591.

[38] R. Gao, Z. Fan, S. Liu, A gradient channel-based novel design of liquid-cooled battery thermal management system for thermal uniformity improvement, J. Energy Stor. 48 (2022) 104014, https://doi.org/10.1016/j.est.2022.104014.

[39] Z. Liu, H. Wang, C. Yang, J. Zhao, Simulation study of lithium-ion battery thermal management system based on a variable flow velocity method with liquid metal, Appl. Therm. Eng. 179 (2020) 115578, https://doi.org/10.1016/j.applthermaleng.2020.115578.

[40] Z. Rao, Z. Qian, Y. Kuang, Y. Li, Thermal performance of liquid cooling based thermal management system for cylindrical lithium-ion battery module with variable contact surface, Appl. Therm. Eng. 123 (2017) 1514–1522, https://doi.org/10.1016/j.applthermaleng.2017.06.059.

[41] Z. Tang, S. Wang, Z. Liu, J. Cheng, Numerical analysis of temperature uniformity of a liquid cooling battery module composed of heat-conducting blocks with gradient contact surface angles, Appl. Therm. Eng. 178 (2020) 115509, https://doi.org/10.1016/j.applthermaleng.2020.115509.

[42] Z. Tang, Z. Zhao, C. Yin, J. Cheng, Orthogonal optimization of a liquid cooling structure with straight microtubes and variable heat conduction blocks for battery module, J. Energy Eng. 148 (2022) 04022017, https://doi.org/10.1061/(ASCE)EY.1943-7897.0000840.

[43] Z. Fan, Y. Fu, H. Liang, R. Gao, S. Liu, A module-level charging optimization method of lithium-ion battery considering temperature gradient effect of liquid cooling and charging time, Energy 265 (2023) 126331, https://doi.org/10.1016/j.energy.2022.126331.

[44] A. Mitra, R. Kumar, D.K. Singh, Thermal management of lithium-ion batteries using carbon-based nanofluid flowing through different flow channel configurations, J. Power Sources 555 (2023) 232351, https://doi.org/10.1016/j.jpowsour.2022.232351.

[45] L. Xie, Y. Huang, H. Lai, Coupled prediction model of liquid-cooling based thermal management system for cylindrical lithium-ion module, Appl. Therm. Eng. 178 (2020) 115599, https://doi.org/10.1016/j.applthermaleng.2020.115599.
[46] B. Yin, S. Zuo, Y. Xu, S. Chen, Performance of liquid cooling battery thermal management system in vibration environment, J. Energy Stor. 53 (2022) 105232, https://doi.org/10.1016/j.est.2022.105232.
[47] W. Cao, C. Zhao, Y. Wang, T. Dong, F. Jiang, Thermal modeling of full-size-scale cylindrical battery pack cooled by channeled liquid flow, Int. J. Heat Mass Transf. 138 (2019) 1178–1187, https://doi.org/10.1016/j.ijheatmasstransfer.2019.04.137.
[48] W. Qi, W. Huang, J. Niu, F. Chen, B. Chen, Y. Chen, Thermal management of power battery based on flexible Swiss roll type liquid cooling micro-channel, Appl. Therm. Eng. 219 (2023) 119491, https://doi.org/10.1016/j.applthermaleng.2022.119491.
[49] Q. Ke, X. Li, J. Guo, W. Cao, Y. Wang, F. Jiang, The retarding effect of liquid-cooling thermal management on thermal runaway propagation in lithium-ion batteries, J. Energy Stor. 48 (2022) 104063, https://doi.org/10.1016/j.est.2022.104063.
[50] J. Bohacek, M. Raudensky, E. Karimi-Sibaki, Polymeric hollow fibers: uniform temperature of Li-ion cells in battery modules, Appl. Therm. Eng. 159 (2019) 113940, https://doi.org/10.1016/j.applthermaleng.2019.113940.
[51] H. Zhou, F. Zhou, Q. Zhang, Q. Wang, Z. Song, Thermal management of cylindrical lithium-ion battery based on a liquid cooling method with half-helical duct, Appl. Therm. Eng. 162 (2019) 114257, https://doi.org/10.1016/j.applthermaleng.2019.114257.
[52] M. Yates, M. Akrami, A.A. Javadi, Analysing the performance of liquid cooling designs in cylindrical lithium-ion batteries, J. Energy Stor. 33 (2021) 100913, https://doi.org/10.1016/j.est.2019.100913.
[53] B. Coleman, J. Ostanek, J. Heinzel, Reducing cell-to-cell spacing for large-format lithium ion battery modules with aluminum or PCM heat sinks under failure conditions, Appl. Energy 180 (2016) 14–26, https://doi.org/10.1016/j.apenergy.2016.07.094.
[54] Z. Liu, X. Liu, H. Meng, L. Guo, Z. Zhang, Numerical analysis of the thermal performance of a liquid cooling battery module based on the gradient ratio flow velocity and gradient increment tube diameter, Int. J. Heat Mass Transf. 175 (2021) 121338, https://doi.org/10.1016/j.ijheatmasstransfer.2021.121338.
[55] L. Sheng, H. Zhang, L. Su, Z. Zhang, H. Zhang, K. Li, Y. Fang, W. Ye, Effect analysis on thermal profile management of a cylindrical lithium-ion battery utilizing a cellular liquid cooling jacket, Energy 220 (2021) 119725, https://doi.org/10.1016/j.energy.2020.119725.
[56] P.R. Tete, M.M. Gupta, S.S. Joshi, Numerical investigation on thermal characteristics of a liquid-cooled lithium-ion battery pack with cylindrical cell casings and a square duct, J. Energy Stor. 48 (2022) 104041, https://doi.org/10.1016/j.est.2022.104041.
[57] M. Tousi, A. Sarchami, M. Kiani, M. Najafi, E. Houshfar, Numerical study of novel liquid-cooled thermal management system for cylindrical Li-ion battery packs under high discharge rate based on AgO nanofluid and copper sheath, J. Energy Stor. 41 (2021) 102910, https://doi.org/10.1016/j.est.2021.102910.
[58] P. K, N. Napa, S. Madichetty, M.K. Agrawal, B. Tamma, Thermal Analysis of Lithium Ion Battery Pack with Different Cooling Media, 2022, https://doi.org/10.4271/2022-28-0043, 2022–28–0043.
[59] Y. Zhou, Z. Wang, Z. Xie, Y. Wang, Parametric investigation on the performance of a battery thermal management system with immersion cooling, Energies 15 (2022) 2554, https://doi.org/10.3390/en15072554.
[60] K. Kant, R. Pitchumani, Analysis and design of battery thermal management under extreme fast charging and discharging, J. Energy Stor. 60 (2023) 106501, https://doi.org/10.1016/j.est.2022.106501.
[61] S. Xin, C. Wang, H. Xi, Thermal management scheme and optimization of cylindrical lithium-ion battery pack based on air cooling and liquid cooling, Appl. Therm. Eng. 224 (2023) 120100, https://doi.org/10.1016/j.applthermaleng.2023.120100.
[62] L. Zhao, W. Li, G. Wang, W. Cheng, M. Chen, A novel thermal management system for lithium-ion battery modules combining direct liquid-cooling with forced air-cooling, Appl. Therm. Eng. 232 (2023) 120992, https://doi.org/10.1016/j.applthermaleng.2023.120992.
[63] A. Angani, H.-W. Kim, M.-H. Hwang, E. Kim, K.-M. Kim, H.-R. Cha, A comparison between zig-Zag plated hybrid parallel pipe and liquid cooling battery thermal management systems for Lithium-ion battery module, Appl. Therm. Eng. 219 (2023) 119599, https://doi.org/10.1016/j.applthermaleng.2022.119599.
[64] A. De Vita, A. Maheshwari, M. Destro, M. Santarelli, M. Carello, Transient thermal analysis of a lithium-ion battery pack comparing different cooling solutions for automotive applications, Appl. Energy 206 (2017) 101–112, https://doi.org/10.1016/j.apenergy.2017.08.184.
[65] M. Akbarzadeh, T. Kalogiannis, J. Jaguemont, L. Jin, H. Behi, D. Karimi, H. Beheshti, J. Van Mierlo, M. Berecibar, A comparative study between air cooling and liquid cooling thermal management systems for a high-energy lithium-ion battery module, Appl. Therm. Eng. 198 (2021) 117503, https://doi.org/10.1016/j.applthermaleng.2021.117503.
[66] T. Han, B. Khalighi, E.C. Yen, S. Kaushik, Li-ion battery pack thermal management: liquid versus air cooling, J. Therm. Sci. Eng. Appl. 11 (2018), https://doi.org/10.1115/1.4041595.
[67] S. Chavan, J. Liu, B. Venkateswarlu, S.W. Joo, S.C. Kim, Numerical simulation of lithium-ion battery thermal management systems: a comparison of fluid flow channels and cooling fluids, J. Energy Stor. 73 (2023) 108940, https://doi.org/10.1016/j.est.2023.108940.
[68] O. Yetik, N. Yilmaz, T.H. Karakoc, Computational modeling of a lithium-ion battery thermal management system with Al2O3-based nanofluids, Int. J. Energy Res. 45 (2021) 13851–13864, https://doi.org/10.1002/er.6718.
[69] D.D. Shetty, M. Sulthan, M. Zuber, I.A. Badruddin, C.R. Kini, Computational design and analysis of a novel battery thermal management system of a single 26650 Li-ion battery cell for electric vehicle application, J. Adv. Res. Fluid Mech. Therm. Sci. 93 (2022) 61–75, https://doi.org/10.37934/arfmts.93.2.6175.
[70] G. Hou, X. Liu, W. He, C. Wang, J. Zhang, X. Zeng, Z. Li, D. Shao, An equivalent circuit model for battery thermal management system using phase change material and liquid cooling coupling, J. Energy Stor. 55 (2022) 105834, https://doi.org/10.1016/j.est.2022.105834.
[71] Y. Gan, J. Wang, J. Liang, Z. Huang, M. Hu, Development of thermal equivalent circuit model of heat pipe-based thermal management system for a battery module with cylindrical cells, Appl. Therm. Eng. 164 (2020) 114523, https://doi.org/10.1016/j.applthermaleng.2019.114523.
[72] P.G. Zadeh, E. Gholamalizadeh, Y. Wang, J.D. Chung, Electrochemical modeling of a thermal management system for cylindrical lithium-ion battery pack considering battery capacity fade, Case Stud. Therm. Eng. 32 (2022) 101878, https://doi.org/10.1016/j.csite.2022.101878.
[73] P.G. Zadeh, Y. Wang, J.D. Chung, Thermal management modeling for cylindrical lithium-ion battery packs considering safety and lifespan, J. Mech. Sci. Technol. 36 (2022) 3727–3733, https://doi.org/10.1007/s12206-022-0646-0.
[74] D. Bernardi, E. Pawlikowski, J. Newman, A general energy balance for battery systems, J. Electrochem. Soc. 132 (1985) 5, https://doi.org/10.1149/1.2113792.
[75] R. Baveja, J. Bhattacharya, S. Panchal, R. Fraser, M. Fowler, Predicting temperature distribution of passively balanced battery module under realistic driving conditions through coupled equivalent circuit method and lumped heat dissipation method, J. Energy Stor. 70 (2023) 107967, https://doi.org/10.1016/j.est.2023.107967.
[76] E. Paccha-Herrera, W.R. Calderón-Muñoz, M. Orchard, F. Jaramillo, K. Medjaher, Thermal modeling approaches for a LiCoO2 Lithium-ion battery—a comparative study with experimental validation, Batteries 6 (2020) 40, https://doi.org/10.3390/batteries6030040.
[77] H. Zhang, C. Li, R. Zhang, Y. Lin, H. Fang, Thermal analysis of a 6s4p Lithium-ion battery pack cooled by cold plates based on a multi-domain modeling framework, Appl. Therm. Eng. 173 (2020) 115216, https://doi.org/10.1016/j.applthermaleng.2020.115216.
[78] J. Wang, S. Lu, Y. Wang, Y. Ni, S. Zhang, Novel investigation strategy for mini-channel liquid-cooled battery thermal management system, Int. J. Energy Res. 44 (2020) 1971–1985, https://doi.org/10.1002/er.5049.
[79] J. Duan, J. Zhao, X. Li, S. Panchal, J. Yuan, R. Fraser, M. Fowler, Modeling and analysis of heat dissipation for liquid cooling Lithium-ion batteries, Energies 14 (2021) 4187, https://doi.org/10.3390/en14144187.
[80] Z. Guo, J. Xu, Z. Xu, M. Mubashir, H. Wang, X. Mei, A lightweight multichannel direct contact liquid-cooling system and its optimization for Lithium-ion batteries, IEEE Trans. Transp. Electrif. 8 (2022) 2334–2345, https://doi.org/10.1109/TTE.2021.3131718.
[81] B. Xia, Y. Liu, R. Huang, Y. Yang, Y. Lai, W. Zheng, H. Wang, W. Wang, M. Wang, Thermal analysis and improvements of the power battery pack with liquid cooling for electric vehicles, Energies 12 (2019) 3045, https://doi.org/10.3390/en12163045.
[82] Z. Shang, H. Qi, X. Liu, C. Ouyang, Y. Wang, Structural optimization of lithium-ion battery for improving thermal performance based on a liquid cooling system, Int. J. Heat Mass Transf. 130 (2019) 33–41, https://doi.org/10.1016/j.ijheatmasstransfer.2018.10.074.
[83] H. Yang, Z. Wang, M. Li, F. Ren, Y. Feng, A manifold channel liquid cooling system with low-cost and high temperature uniformity for lithium-ion battery pack thermal management, Therm. Sci. Eng. Prog. 41 (2023) 101857, https://doi.org/10.1016/j.tsep.2023.101857.
[84] J. E, D. Han, A. Qiu, H. Zhu, Y. Deng, J. Chen, X. Zhao, W. Zuo, H. Wang, J. Chen, Q. Peng, Orthogonal experimental design of liquid-cooling structure on the cooling effect of a liquid-cooled battery thermal management system, Appl. Therm. Eng. 132 (2018) 508–520, https://doi.org/10.1016/j.applthermaleng.2017.12.115.
[85] N. Mei, X. Xu, R. Li, Heat dissipation analysis on the liquid cooling system coupled with a flat heat pipe of a Lithium-ion battery, ACS Omega 5 (2020) 17431–17441, https://doi.org/10.1021/acsomega.0c01858.
[86] C. Lan, J. Xu, Y. Qiao, Y. Ma, Thermal management for high power lithium-ion battery by minichannel aluminum tubes, Appl. Therm. Eng. 101 (2016) 284–292, https://doi.org/10.1016/j.applthermaleng.2016.02.070.
[87] C. Wang, G. Zhang, L. Meng, X. Li, W. Situ, Y. Lv, M. Rao, Liquid cooling based on thermal silica plate for battery thermal management system, Int. J. Energy Res. 41 (2017) 2468–2479, https://doi.org/10.1002/er.3801.
[88] C. Wang, G. Zhang, X. Li, J. Huang, Z. Wang, Y. Lv, L. Meng, W. Situ, M. Rao, Experimental examination of large capacity liFePO4 battery pack at high temperature and rapid discharge using novel liquid cooling strategy, Int. J. Energy Res. 42 (2018) 1172–1182, https://doi.org/10.1002/er.3916.
[89] Y. Chung, M.S. Kim, Thermal analysis and pack level design of battery thermal management system with liquid cooling for electric vehicles, Energy Convers. Manag. 196 (2019) 105–116, https://doi.org/10.1016/j.enconman.2019.05.083.
[90] H. Wang, L. Ma, Thermal management of a large prismatic battery pack based on reciprocating flow and active control, Int. J. Heat Mass Transf. 115 (2017) 296–303, https://doi.org/10.1016/j.ijheatmasstransfer.2017.07.060.
[91] Y. Yang, W. Li, X. Xu, G. Tong, Heat dissipation analysis of different flow path for parallel liquid cooling battery thermal management system, Int. J. Energy Res. 44 (2020) 5165–5176, https://doi.org/10.1002/er.5089.

[92] G. Chang, X. Cui, Y. Li, Y. Ji, Effects of reciprocating liquid flow battery thermal management system on thermal characteristics and uniformity of large lithium-ion battery pack, Int. J. Energy Res. 44 (2020) 6383–6395, https://doi.org/10.1002/er.5363.
[93] Y. Yang, J. Wu, X. Song, Z. Gu, Thermal management performance of Lithium-ion battery using supercritical CO2 as cooling fluid, Heat Transf. Eng. 44 (2023) 1452–1465, https://doi.org/10.1080/01457632.2022.2134082.
[94] X.-H. Yang, S.-C. Tan, J. Liu, Thermal management of Li-ion battery with liquid metal, Energy Convers. Manag. 117 (2016) 577–585, https://doi.org/10.1016/j.enconman.2016.03.054.
[95] H. Liu, E. Chika, J. Zhao, Investigation into the effectiveness of nanofluids on the mini-channel thermal management for high power lithium ion battery, Appl. Therm. Eng. 142 (2018) 511–523, https://doi.org/10.1016/j.applthermaleng.2018.07.037.
[96] Z. An, L. Jia, X. Li, Y. Ding, Experimental investigation on lithium-ion battery thermal management based on flow boiling in mini-channel, Appl. Therm. Eng. 117 (2017) 534–543, https://doi.org/10.1016/j.applthermaleng.2017.02.053.
[97] L. Sheng, L. Su, H. Zhang, K. Li, Y. Fang, W. Ye, Y. Fang, Numerical investigation on a lithium ion battery thermal management utilizing a serpentine-channel liquid cooling plate exchanger, Int. J. Heat Mass Transf. 141 (2019) 658–668, https://doi.org/10.1016/j.ijheat-masstransfer.2019.07.033.
[98] R. Guo, L. Li, Heat dissipation analysis and optimization of lithium-ion batteries with a novel parallel-spiral serpentine channel liquid cooling plate, Int. J. Heat Mass Transf. 189 (2022) 122706, https://doi.org/10.1016/j.ijheatmasstransfer.2022.122706.
[99] N. Wang, C. Li, W. Li, X. Chen, Y. Li, D. Qi, Heat dissipation optimization for a serpentine liquid cooling battery thermal management system: An application of surrogate assisted approach, J. Energy Stor. 40 (2021) 102771, https://doi.org/10.1016/j.est.2021.102771.
[100] D. Zhao, C. An, Z. Jia, Z. Lei, Structure optimization of liquid-cooled plate for electric vehicle lithium-ion power batteries, Int. J. Therm. Sci. 195 (2024) 108614, https://doi.org/10.1016/j.ijthermalsci.2023.108614.
[101] S. Chen, X. Peng, N. Bao, A. Garg, A comprehensive analysis and optimization process for an integrated liquid cooling plate for a prismatic lithium-ion battery module, Appl. Therm. Eng. 156 (2019) 324–339, https://doi.org/10.1016/j.applthermaleng.2019.04.089.
[102] S. Chen, N. Bao, L. Gao, X. Peng, A. Garg, An experimental investigation of liquid cooling scheduling for a battery module, Int. J. Energy Res. 44 (2020) 3020–3032, https://doi.org/10.1002/er.5132.
[103] A. Karthik, P. Kalita, A. Garg, L. Gao, S. Chen, X. Peng, A novel MOGA approach for power saving strategy and optimization of maximum temperature and maximum pressure for liquid cooling type battery thermal management system, Int. J. Green Energy 18 (2021) 80–89, https://doi.org/10.1080/15435075.2020.1831507.
[104] P. Li, J. Zhao, S. Zhou, J. Duan, X. Li, H. Zhang, J. Yuan, Design and optimization of a liquid cooling thermal management system with flow distributors and Spiral Channel cooling plates for Lithium-ion batteries, Energies 16 (2023) 2196, https://doi.org/10.3390/en16052196.
[105] Y. Fan, Z. Wang, T. Fu, H. Wu, Numerical investigation on lithium-ion battery thermal management utilizing a novel tree-like channel liquid cooling plate exchanger, Int. J. Heat Mass Transf. 183 (2022) 122143, https://doi.org/10.1016/j.ijheatmasstransfer.2021.122143.
[106] X. Fan, C. Meng, Y. Yang, J. Lin, W. Li, Y. Zhao, S. Xie, C. Jiang, Numerical optimization of the cooling effect of a bionic fishbone channel liquid cooling plate for a large prismatic lithium-ion battery pack with high discharge rate, J. Energy Stor. 72 (2023) 108239, https://doi.org/10.1016/j.est.2023.108239.
[107] D. Zhao, Z. Lei, C. An, Research on battery thermal management system based on liquid cooling plate with honeycomb-like flow channel, Appl. Therm. Eng. 218 (2023) 119324, https://doi.org/10.1016/j.applthermaleng.2022.119324.
[108] M. Xiong, N. Wang, W. Li, A. Garg, L. Gao, Study on the heat dissipation performance of a liquid cooling battery pack with different pin-fins, Batteries 9 (2023) 44, https://doi.org/10.3390/batteries9010044.
[109] Z. Tang, Z. Liu, J. Li, J. Cheng, A lightweight liquid cooling thermal management structure for prismatic batteries, J. Energy Stor. 42 (2021) 103078, https://doi.org/10.1016/j.est.2021.103078.
[110] X. Xu, T. Xiao, S. Chen, S. Lin, Exploring the heat transfer performance of nanofluid as a coolant for power battery pack, Heat Transfer—Asian Res. 48 (2019) 2974–2988, https://doi.org/10.1002/htj.21526.
[111] H. Fathabadi, A novel design including cooling media for Lithium-ion batteries pack used in hybrid and electric vehicles, J. Power Sources 245 (2014) 495–500, https://doi.org/10.1016/j.jpowsour.2013.06.160.
[112] P.T. Coman, E.C. Darcy, C.T. Veje, R.E. White, Numerical analysis of heat propagation in a battery pack using a novel technology for triggering thermal runaway, Appl. Energy 203 (2017) 189–200, https://doi.org/10.1016/j.apenergy.2017.06.033.
[113] B.J. Azuaje-Berbecí, H.B. Ertan, A model for the prediction of thermal runaway in lithium–ion batteries, J. Energy Stor. 90 (2024) 111831, https://doi.org/10.1016/j.est.2024.111831.
[114] M. Khasin, M.R. Mehta, C. Kulkarni, J.W. Lawson, Thermal data-driven model reduction for enhanced battery health monitoring, J. Power Sources 604 (2024) 234442, https://doi.org/10.1016/j.jpowsour.2024.234442.
[115] P. Zhao, L. Liu, Y. Chen, H. Ge, Theoretical and numerical analysis for thermal runaway propagation within a single cell, Int. J. Heat Mass Transf. 181 (2021) 121901, https://doi.org/10.1016/j.ijheatmasstransfer.2021.121901.